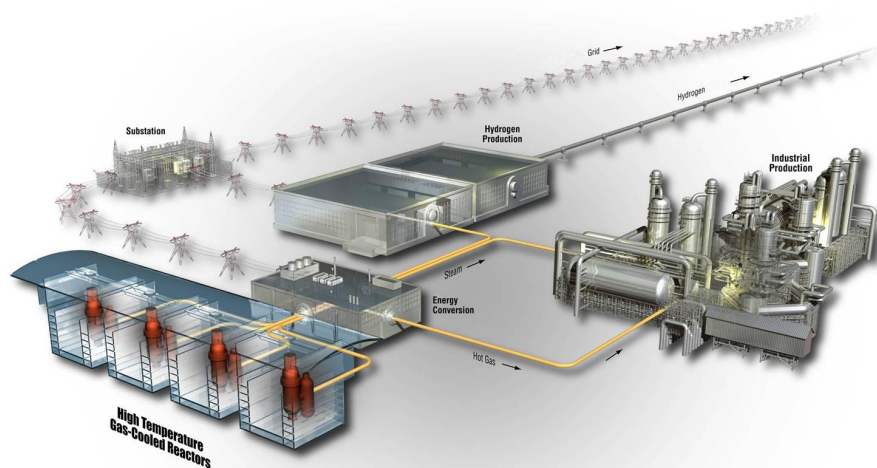


# AGR-3/4 Irradiation Test Final As-Run Report

Blaise P. Collin

June 2015

The INL is a  
U.S. Department of Energy  
National Laboratory  
operated by  
Battelle Energy Alliance



#### **DISCLAIMER**

This information was prepared as an account of work sponsored by an agency of the U.S. Government. Neither the U.S. Government nor any agency thereof, nor any of their employees, makes any warranty, expressed or implied, or assumes any legal liability or responsibility for the accuracy, completeness, or usefulness, of any information, apparatus, product, or process disclosed, or represents that its use would not infringe privately owned rights. References herein to any specific commercial product, process, or service by trade name, trade mark, manufacturer, or otherwise, does not necessarily constitute or imply its endorsement, recommendation, or favoring by the U.S. Government or any agency thereof. The views and opinions of authors expressed herein do not necessarily state or reflect those of the U.S. Government or any agency thereof.

# **AGR-3/4 Irradiation Test Final As-Run Report**

**Blaise P. Collin**

**June 2015**

**Idaho National Laboratory  
INL ART Program  
Idaho Falls, Idaho 83415**

**<http://www.inl.gov>**

**Prepared for the  
U.S. Department of Energy  
Assistant Secretary for the Office of Nuclear Energy  
Under DOE Idaho Operations Office  
Contract DE-AC07-05ID14517**





## INL ART Program

# AGR-3/4 Irradiation Test Final As-Run Report

INL/EXT-15-35550

Revision 0


June 2015

Prepared by:


  
Blaise P. Collin

6-29-2015  
Date

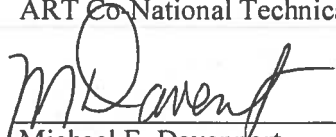
Approved by:

  
John T. Maki  
Fuel Performance Lead

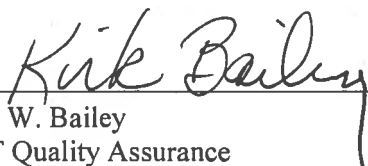
6-29-2015  
Date

  
David A. Petti  
ART Co-National Technical Director

6-29-2015  
Date

  
Michael E. Davenport  
Technical Lead

6/29/2015  
Date

  
Kirk W. Bailey  
ART Quality Assurance

6-25-2015  
Date

## REVISION LOG

Rev.	Date	Affected Pages	Revision Description
0	06/29/2015	All	Initial issue of the AGR-3/4 Irradiation Test Final As-Run Report

## SUMMARY

This document presents the as-run analysis of the AGR-3/4 irradiation experiment. AGR-3/4 is the combined third and fourth planned irradiations of the Advanced Gas Reactor (AGR) Fuel Development and Qualification Program. Funding for this program is provided by the U.S. Department of Energy as part of the Idaho National Laboratory (INL) Advanced Reactor Technologies Technology Development Office program. The objectives of the AGR-3/4 experiment are to:

1. Irradiate fuel containing uranium oxycarbide (UCO) designed-to-fail (DTF) fuel particles that will provide a known source of fission products for subsequent transport through compact matrix and structural graphite materials.
2. Assess the effects of sweep gas impurities, such as CO, H<sub>2</sub>O, and H<sub>2</sub> typically found in the primary coolant circuit of high temperature gas-cooled reactors, on fuel performance and subsequent fission product transport.
3. Provide irradiated fuel and material samples for post-irradiation examination (PIE) and safety testing.
4. Support the refinement of fuel performance and fission product transport models with on-line, PIE and safety test data.

The AGR-3/4 experiment was designed as a time-at-temperature experiment in which each capsule is thermally controlled within a range of temperatures suitable for the measurement of fission product diffusion in compact matrix and structural graphite materials. The primary objective of the test was directed towards providing data on fission product transport from particles with failed coatings using DTF particles. From the irradiation, data on fission product diffusivities in fuel kernels and sorptivities and diffusivities in compact matrix and structural graphite materials will be derived for use in the upgrade of fission product transport models.

In order to achieve the test objectives, the AGR-3/4 experiment was irradiated in the northeast flux trap position of the Advanced Test Reactor (ATR) at INL for a total irradiation duration of 369.1 effective full power days. The northeast flux trap location was selected because its larger diameter provided greater flexibility for test train design, significantly enhancing the capability for these combined irradiations. Irradiation began on December 14, 2011, and ended on April 12, 2014, spanning ten ATR cycles and approximately two and a half calendar years. The test train contained 12 separate and independently controlled and monitored capsules. Each capsule contained four 12.51 mm long compacts filled with both UCO unaltered “driver” fuel particles and UCO designed-to-fail fuel particles. The DTF fraction was specified to be  $1 \times 10^{-2}$ .

Final burnup values on a per compact basis ranged from 4.85 to 15.27% fissions per initial heavy-metal atom, while fast fluence values ranged from 1.19 to  $5.32 \times 10^{25}$  n/m<sup>2</sup> (E > 0.18 MeV). Time-average volume-average fuel temperatures on a capsule basis at the end of irradiation ranged from 845°C in Capsule 12 to 1276°C in Capsule 7. By the end of the irradiation, five out of 27 installed thermocouples had failed.

The AGR-3/4 experiment was globally successful in keeping the control temperatures of the 12 capsules in the temperature range of interest for the measurement of fission product diffusion in compact matrix and structural graphite materials.

Fission product release-to-birth (R/B) ratios reached values in the  $10^{-4}$ - $10^{-3}$  range early during irradiation as DTF particles started to fail during the first AGR-3/4 cycle. The hotter Capsule 7 reached the highest R/B value of around  $3 \times 10^{-3}$ .

Identifying individual DTF failures was not trivial because of simultaneous failures and increasing background from already failed DTF particles. At the end of irradiation, a best-estimate total of 780 DTF

particles had failed out of the 960 initial DTF particles in the entire test train, but minimum and maximum values of 562 and 1159 were also derived from the detection process to account for uncertainty in the failure counts. Based on AGR-1 irradiation fuel performance, it is reasonable to assume that there were no in-pile particle failures among the qualified driver fuel particles. Thus, the total number of fuel particle failures in each AGR-3/4 capsule should be capped at a maximum of 80 failures. Two capsules (Capsules 6 and 12) had maximum counts more than 30% lower than 80 failures.

Impurities added to the sweep gas did not appear to have an appreciable impact on fuel performance or fission product transport, but very small quantities of iodine isotope I-131 were identified in the sweep gas following the injection of the impurities and its transport to the detection system is believed to have been facilitated by the injected moisture.

## CONTENTS

SUMMARY .....	ix
ACRONYMS .....	xiv
1. INTRODUCTION .....	1
1.1 Test Objectives .....	2
1.2 Experimental Approach .....	2
1.3 Management and Qualification of AGR-3/4 Data .....	8
2. PHYSICS ANALYSIS .....	10
2.1 Advanced Test Reactor Power History .....	10
2.2 Neutronics Analysis Methodology .....	12
2.3 As-Run Neutronics Analysis Results .....	12
2.4 Axial Flux Wire Analysis .....	25
3. THERMAL ANALYSIS .....	28
3.1 Thermal Calculation Methodology .....	28
3.2 As-Run Thermal Analysis Results .....	39
4. FISSION PRODUCT GAS RELEASE ANALYSIS .....	44
4.1 Birth Rate Calculations Methodology .....	44
4.2 Release Rate Calculations Methodology .....	45
4.3 Release Rate to Birth Rate Ratio Results .....	45
4.4 Fuel Failure Particle Count .....	48
4.5 Release-to-Birth Ratio Per Failed Particle .....	49
5. AGR-3/4 OPERATIONAL ASSESSMENT .....	50
5.1 Power Increase .....	50
5.2 Temperature Control .....	50
5.3 Thermocouple Performance .....	54
5.4 Thermocouple Set Points Adjustments .....	61
6. CONCLUSIONS .....	63
7. REFERENCES .....	64
Appendix A As-Manufactured Fuel Data .....	67
Appendix B Compact Burnup and Fast Fluence by Cycle .....	73
Appendix C Matrix ring, graphite ring, and graphite sink temperatures .....	88

## FIGURES

Figure 1. ATR core cross section displaying the NEFT position. ....	3
---	---

Figure 2. Axial schematic of the AGR-3/4 capsules.....	4
Figure 3. Radial schematic of an AGR-3/4 capsule.....	5
Figure 4. Simplified flow path for AGR-3/4 sweep gas. ....	6
Figure 5. Schematic of an AGR-3/4 compact with DTF fuel particles placed along the axis. ....	8
Figure 6. Calculated average power density for Capsules 7-12 versus irradiation time in EFPD. ....	14
Figure 7. Calculated average power density for Capsules 1-6 versus irradiation time in EFPD. ....	15
Figure 8. Maximum instantaneous peak particle power versus irradiation time in EFPD for AGR-3/4 compacts. ....	16
Figure 9. Burnup versus irradiation time in EFPD for Capsules 7-12. ....	17
Figure 10. Burnup versus irradiation time in EFPD for Capsules 1-6. ....	18
Figure 11. Fast neutron fluence ( $E > 0.18$ MeV) versus irradiation time in EFPD for Capsules 7-12. ....	19
Figure 12. Fast neutron fluence ( $E > 0.18$ MeV) versus irradiation time in EFPD for Capsules 1-6. ....	20
Figure 13. Fast neutron fluence ( $E > 0.18$ MeV) versus burnup for AGR 3/4 compacts (top) and capsules (bottom). ....	21
Figure 14. Average thermal fluence rate or thermal flux for the four flux wires (Cycle 154B). ....	26
Figure 15. Average fast fluence rate or fast flux for the four flux wires (Cycle 154B). ....	27
Figure 16. Cutaway view (left) and three-dimensional rendering of ABAQUS finite element mesh (right) of a single AGR 3/4 capsule. ....	29
Figure 17. Three-dimensional plot of the AGR-3/4 fuel compact thermal conductivity as a function of fast neutron fluence ( $E > 0.18$ MeV) and temperature. ....	30
Figure 18. Three-dimensional plot of the AGR-3/4 matrix thermal conductivity as a function of fast neutron fluence ( $E > 0.18$ MeV) and temperature. ....	30
Figure 19. Three-dimensional plot of the ratio of irradiated over unirradiated AGR-3/4 graphite thermal conductivity as a function of temperature and displacements per atom (dpa). ....	31
Figure 20. Three-dimensional plot of the AGR-3/4 sweep gas thermal conductivity as a function of temperature and helium mole fraction. ....	32
Figure 21. Temperature contour plot cutaway view Capsule 12. ....	33
Figure 22. Calculated daily minimum, maximum, and volume-average fuel temperatures for Capsules 7-12. ....	34
Figure 23. Calculated daily minimum, maximum, and volume-average fuel temperatures for Capsules 1-6. ....	35
Figure 24. Calculated time-average minimum, time-average maximum, and time-average volume-average fuel temperatures for Capsules 7-12. ....	36
Figure 25. Calculated time-average minimum, time-average maximum, and time-average volume-average fuel temperatures for Capsules 1-6. ....	37
Figure 26. Temperature ( $^{\circ}\text{C}$ ) contour of compacts (a), matrix (b), graphite ring (c), and graphite sink (d). ....	38

Figure 27. Time-average minimum (TA Min), time-average volume-average (TAVA), and time-average peak (TA Peak) temperatures of AGR-3/4 compacts.....	42
Figure 28. Three-dimensional scatter plots of the irradiation characteristics of the AGR 3/4 compacts, with projections on two-dimensional plans in blue (burnup vs. fast fluence), green (burnup vs. TAVA temperature), and red (fast fluence vs. TAVA temperature). .....	42
Figure 29. Time-average volume-average temperature (°C) versus burnup for AGR 3/4 compacts.....	43
Figure 30. Time-average volume-average temperature (°C) versus fast neutron fluence ( $E > 0.18$ MeV) for AGR 3/4 compacts. ....	43
Figure 31. R/B values from daily birth rates for Kr 85m, Kr 88, and Xe 138 for Capsules 1-6.....	46
Figure 32. R/B values from daily birth rates for Kr 85m, Kr 88, and Xe 138 for Capsules 7-12.....	47
Figure 33. DTF best-estimate failure counts.....	49
Figure 34. Calculated daily control temperatures for Capsules 7-12.....	52
Figure 35. Calculated daily control temperatures for Capsules 1-6.....	53
Figure 36. Cutaway view of a capsule showing the position of TCs.....	55
Figure 37. Measured TC temperatures for Capsules 7-12. ....	57
Figure 38. Measured TC temperatures for Capsules 1-6. ....	58
Figure 39. Difference between measured and calculated TC temperatures versus EFPD for Capsules 7-12. ....	59
Figure 40. Difference between measured and calculated TC temperatures versus EFPD for Capsules 1-6. ....	60

## TABLES

Table 1. AGR 3/4 capsule rings.....	8
Table 2. ATR power history during AGR 3/4 irradiation.....	10
Table 3. Burnup and fast neutron fluence for Capsules 7-12 at the end of irradiation. ....	22
Table 4. Burnup and fast neutron fluence for Capsules 1-6 at the end of irradiation. ....	23
Table 5. Minimum, average, and peak compact burnup and fast fluence at the end of irradiation. ....	24
Table 6. Compact temperature data for Capsules 7-12 at end of irradiation. ....	40
Table 7. Compact temperature data for Capsules 1-6 at end of irradiation. ....	41
Table 8. AGR-3/4 DTF fuel failure total count (best-estimate, maximum, and minimum). ....	48
Table 9. AGR-3/4 temperature matrix. ....	50
Table 10. TC types, locations, and conditions in AGR 3/4 test train.....	55
Table 11. AGR-3/4 capsule TC set points (°C). NF indicates capsule running on set neon flow. ....	62

## ACRONYMS

AGR	Advanced Gas Reactor
ART	Advanced Reactor Technologies
ATR	Advanced Test Reactor
BE	best-estimate
BWXT	BWX Technologies
DNE	DIDO Nickel Equivalent
DTF	design-to-fail
EFPD	effective full-power days
FIMA	fissions per initial heavy-metal atom
FPM	fission product monitor
FPMS	fission product monitoring system
HPGe	high-purity germanium
HTGR	high temperature gas-cooled reactor
INL	Idaho National Laboratory
IPyC	inner pyrolytic carbon
LEU	low-enriched uranium
MCNP	Monte Carlo N-Particle transport code
NDMAS	Nuclear Data Management and Analysis System
NEFT	northeast flux trap
NQA	Nuclear Quality Assurance
OPyC	outer pyrolytic carbon
ORNL	Oak Ridge National Laboratory
PALM	powered axial locator mechanism
PIE	post-irradiation examination
R/B	release rate to birth rate ratio
SiC	silicon carbide
TAVA	time-average volume-average
TC	thermocouple
TDO	Technology Development Office
TRISO	tristructural isotropic
UCO	uranium oxycarbide



# AGR-3/4 Irradiation Test Final As-Run Report

## 1. INTRODUCTION

Several fuel and material irradiation experiments have been planned for the Idaho National Laboratory (INL) Advanced Reactor Technologies (ART) Technology Development Office (TDO) Advanced Gas Reactor (AGR) Fuel Development and Qualification Program (referred to as the INL ART TDO/AGR fuel program hereafter), which supports the development and qualification of tristructural-isotropic (TRISO) coated particle fuel for use in high temperature gas-cooled reactors (HTGRs). The goals of these experiments are to provide irradiation performance data to support fuel process development, qualify fuel for normal operating conditions, support development and validation of fuel performance and fission product transport models and codes, and provide irradiated fuel and materials for post-irradiation examination (PIE) and safety testing (INL, 2015b). AGR-3/4 combined the third and fourth in this series of planned experiments to test TRISO coated low enriched uranium (LEU) oxycarbide (UCO) fuel.

This combined experiment was intended to support the refinement of fission product transport models and to assess the effects of sweep gas impurities on fuel performance and fission product transport by irradiating designed-to-fail fuel particles and by measuring subsequent metallic fission product transport in fuel-compact matrix material and fuel-element graphite.

The AGR-3/4 fuel test was successful in irradiating the fuel compacts to the burnup and fast fluence target ranges, considering the experiment was terminated slightly before its initial target of 400 effective full power days (EFPD) (Collin, 2015). Out of the 48 AGR-3/4 compacts, 42 achieved the specified burnup of at least 6% fissions per initial heavy-metal atom (FIMA). Three capsules had a maximum fuel compact average burnup less than 10% FIMA, one more than originally specified, and the maximum fuel compact average burnup was less than 19% FIMA for the remaining capsules, as specified. Fast neutron fluence fell in the expected range of  $1.0$  to  $5.5 \times 10^{25}$  n/m<sup>2</sup> ( $E > 0.18$  MeV) for all compacts.

In addition, the AGR-3/4 experiment was globally successful in keeping the temperature in the 12 capsules relatively flat in a range of temperatures suitable for the measurement of fission product diffusion in compact matrix and structural graphite materials.

Designed-to-fail (DTF) particles failed mostly as intended, with the majority failing during the first AGR-3/4 cycle. A few capsules experienced additional DTF failures starting about two thirds of the way into irradiation. Overall, the particle failure count was estimated to be lower than the number of DTF particles in the capsules, signaling that in most capsules not all DTF particles had failed.

Once PIE is completed, this test will provide irradiated fuel performance data and safety testing performance fuel data to improve understanding of fission product transport in HTGRs. Additionally, PIE data will provide a better and more comprehensive assessment of the effects of sweep gas impurities on fuel performance and fission product transport.

This document presents the AGR-3/4 data collected and the analysis results of the as-run fuel irradiation conditions, including a summary of the experimental approach, as-run reactor physics and thermal analysis, fission product release-to-birth (R/B) ratio calculations and measurements, issues encountered during the test, and a summary of data qualification work. All AGR-3/4 work and analysis were performed in accordance to quality standards described by the INL ART TDO Quality Assurance Program Plan (INL, 2015a).

At the time this report was released, the AGR-3/4 test train had been unloaded from the reactor and some initial post-irradiation observations have been made, but PIE is not complete and will be documented in another report.

## 1.1 Test Objectives

As defined in the Technical Program Plan for the INL ART TDO/AGR fuel program (INL, 2015b), the objectives of the AGR-3/4 experiment are to:

1. Irradiate fuel containing UCO designed-to-fail fuel particles that will provide a known source of fission products for subsequent transport through compact matrix and structural graphite materials.
2. Assess the effects of sweep gas impurities, such as CO, H<sub>2</sub>O, and H<sub>2</sub> typically found in the primary coolant circuit of HTGRs, on fuel performance and subsequent fission product transport.
3. Provide irradiated fuel and material samples for post-irradiation examination and safety testing.
4. Support the refinement of fuel performance and fission product transport models with on-line, PIE and safety test data.

## 1.2 Experimental Approach

To achieve the test objectives outlined above, in accordance with requirements from the Technical Program Plan (INL, 2015b) and the Irradiation Test Specification (Maki, 2011), AGR-3/4 was irradiated in the northeast flux trap position (NEFT) of the Advanced Test Reactor (ATR) at INL. A cross-sectional view of the ATR core indicating this location is displayed in Figure 1.

Preliminary physics calculations (Chang, 2011) have shown that the best ATR position to achieve significant end-of-irradiation conditions (i.e., peak compact burnup exceeding 16 % FIMA and maximum fast neutron fluence of about  $5.5 \times 10^{25}$  n/m<sup>2</sup>, E > 0.18 MeV) after 400 EFPDs, for a test train of sufficient size to accommodate test fuel and test articles, is obtained from irradiation in the NEFT. Contrary to the Large B positions used for AGR-1 and AGR-2, its larger diameter also provides greater flexibility for test train design, significantly enhancing the capability for the combined irradiations. Specifically, AGR-3/4 irradiation in the NEFT position:

- maximizes space for different fission product retention materials,
- minimizes irradiation time due to a higher flux rate,
- minimizes flux gradient across the test train, and
- allows power level control (corner lobes controlled independently).

In addition, the rate of burnup and fast fluence accumulation, or acceleration, in this position is less than three times that expected in the HTGR. Past U.S. and German experience indicates that by keeping the acceleration factor under three, an irradiation test is more prototypic of an actual reactor irradiation (Petti, 2002).

The AGR-3/4 test train is a multi-capsule, instrumented lead experiment designed for irradiation in the 133.4-mm diameter NEFT position of ATR. The best geometry to obtain fission product transport data was determined to be an AGR-3/4 capsule consisting of a single stack of fuel compacts containing a known fraction of DTF particles surrounded by three concentric annular rings of test material: (1) an annulus of fuel-compact matrix material; (2) an annulus of fuel-element graphite; and (3) an annulus of graphite operating at lower temperature to act as a sink for fission products. This configuration best reduces axial thermal gradients and, hence, axial diffusion. The test reactor's axial flux distribution and space considerations within the test train impose a practical limit of 12 independently controlled and monitored capsules per test train. An axial view of the test train is illustrated in Figure 2. Figure 3 illustrates a radial view of a capsule.

Steep temperature gradients occurred in the capsules between the fuel stack and the successive concentric rings. Since peak temperatures in the fuel were limited by specifications, the temperature in the

graphite rings fell below the range of interest for the study of fission product transport. Taking advantage of the relative higher temperatures experienced in the matrix ring, the matrix material in Capsules 3, 8, and 10 was replaced by graphite to allow the study of fission product diffusion in graphite in a wider range of temperatures.

There are two styles of capsules: a “fuel body” style where the graphite layer incorporates a floor and a lid (Capsules 2, 4, 6, 9 and 11) and a standard style where the graphite layer is simply a ring (seven remaining capsules). The floor and lid hold the inner part of the capsule (fuel + matrix ring + graphite ring) as a single piece, allowing it to be removed after irradiation and to be heated in a furnace for fission product migration measurements. The former style capsule is 111.3 mm long and the latter style capsule is 101.6 mm long. Each of the 12 AGR-3/4 capsules hosts four 12.51 mm long compacts.

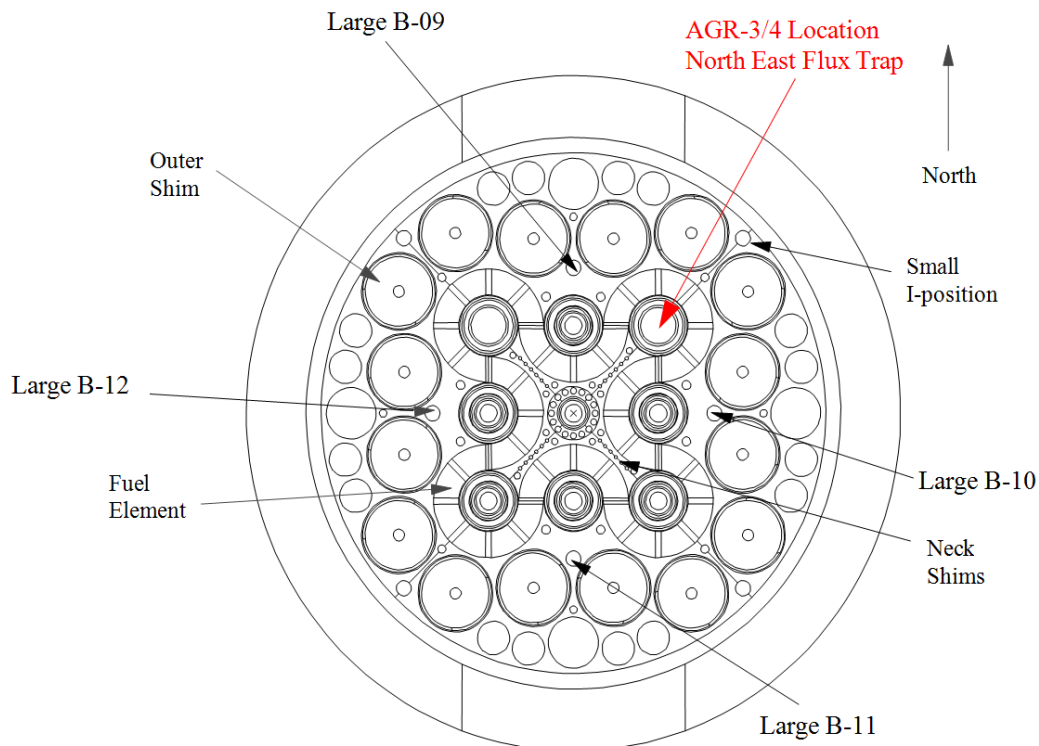


Figure 1. ATR core cross section displaying the NEFT position.

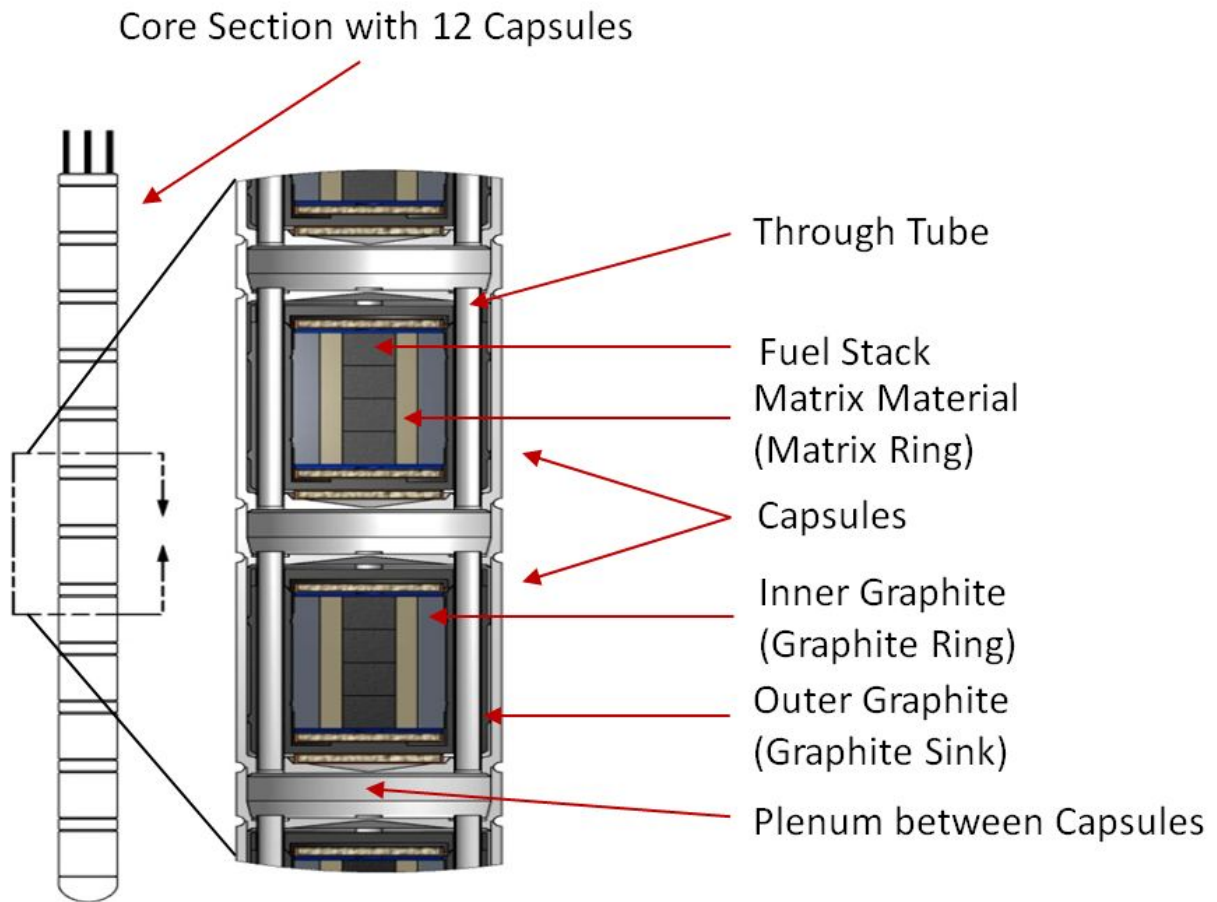


Figure 2. Axial schematic of the AGR-3/4 capsules.

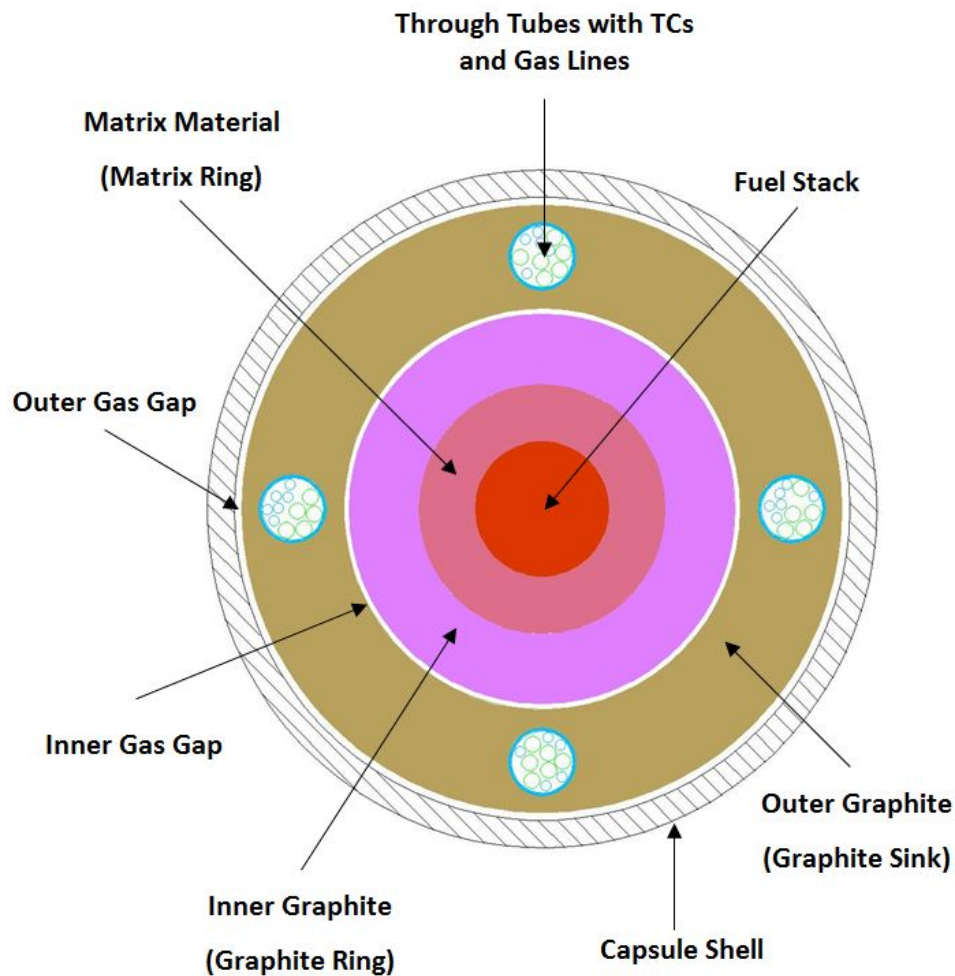


Figure 3. Radial schematic of an AGR-3/4 capsule.

Independent gas lines route a mixture of helium and neon gases through each of the 12 capsules to provide temperature control and to sweep released fission product gases to the fission product monitoring system (FPMS). Temperature control is based on temperature feedback from the thermocouples (TCs) in each capsule and is performed by varying the sweep gas composition (between 100% helium for high conductivity and 100% neon for low conductivity). Each capsule has two temperature control gaps fed by a single gas blend supply: one gap between the graphite ring and the graphite sink and the other between the graphite sink and the stainless steel capsule shell. The purpose of the dual gas gaps is to run the sink at a much cooler temperature, resulting in effective fission product retention, and to decrease the operating temperature of the instrumentation placed in the sink ring, resulting in a prolonged life of the thermocouples in this ring. The gas gaps between the other layers are set to a fixed minimum width to minimize the temperature difference between the layers. Reactor coolant water flows on the outside of the stainless steel capsule shell. The blending of sweep gases is accomplished by a computerized mass flow controller before the gas enters the test train. In addition to the helium and neon sweep gas mixture necessary to provide thermal control of the experiment, Capsule 11 was injected with impurities (carbon monoxide, water, and hydrogen) typically found in the primary coolant circuit helium of HTGRs. These impurities were injected in Capsule 11 during the last three cycles of AGR-3/4 to assess their effects on fuel performance and fission product transport. Figure 4 shows a schematic diagram of the FPMS.

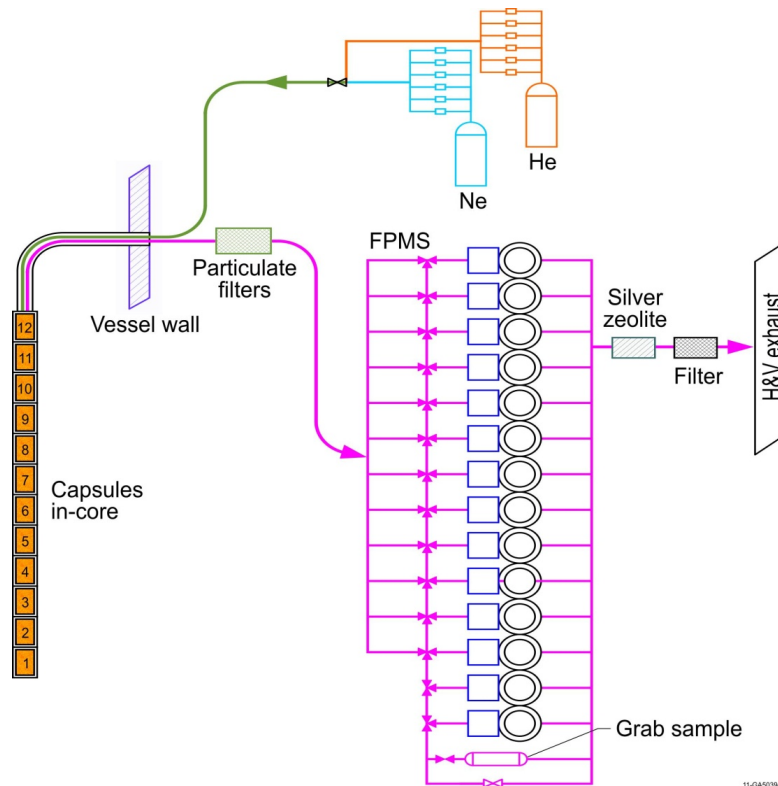


Figure 4. Simplified flow path for AGR-3/4 sweep gas.

(Hartwell, 2005) provides a detailed description of the FPMS. This system continuously measures the gamma activity of the sweep gas from each AGR-3/4 capsule to provide an indicator of fuel irradiation performance. Spectrometer detector systems measure the concentrations of various krypton and xenon isotopes in the sweep gas from each capsule. Eight-hour counting intervals were used to measure the concentrations of Kr-85m, Kr-87, Kr-88, Kr-89, Kr-90, Xe-131m, Xe-133, Xe-135, Xe-135m, Xe-137, Xe-138, and Xe-139. These concentrations, along with gas flow data, were used to determine release rates. The release rates were paired with calculated birth rates to obtain the release-to-birth ratio values used as indicators of initial fuel quality and fuel performance during irradiation.

The FPMS incorporates 14 individual monitoring systems, one for each of the individual capsule effluent lines, and two backup spares. Each monitor consists of a high purity germanium (HPGe), detector-based, gamma-ray spectrometer and a sodium iodide [NaI(Tl)] scintillation detector-based total radiation detector (often termed the “gross” gamma detector). The gross gamma detectors are able to detect the failure of individual TRISO particles, while the gamma-ray spectrometer is used for isotopic quantification of noble gas release. These detector units are located in the ATR 1A Primary cubicle.

The sweep gas from each test capsule is routed via sampling lines to the monitoring station associated with that capsule. The sample lines, valves, and filters are predominately contained in the 1A Primary cubicle. The sample lines have only two short, shielded segments in the 1A Primary cubicle. These short segments run through the gross detector monitoring station and into the HPGe spectrometer shield.

Each gross detector monitoring station (14 stations implemented) incorporates a thallium-activated NaI(Tl) scintillation detector viewing a 25-mm long segment of the capsule effluent line just before its entry into the HPGe spectrometer shield. The scintillation detector counting rate is monitored using a computer-controlled multi-channel scaler.

Fuel for AGR-3/4 contains conventional driver fuel coated particles similar to the baseline fuel used in the AGR-1 experiment (Barnes, 2006a) and designed-to-fail fuel particles whose kernels are identical to the driver fuel kernels and whose coatings are designed to fail under irradiation, leaving fission products to migrate through the surrounding materials (Barnes, 2006b and Marshall, 2011):

- Driver fuel consists of TRISO coated particles that are slightly less than 1 mm in diameter. Each particle has a central reference kernel containing the fuel material, a porous carbon buffer layer, an inner pyrolytic carbon (IPyC) layer, a silicon carbide (SiC) barrier coating, and an outer pyrolytic carbon (OPyC) layer.
- DTF fuel consists of reference kernels with a 20- $\mu$ m-thick pyrolytic carbon (PyC) seal coating. This coating was designed to fail early in the irradiation and provide a known source of fission products. The coating properties of the DTF particles are not a significant factor, given that the coatings are designed to fail early in these irradiations, and for this reason they were produced in a laboratory-scale coater.

Kernels for AGR-3/4 consist of LEU UCO fuel. The kernels were fabricated by BWX Technologies (BWXT, 2006) in accordance with the AGR-3/4 Fuel Product Specification (Marshall, 2011). The UCO kernels were coated and characterized by ORNL (Hunn, 2007 and Hunn, 2011a). Coating was performed in accordance with the AGR-3/4 Fuel Product Specification (Barnes, 2006a and Marshall, 2011).

After coating, AGR-3/4 fuel was formed into right cylindrical compacts. The compact matrix material is composed of a thermosetting carbonaceous material. Prior to compacting, the fuel particles were overcoated with thick layers of the compact matrix material. This overcoat is intended to prevent particle-to-particle contact and help achieve the desired packing fraction of fuel particles. Each AGR-3/4 compact contains driver fuel particles and 20 DTF particles (about 1 % of the particles) placed along its axis as shown in Figure 5. AGR-3/4 compacts are nominally 12.51 mm in length and 12.31 mm in diameter. The compacts are fabricated with fuel-free end caps of matrix material less than 0.5 mm thick. These end caps ensure smooth, protected surfaces that help to prevent fuel particle damage during handling.

The AGR-3/4 fuel compacts are surrounded by three concentric annular rings of test material consisting of fuel-compact matrix material (matrix ring) and fuel-element graphite (graphite ring and sink). The matrix rings have average nominal inside and outside diameters of 12.4 and 24.2 mm, respectively, and a length of 50.8 mm. This leads to a wall thickness of about 6 mm, which has been determined to be adequate to study the diffusion of fission product in matrix material. For the same reason, the surrounding layers (graphite rings and sinks) were also designed with wall thicknesses greater than 6 mm, essentially as thick as the capsule shells permit: the graphite rings and graphite sinks have nominal diameters of 39.0 and 63.3 mm, respectively, leading to wall thicknesses of 7.3 and 12.2 mm, respectively. These values vary somewhat from capsule to capsule, depending on their gas gap widths. The materials used to fabricate the AGR-3/4 graphite rings and sinks are two candidate nuclear-grade graphites considered for high-dose regions in conceptual high temperature reactors (Marshall 2011): IG-110 and PCEA. IG-110 is an isostatically molded graphite with a very fine grain structure, whereas PCEA is an extruded graphite. As indicated in Table 1, Capsules 8 and 9 contain IG-110 graphite rings and sinks while all the other capsules contain PCEA. Table 1 also lists the “fuel body” and standard capsules. Capsules 3, 8, and 9 had their matrix material replaced by graphite to allow study of fission product diffusion in graphite at higher temperatures. Capsule 11 received impurities to study their effects on fuel performance and fission product transport.

Appendix A contains as-manufactured fuel data. Characterization data for the fuel particles, fuel compacts, and rings are detailed in the AGR-3/4 Irradiation Experiment Test Plan (Collin, 2015).



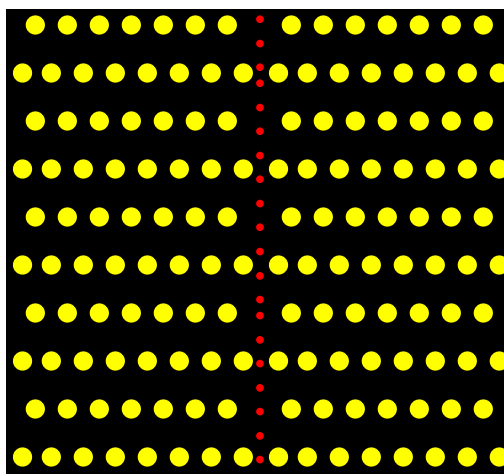


Figure 5. Schematic of an AGR-3/4 compact with DTF fuel particles placed along the axis.

Table 1. AGR 3/4 capsule rings.

Capsule	Capsule Type	Graphite Type	Impurities
12	Standard	PCEA	No
11	Fuel body	PCEA	Yes
10 <sup>(a)</sup>	Standard	PCEA	No
9	Fuel body	IG-110	No
8 <sup>(a)</sup>	Standard	IG-110	No
7	Standard	PCEA	No
6	Fuel body	PCEA	No
5	Standard	PCEA	No
4	Fuel body	PCEA	No
3 <sup>(a)</sup>	Standard	PCEA	No
2	Fuel body	PCEA	No
1	Standard	PCEA	No

a. Matrix material in Capsules 3, 8, and 10 was replaced by graphite.

### 1.3 Management and Qualification of AGR-3/4 Data

The AGR-3/4 test spanned ten cycles of ATR operation, eight of which generated five major streams of data. The test train was removed from its NEFT location and moved to the ATR canal during two cycles, for which no data were recorded. Of the eight cycles spent in ATR and for which data were recorded, seven were power cycles and one was a low power cycle during which little burnup was accumulated. At the outset, detailed data provided a description of the fuel fabrication process and the contents of each compact. Data streams resulting from neutronics and thermal modeling of the experiment as run in ATR were created both during the experiment and more recently during the post-experiment evaluation. Particularly, the most accurate post-experiment calculations, summarized in the remainder of this document, are important for future reference. Finally, during the entire course of irradiation, the following three streams of data were generated on an ongoing basis:

- Fuel irradiation data, which include thermocouple readings, sweep gas compositions, flow rates and pressures, and moisture monitor readings



- FPMS data, which include both isotopic release data and gross gamma counts
- ATR operating conditions data, which include lobe powers, outer shim control cylinder positions, neck shim positions, and control rod positions.

AGR-3/4 data also include calculated quantities during the experiment such as fission product isotope birth rates and effective full-power days at the start of each ATR cycle.

Preservation and management of these data are critical contributions to the experiment's ability to meet its objectives. The INL ART program established the Nuclear Data Management and Analysis System (NDMAS) to ensure that INL ART data are qualified for use, stored in a readily accessible electronic form, and analyzed to extract useful results. The system is described in the Nuclear Data Management and Analysis System Plan (Hull, 2015).

The NDMAS provides a single controlled repository for all of AGR-3/4 data and makes the data available to users on an easily-accessible website. During the experiment, the website showed progress of irradiation in almost real time after data were generated. The gross gamma data were displayed almost daily, and other irradiation, FPMS, and ATR operational data were displayed within a week or so of real time. In addition to displays of the data as it accrues in time, summaries of the data are provided by the NDMAS. Many of the plots in this document are examples of the displays that this system provides.

Another important function of NDMAS is the facilitation of data qualification and storage of the associated documentation. Specific data qualification activities within NDMAS depend on the data qualification category for each data entity as assigned by the data generator. Activities include: (1) capture testing to confirm data stored within NDMAS are identical to the raw data supplied, (2) accuracy testing to confirm data are an accurate representation of the system or object being measured, and (3) documentation that data were collected under a Nuclear Quality Assurance NQA-1 or equivalent quality assurance program. Within the INL ART program, the NQA-1 requirements are implemented through INL ART TDO Quality Assurance Program Plan (INL, 2015a). "Capture tested" data are data whose capture has been verified by showing that data pushed to the database match the raw data provided by the generator. Data captured using approved and controlled code are considered verified, i.e. "capture passed", data. Data loaded into the system using an approved code are verified through manual inspection. If data fail capture verification, the capture process is reviewed and modified until the captured data are correct. "Capture failed" is a short-lived data state.

The status of these data streams is summarized below (Pham, 2015):

1. Fuel fabrication data – All data have been processed into the NDMAS database and qualified (953 records).
2. Fuel irradiation data – Data from eight AGR-3/4 reactor cycles have been processed into the NDMAS database and tested. Of these, 91.5% have been qualified, 0.6% were considered "trend", and 7.9% have failed NDMAS accuracy testing.
3. FPMS data – Data from eight AGR-3/4 reactor cycles have been processed into the database and capture tested. Qualification of these data (Scates, 2015) has been recorded in NDMAS.
4. ATR Operating Conditions Data – Data for all AGR-3/4 cycles have been stored and capture tested. These data, which come from outside the INL ART program, are assumed to be qualified by ATR quality control procedures.
5. Neutronics and Thermal Modeling Data – All data have been stored in NDMAS and capture passed. Qualification of these data (Sterbentz, 2015 and Hawkes, 2015b) has been recorded in NDMAS.

## 2. PHYSICS ANALYSIS

This section summarizes the physics analyses used to characterize the neutron flux environment and burnup of the fuel compacts. It gives the operational history of ATR during AGR-3/4 irradiation, followed by a description of the methodology used to analyze the test train. Key parameters, such as burnup and fast fluence of the fuel compacts, are included.

### 2.1 Advanced Test Reactor Power History

The AGR-3/4 irradiation experiment lasted for a total of ten ATR cycles including seven normal cycles, one low power cycle, one unplanned outage cycle, and one Power Axial Locator Mechanism (PALM) cycle. The AGR-3/4 test train was irradiated for seven power cycles, from December 2011 until April 2014. The test train was located in the NEFT location during these seven power cycles, and it was moved to the ATR canal during the unplanned outage cycle 153A to prevent over-heating of the fuel compacts during the following PALM cycle 153B. Cycle 152A was a low power testing cycle during which little burnup was accumulated. These three cycles are not discussed in this report.

Table 2 shows the irradiation history, including start and stop times and dates for each power cycle, and unplanned outages. Times of reactor events are given to the nearest hour and the total irradiation time in EFPD is based on ATR power history data. The total irradiation time of the AGR-3/4 test train was 369.1 EFPD. Also shown is the average northeast lobe power for each cycle, which was progressively increased from approximately 14 to 16 to 18 to 19 MW during the course of the AGR-3/4 irradiation in order to maintain temperature in the capsules as U-235 depleted.

Table 2. ATR power history during AGR 3/4 irradiation.

AGR-3/4 Cycle	ATR Cycle	Average Northeast Lobe Power (MW)	Cycle EFPD	Cumulative EFPD	Date (M-D-Y)	Time <sup>(a)</sup>	Reactor Event
1	151A	14.4	56.1	0.0	12-14-11	0100	Reactor start-up
				0.4	12-14-11	1700	Full power reached
				11.1	12-25-11	1000	Unplanned reactor scram
				11.1	12-28-11	0400	Reactor re-start
				11.5	12-28-11	2000	Full power reached
				56.1	02-11-12	1100	Reactor down
2	151B	14.3	51.3	56.1	03-01-12	0600	Reactor start-up
				56.3	03-01-12	1600	Full power reached
				77.3	03-22-12	1700	Unplanned reactor scram
				77.3	03-25-12	0900	Reactor restart
				77.5	03-25-12	2100	Full power reached
				79.3	03-27-12	1500	Unplanned reactor scram
				79.3	04-07-12	0000	Reactor restart
				79.5	04-07-12	1400	Full power reached
				107.4	05-05-12	1100	Reactor down

Table 2. (continued)

AGR-3/4 Cycle	ATR Cycle	Average Northeast Lobe Power (MW)	Cycle EFPD	Cumulative EFPD	Date (M-D-Y)	Time <sup>(a)</sup>	Reactor Event
3	152B	15.8	51.0	107.4	11-27-12	0400	Reactor start-up
				107.8	11-28-12	2100	Full power reached
				158.4	01-18-13	1100	Reactor down
4	154A	16.0	52.3	158.4	05-19-13	0300	Reactor start-up
				158.6	05-19-13	1500	Full power reached
				160.3	05-21-13	0600	Unplanned reactor scram
				160.3	05-23-13	2000	Reactor re-start
				160.4	05-24-13	0300	Full power reached
				210.7	07-13-13	1100	Reactor down
5	154B	17.6	53.4	210.7	08-23-13	1500	Reactor start-up
				210.9	08-24-13	0600	Full power reached
				264.1	10-16-13	1100	Reactor down
6	155A	17.9	55.1	264.1	11-08-13	0100	Reactor start-up
				264.1	11-08-13	1800	Full power reached
				268.5	11-13-13	0200	Unplanned reactor scram
				268.5	11-27-13	0300	Reactor re-start
				268.5	11-27-13	2200	Full power reached
				319.2	01-17-14	1600	Reactor down
7	155B	18.6	49.9	319.2	02-13-14	0500	Reactor start-up
				319.5	02-13-14	2100	Full power reached
				354.9	03-21-14	0800	Unplanned reactor scram
				354.9	03-28-14	1700	Reactor re-start
				355.1	03-29-14	0400	Full power reached
				369.1	04-12-14	0500	Reactor down

a. Reactor event time was obtained from hourly ATR Surveillance Data Reports. Events are observed at the nearest full hour increment.

## 2.2 Neutronics Analysis Methodology

Neutronics analysis of the AGR-3/4 test train was performed using JMOCUP, a coupling code developed at INL that combines the continuous energy Monte Carlo N-Particle (MCNP) transport code (LANL, 2004) and the depletion code ORIGEN (Croff, 1983). The JMOCUP depletion methodology was used to model and deplete the AGR-3/4 TRISO fuel compacts in the northeast flux trap of ATR. The AGR-3/4 calculations here use the same JMOCUP Monte Carlo depletion methodology and software modules previously used in the AGR-1 physics calculations (Sterbentz, 2013). Verification that the calculation executed properly was done through both technical checkers and post-processing of calculated data. A detailed description of the JMOCUP system, along with Verification and Validation of the JMOCUP depletion calculation is documented in (Sterbentz, 2015).

The AGR-3/4 experiment was modeled in MCNP format as a collection of cells describing the AGR-3/4 experiment in detail using the as-manufactured data provided in Appendix A. Calculations with a particle model allowed for self-shielding of U-238 in the kernels and are expected to produce more accurate isotopic concentrations for actinides and fission products. Each AGR-3/4 compact was subdivided into two equal-volume axial sections, with each section containing seven layers of particles and each layer containing 135 particles, or 945 particles per section and 1890 particles per compact. The particle model calculated the data averaged over half a compact. The graphite annuli (matrix, ring, and sink) were subdivided into four azimuthal quadrants.

The AGR-3/4 JMOCUP depletion calculation coordinated three depletions: (1) ATR driver core, (2) AGR-3/4 TRISO compacts, and (3) AGR-3/4 hafnium capsule shroud. The ATR driver core consists of 840 depletion cells in the MCNP model, or three radial and seven axial cells per each of the 40 driver elements in the serpentine ATR core. The 48 fuel compacts of the AGR-3/4 experiment were split in half for a total of 96 depletion cells. The hafnium shroud had 48 depletion cells or four azimuthal segments per capsule. Therefore, there were 984 depletion cells in the particle model. JMOCUP depleted each cell at each time step.

The ATR driver fuel depletion cells each contain nine actinides and 24 fission product isotopes that are tracked along with their fission and radiative capture cross sections, which must be updated at each time step. Similarly, the compacts have 21 tracked actinides and 71 fission products. In the hafnium shroud cells, the six naturally-occurring hafnium isotopes are tracked. The MCNP code calculates the cell flux and specified nuclear reaction rate(s) for every isotope in each depletion cell at every time step. Using these data, updated one-group cross sections are fed to the ORIGEN input files for the next ORIGEN depletion calculation.

The neutron transport problem in the JMOCUP method is solved using the KCODE option in the MCNP code. In order for the KCODE option to be effective, the reactor core, in this case the ATR driver fuel must be simultaneously depleted along with the AGR-3/4 experiment depletions. Modeling the depletion of the entire ATR core provides a realistic neutron and gamma source for analyzing the AGR-3/4 experiment's radiation environment. The effects of important operational details (such as the positions of the outer shim control cylinders) can be taken into account on a daily-averaged basis using this methodology.

## 2.3 As-Run Neutronics Analysis Results

Figure 6 and Figure 7 show the calculated capsule compact heat rates for the 12 AGR-3/4 capsules over the full irradiation. The heat rate in each capsule is the sum of all four compacts or eight half-cell compacts. Capsule 6 was just below the ATR core midplane and exposed to the highest thermal neutron fluence. Its compacts sustained the greatest burnups of all compacts along with the compacts in Capsule 7, which was just above core midplane. The surrounding Capsules 5 and 8, and to a lesser extent Capsules 4 and 9, also received significant fast fluence and accumulated high burnups. The heat rate in these middle capsules burned down as each cycle progressed. The capsule heat rates jumped up at the

start of every cycle in which the northeast lobe power was increased (see Table 2). The burnup of U-235 in the compacts corresponded directly to the decrease in the capsule heat rates during the cycle.

Capsules 1 and 12 were at the bottom and top of the active core, respectively, and sustained substantially lower U-235 burnup. The heat rate behavior in these capsules and in their neighbor Capsules 2 and 11 is quite different from the middle capsules. It tended to remain relatively flat throughout irradiation and increased slightly over the course of each cycle. The slight increase is attributable to rotation of the outer shim control cylinders and a corresponding increase in local thermal flux. One can also detect a slight increase in the heat rate at the beginning of those cycles in which the lobe power increased relative to the last cycle. The design goal of a flat power or heat rate profile appears to have been achieved for the capsules near the top and bottom of the test train (Capsules 1, 2, 11, and 12). The heat rates of Capsules 3 and 10 exhibit a behavior intermediate to the capsules around midplane and the capsules on top and bottom.

Figure 8 displays the maximum instantaneous peak power per particle for AGR-3/4 compacts. The location of the maximum instantaneous peak can move from one compact to another, so the curves show the maximum values reached at each time step.

The evolution of burnup with irradiation time is shown in Figure 9 and Figure 10. Capsule average burnup is shown for each capsule, along with the peak and minimum compact values in each capsule. The capsule at the top of the reactor (Capsule 12) had the lowest average burnup at the end of irradiation, with higher values found towards the center. Capsule-average burnups ranged from 5.35% FIMA in Capsule 12 to 15.24% FIMA in Capsule 6. Figure 11 and Figure 12 show the evolution of the fast neutron fluence ( $E > 0.18$  MeV) with irradiation time. As would be expected, the trends of fast fluence follow closely those of burnup. The capsule with the lowest average fluence at the end of the irradiation was Capsule 12, with a value of  $1.50 \times 10^{25}$  n/m<sup>2</sup>, and the capsule with the highest average fluence was Capsule 6, with a value of  $5.31 \times 10^{25}$  n/m<sup>2</sup>. In addition, Figure 13 shows the correlation between burnup and fast fluence for the 48 compacts and 12 capsules of the AGR-3/4 test train. A three-dimensional scatter plot of the irradiation characteristics of the 48 AGR-3/4 compacts is presented in Figure 28 (see Section 3.13.1).

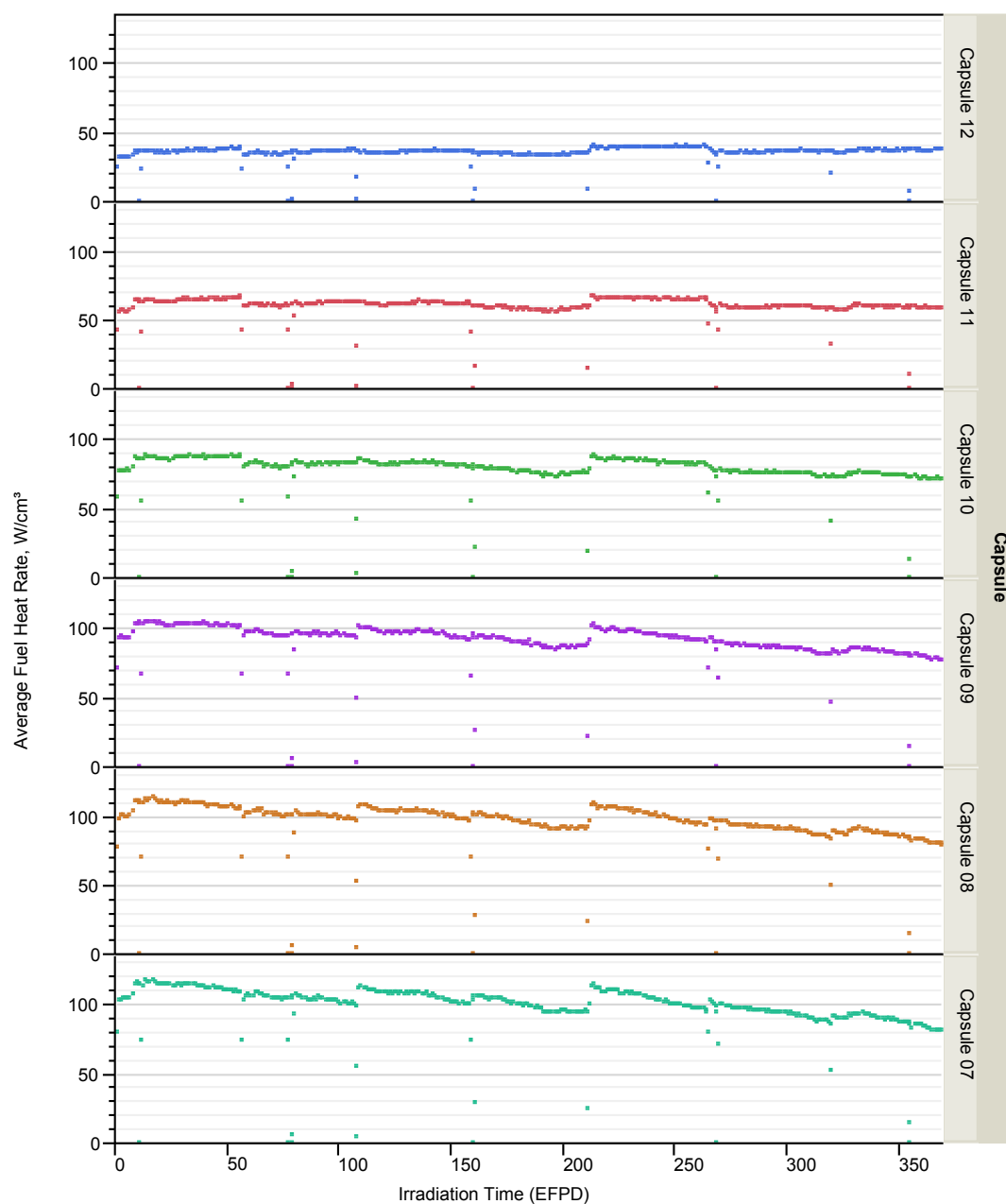


Figure 6. Calculated average power density for Capsules 7-12 versus irradiation time in EFPD.

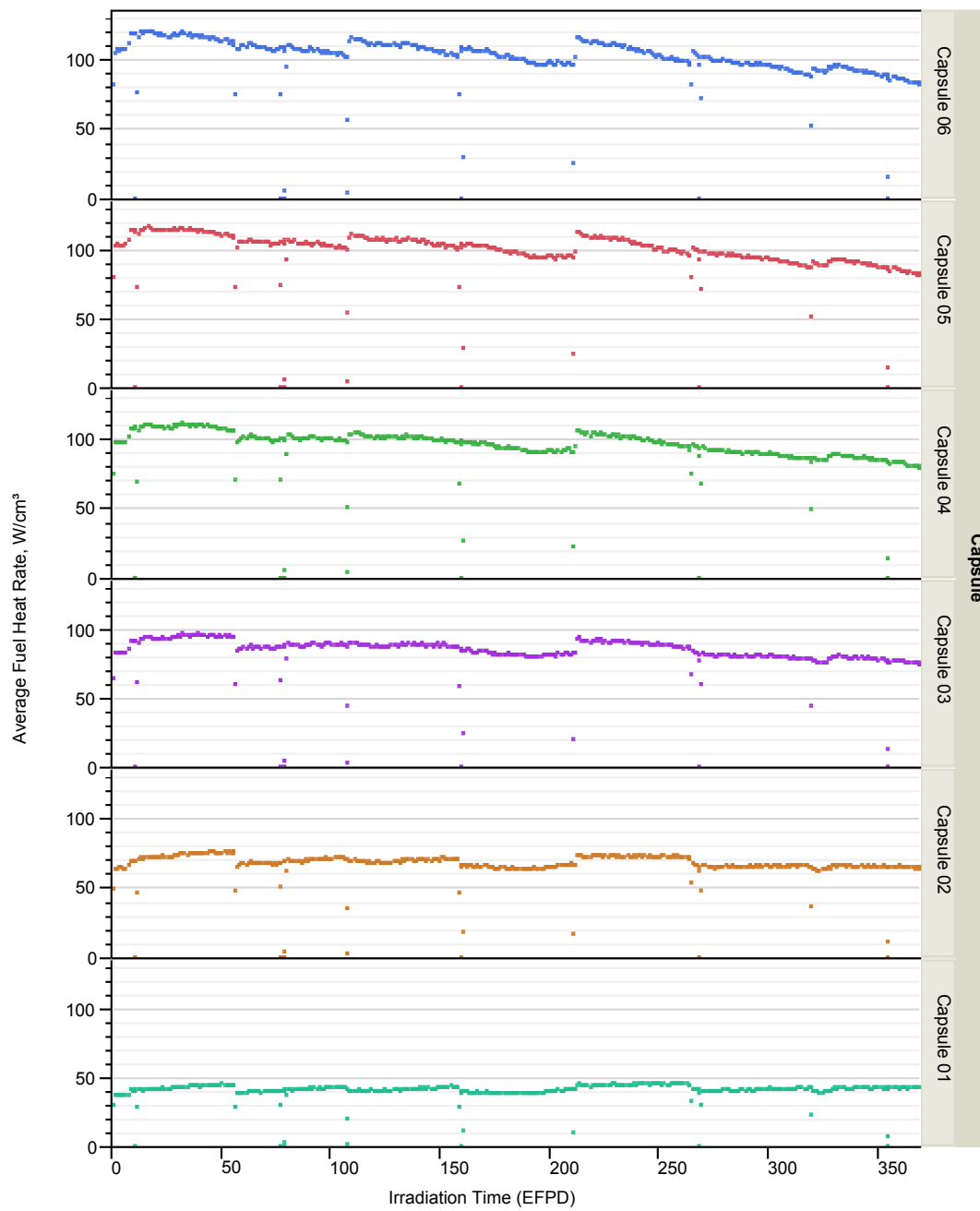


Figure 7. Calculated average power density for Capsules 1-6 versus irradiation time in EFPD.

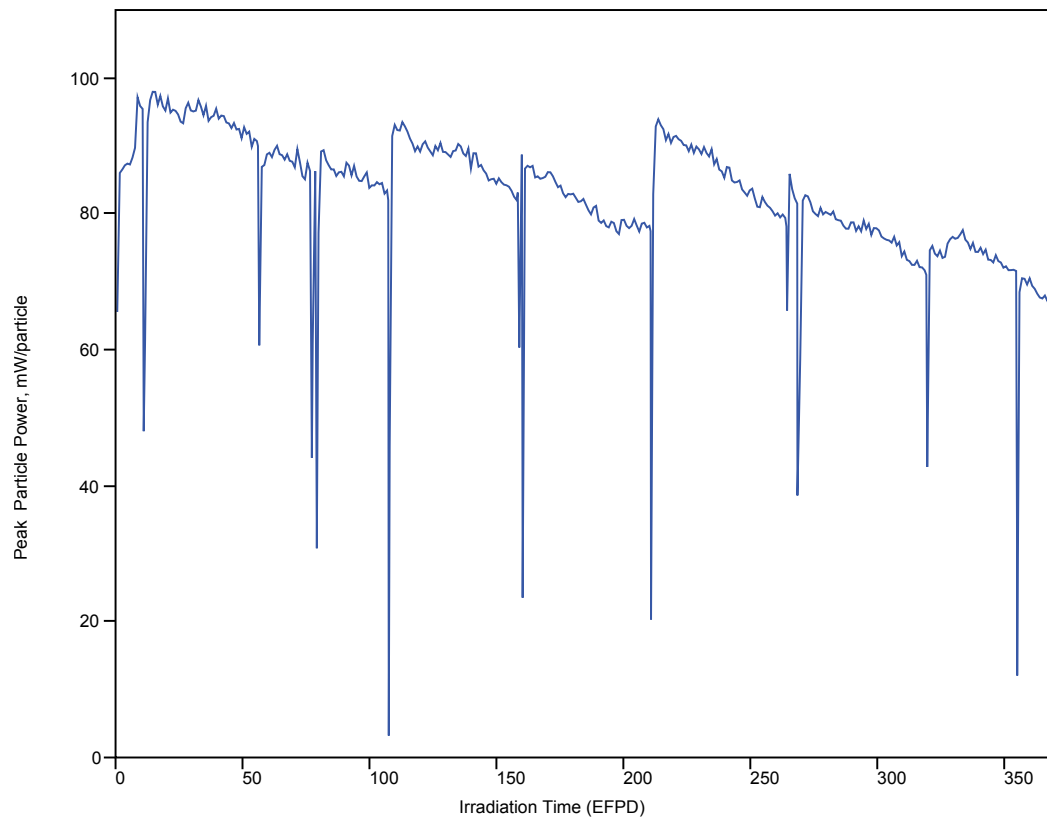


Figure 8. Maximum instantaneous peak particle power versus irradiation time in EFPD for AGR-3/4 compacts.



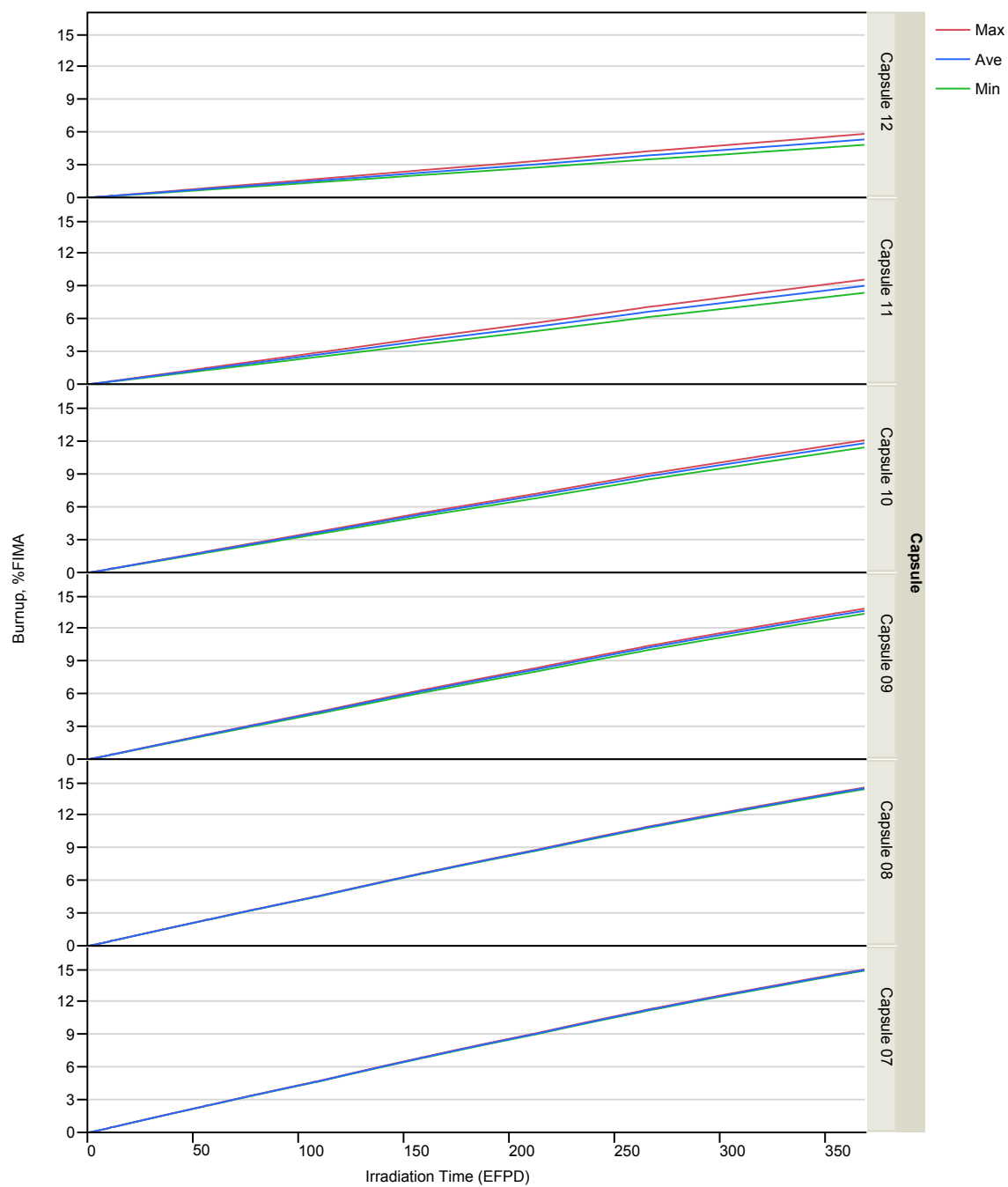


Figure 9. Burnup versus irradiation time in EFPD for Capsules 7-12.

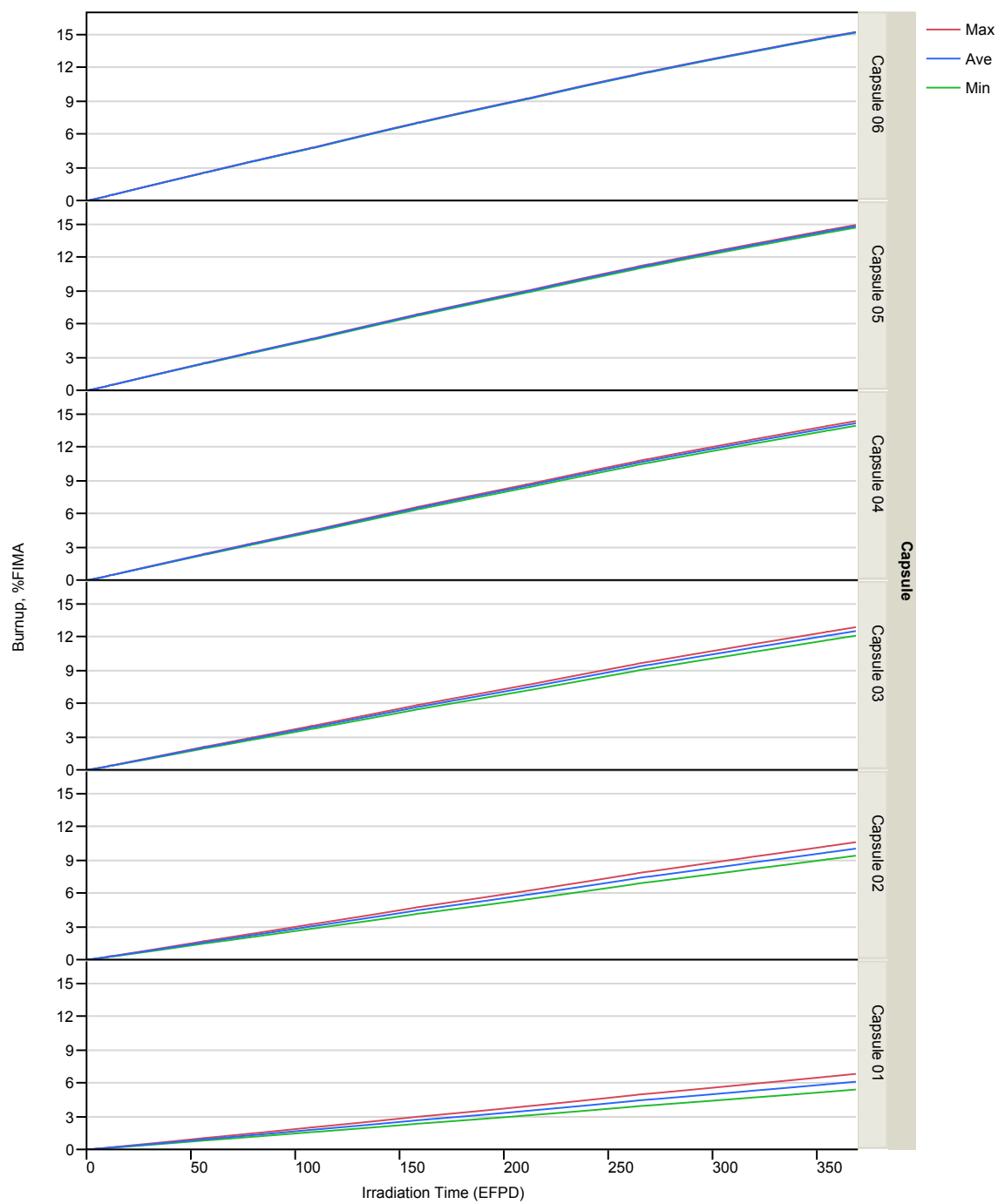


Figure 10. Burnup versus irradiation time in EFPD for Capsules 1-6.

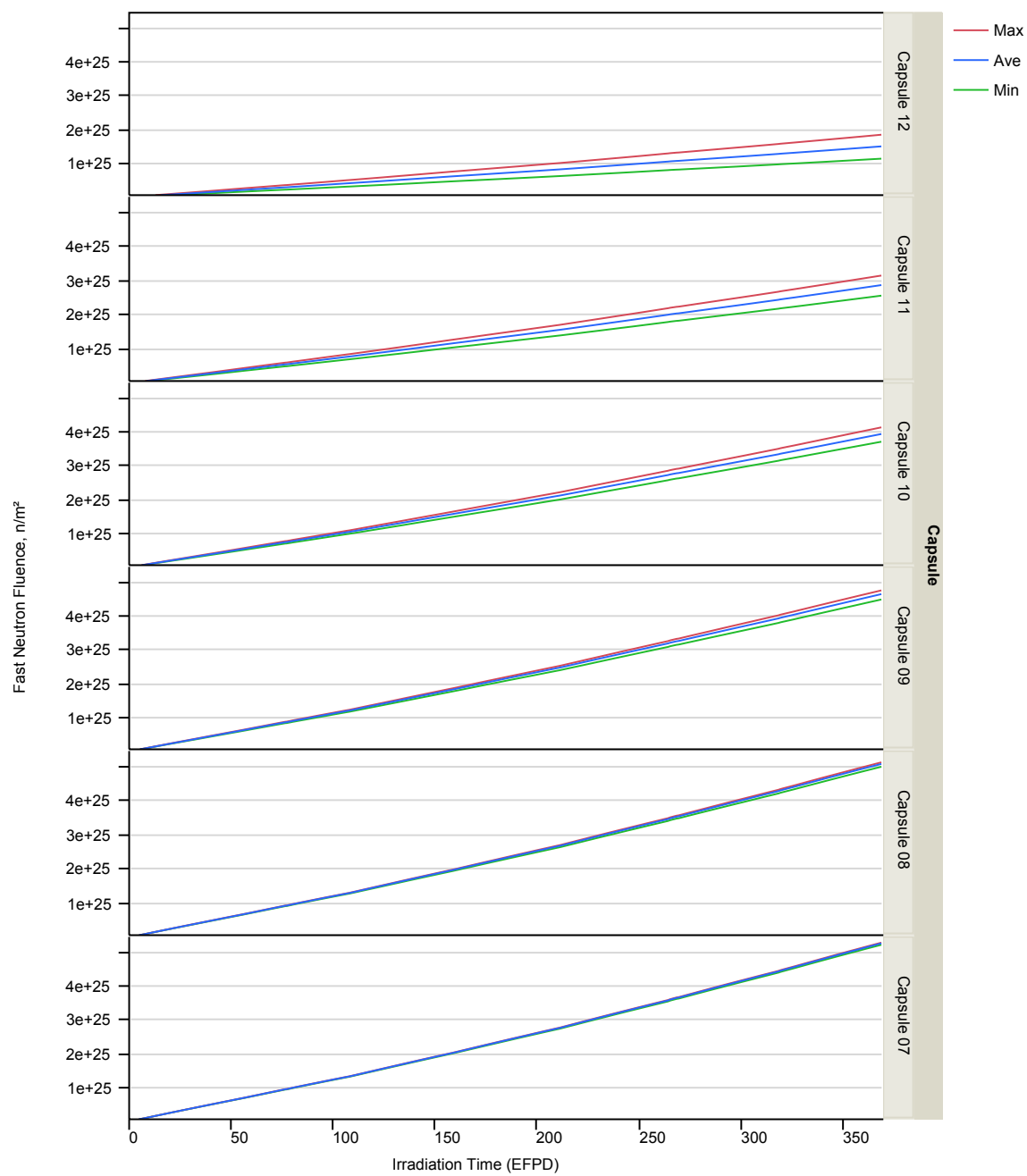


Figure 11. Fast neutron fluence ( $E > 0.18$  MeV) versus irradiation time in EFPD for Capsules 7-12.

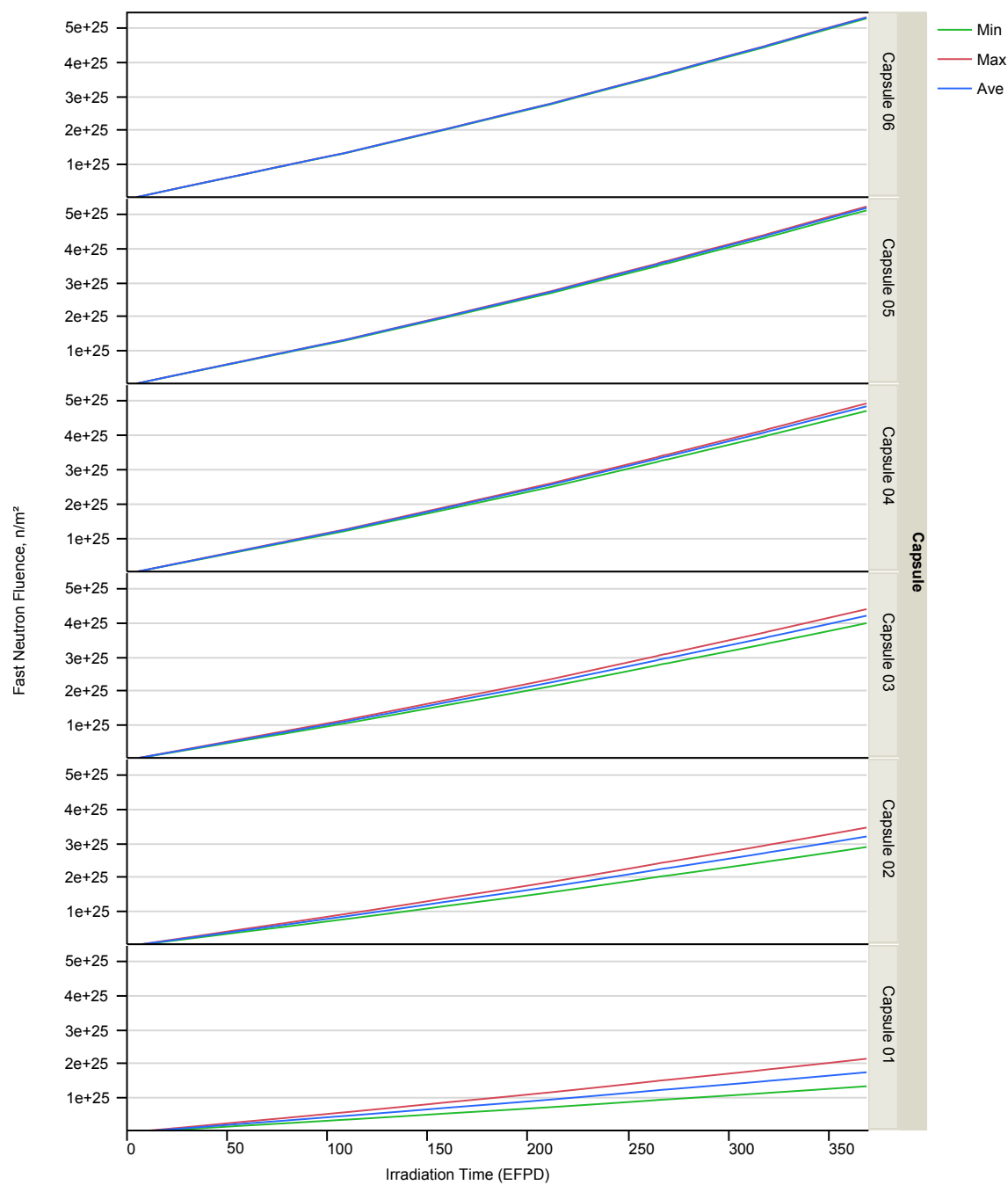


Figure 12. Fast neutron fluence ( $E > 0.18$  MeV) versus irradiation time in EFPD for Capsules 1-6.

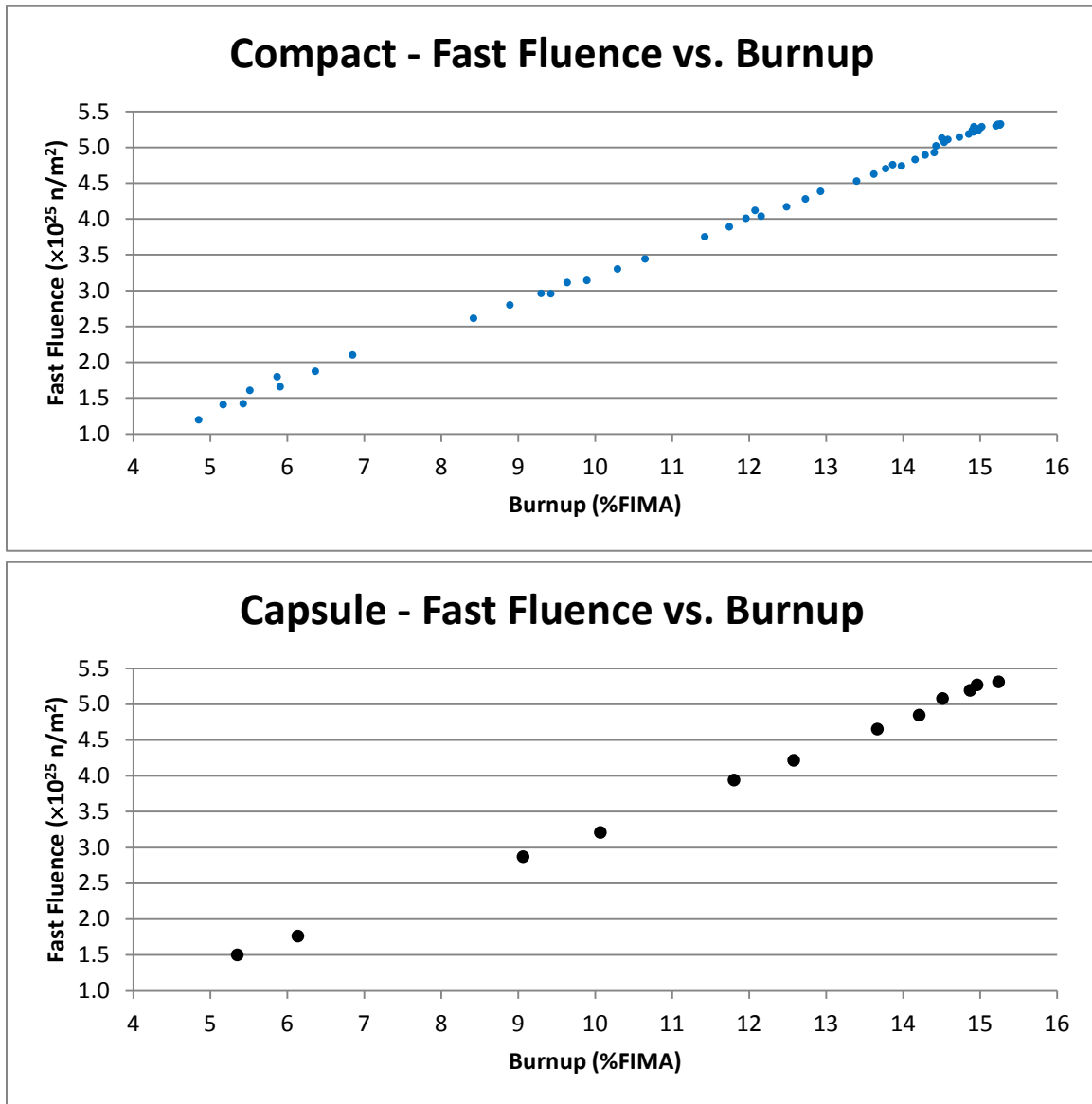


Figure 13. Fast neutron fluence ( $E > 0.18 \text{ MeV}$ ) versus burnup for AGR 3/4 compacts (top) and capsules (bottom).

Table 3 and Table 4 show burnup and fast fluence at the end of irradiation for all the compacts in the test train – capsule averages are also included. From these tables, one can see that burnup on a compact basis ranged from 4.85 to 15.27% FIMA and the compact fast fluence ranged from  $1.19 \times 10^{25}$  to  $5.32 \times 10^{25} \text{ n/m}^2$ . There is some noticeable axial asymmetry in the average compact burnups. One might expect more symmetry considering six capsules were above the ATR core midplane, six capsules were below, and the six corresponding pairs of capsules were equidistant from midplane. The asymmetric burnup is attributed to the hafnium safety rods. The safety rods are above the north, west, east, southwest, south, and southeast flux traps. The rod tips are parked about 8 cm into the top of the active core and depress the thermal neutron and upset the overall axial thermal neutron flux profile in the active core (Sterbentz, 2015).

These data are also summarized in Table 5 with peak, minimum, and capsule average values given for fast fluence and burnup. Appendix B gives burnup and fast fluence at the end of each AGR-3/4 cycle for all compacts.

Table 3. Burnup and fast neutron fluence for Capsules 7-12 at the end of irradiation.

Capsule	Compact	Burnup (% FIMA)	Fast Neutron Fluence ( $10^{25}$ n/m <sup>2</sup> , E > 0.18 MeV)
12	4	4.85	1.19
	3	5.17	1.41
	2	5.52	1.60
	1	5.87	1.80
Capsule 12 Average		5.35	1.50
11	4	8.42	2.61
	3	8.89	2.80
	2	9.30	2.96
	1	9.64	3.11
Capsule 11 Average		9.06	2.87
10	4	11.43	3.75
	3	11.75	3.89
	2	11.96	4.01
	1	12.08	4.12
Capsule 10 Average		11.80	3.94
9	4	13.40	4.53
	3	13.63	4.63
	2	13.78	4.70
	1	13.87	4.76
Capsule 9 Average		13.67	4.65
8	4	14.43	5.02
	3	14.54	5.07
	2	14.58	5.11
	1	14.51	5.13
Capsule 8 Average		14.51	5.08
7	4	14.90	5.24
	3	15.00	5.27
	2	15.02	5.29
	1	14.92	5.28
Capsule 7 Average		14.96	5.27

Table 4. Burnup and fast neutron fluence for Capsules 1-6 at the end of irradiation.

Capsule	Compact	Burnup (% FIMA)	Fast Neutron Fluence ( $10^{25}$ n/m <sup>2</sup> , E > 0.18 MeV)
6	4	15.26	5.31
	3	15.27	5.32
	2	15.23	5.32
	1	15.21	5.30
Capsule 6 Average		15.24	5.31
5	4	14.98	5.23
	3	14.92	5.22
	2	14.86	5.18
	1	14.74	5.14
Capsule 5 Average		14.87	5.19
4	4	14.41	4.92
	3	14.29	4.89
	2	14.16	4.83
	1	13.98	4.74
Capsule 4 Average		14.21	4.85
3	4	12.93	4.38
	3	12.73	4.28
	2	12.49	4.17
	1	12.16	4.04
Capsule 3 Average		12.58	4.22
2	4	10.65	3.44
	3	10.29	3.30
	2	9.90	3.14
	1	9.43	2.95
Capsule 2 Average		10.07	3.21
1	4	6.85	2.10
	3	6.37	1.87
	2	5.91	1.66
	1	5.43	1.42
Capsule 1 Average		6.14	1.76

Table 5. Minimum, average, and peak compact burnup and fast fluence at the end of irradiation.

Capsule	Compact Burnup (% FIMA)			Compact Fast Neutron Fluence ( $10^{25}$ n/m <sup>2</sup> , E > 0.18 MeV)		
	Minimum Compact	Capsule Average	Peak Compact	Minimum Compact	Capsule Average	Peak Compact
12	4.85	5.35	5.87	1.19	1.50	1.80
11	8.42	9.06	9.64	2.61	2.87	3.11
10	11.43	11.80	12.08	3.75	3.94	4.12
9	13.40	13.67	13.87	4.53	4.65	4.76
8	14.43	14.51	14.58	5.02	5.08	5.13
7	14.90	14.96	15.02	5.24	5.27	5.29
6	15.21	15.24	15.27	5.30	5.31	5.32
5	14.74	14.87	14.98	5.14	5.19	5.23
4	13.98	14.21	14.41	4.74	4.85	4.92
3	12.16	12.58	12.93	4.04	4.22	4.38
2	9.43	10.07	10.65	2.95	3.21	3.44
1	5.43	6.14	6.85	1.42	1.76	2.10

The neutronics specifications of irradiation as enumerated in the AGR-3/4 Irradiation Test Specification (Maki, 2011) are listed below with comments on the performance of the experiment with respect to each:

- The minimum fuel compact average burnup shall be >6% FIMA.*

42 of 48 compacts exceeded an average burnup of 6% FIMA. Five compacts had an average burnup between 5 and 6% FIMA, and one compact had a burnup lower than 5% (Compact 12-4 with an average burnup of 4.85%).
- The maximum fuel compact average burnup goal should be <10 % FIMA for two capsules, and should be <19% FIMA for the remaining capsules.*

Three capsules had a maximum fuel compact average burnup < 10% FIMA and the maximum fuel compact average burnup for the entire test train was 15.27% (Compact 6-3).
- The maximum average fast neutron fluence for each fuel compact shall be <  $5.5 \times 10^{25}$  n/m<sup>2</sup>, E > 0.18 MeV.*

The fast neutron fluence reached a maximum average of  $5.32 \times 10^{25}$  n/m<sup>2</sup>, E > 0.18 MeV (Compact 6-3).
- The minimum average fast neutron fluence for each fuel compact shall be >  $1.0 \times 10^{25}$  n/m<sup>2</sup>, E > 0.18 MeV.*



The compact fast neutron fluence had a minimum average of  $1.19 \times 10^{25}$  n/m<sup>2</sup>, E > 0.18 MeV (Compact 12-4).

- *The instantaneous peak power per particle shall be < 400 mW/particle.*

The instantaneous peak power was limited to 100 mW/particle.

## 2.4 Axial Flux Wire Analysis

During the AGR-3/4 irradiation, there were some questions over whether the used ATR driver fuel in the northeast lobe was creating axial asymmetries in the compact heat rates (Sterbentz, 2015).

The issue arose when axial asymmetries were observed between thermocouple measurements and predicted thermocouple temperatures using the AGR-3/4 thermal analysis models. Because the calculated compact heat rates feed directly into the thermal models, the calculated compact heat rates relative to the actual compact heat rates in ATR came into question. The three capsule temperatures near the top of the capsule stack were consistently predicted to be hotter than the thermocouple measurements, and capsules near the middle to bottom were consistently predicted to be colder than the thermocouple measurements, leading to a possible axial asymmetry not accounted for in the physics model.

The primary suspicion centered on the used driver fuel and potential axial asymmetries in driver fuel burnup, in particular the U-235 distribution and axial fission rate profiles, because ATR fuel elements usually burn U-235 fastest around the center region of the element, which is exposed to the highest midplane thermal neutron fluence.

Indeed, the seven ATR cycles that composed the AGR-3/4 test used almost exclusively used fuel elements in the northeast lobe. Used elements populated the northeast lobe intentionally because of their reduced reactivity and the desire to maintain a relatively low lobe power for the AGR-3/4 test. Once-, twice-, and even three-times burned elements could then end up in the northeast lobe positions. It was these elements with their potentially asymmetric axial burnup histories that were of concern, even though ATR used elements typically do not reach this severe burnout even after two or three cycles.

The other possibility that could produce axial asymmetric burnup of ATR driver elements is the influence of fueled or highly absorbing experiments in a flux trap with axial variations. These experiments could possibly enhance or depress the local thermal neutron flux, leading to greater or lesser U-235 driver fuel element burnup. However, these possibilities are substantially mitigated by ATR operational requirements (Tomberlin, 2000).

However, with the possibility in mind that used driver fuel elements were possibly creating axial asymmetries in the compact heats, a method to measure such asymmetries was developed and implemented to address this issue. The method chosen was to instrument the northeast flux trap with full-length flux wires. Four aluminum flux wire holders contained the flux wires and each holder was positioned vertically in the light water coolant between the AGR-3/4 neutron filter and the ATR flux trap aluminum baffle. The holders were equally spaced on a fixed radius from the center of the flux trap at the four cardinal positions. The bottom end of each wire was at the bottom of the active core and extended above the top of the active core. Two flux wires, one nickel and one 0.1%cobalt-aluminum were placed in each aluminum holder. The mounted full-length flux wires were irradiated, activated, removed, chopped, and activities measured.

Although deviations between the thermal model predictions and the thermocouple measurements had been observed from the beginning of the AGR-3/4 irradiation, it was not until the beginning of the fifth AGR-3/4 power cycle (Cycle 154B) that flux wires were actually installed. Flux wires were installed thereafter for the last two cycles (Cycles 155A and 155B).

To compare the thermal and fast flux values from measurements to calculated values, the MCNP models from the JMOCUP depletion calculation were modified by adding the four flux wire holders to

the northeast flux trap (Sterbentz, 2015). Excellent agreement between calculated and measured axial profiles was seen in all four flux wire positions, for both the axial thermal and fast fluxes, as seen in Figure 14 (thermal flux) and Figure 15 (fast flux) for Cycle 154B.

Although the analysis was based primarily on Cycle 154B, the other two AGR-3/4 cycles that included flux wire measurements (Cycles 155A and 155B) both exhibited similar behavior as Cycle 154B. Therefore, one could conclude that the calculated compact heat rates do not appear to be introducing any usual axial asymmetries and, therefore, are probably not the reason for the observed differences between the thermal analysis and the thermocouple readings during the AGR-3/4 cycle irradiations.

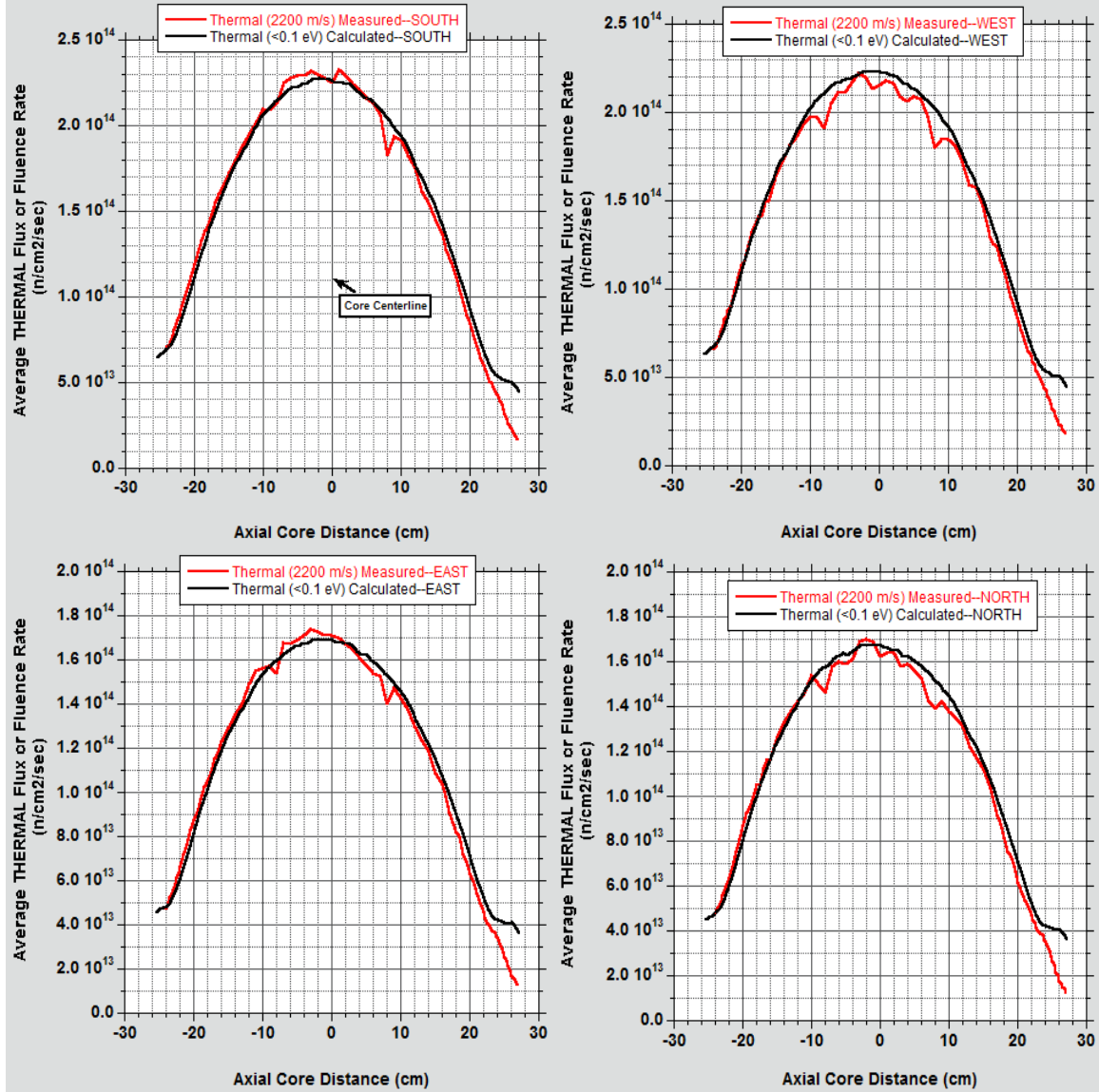


Figure 14. Average thermal fluence rate or thermal flux for the four flux wires (Cycle 154B).

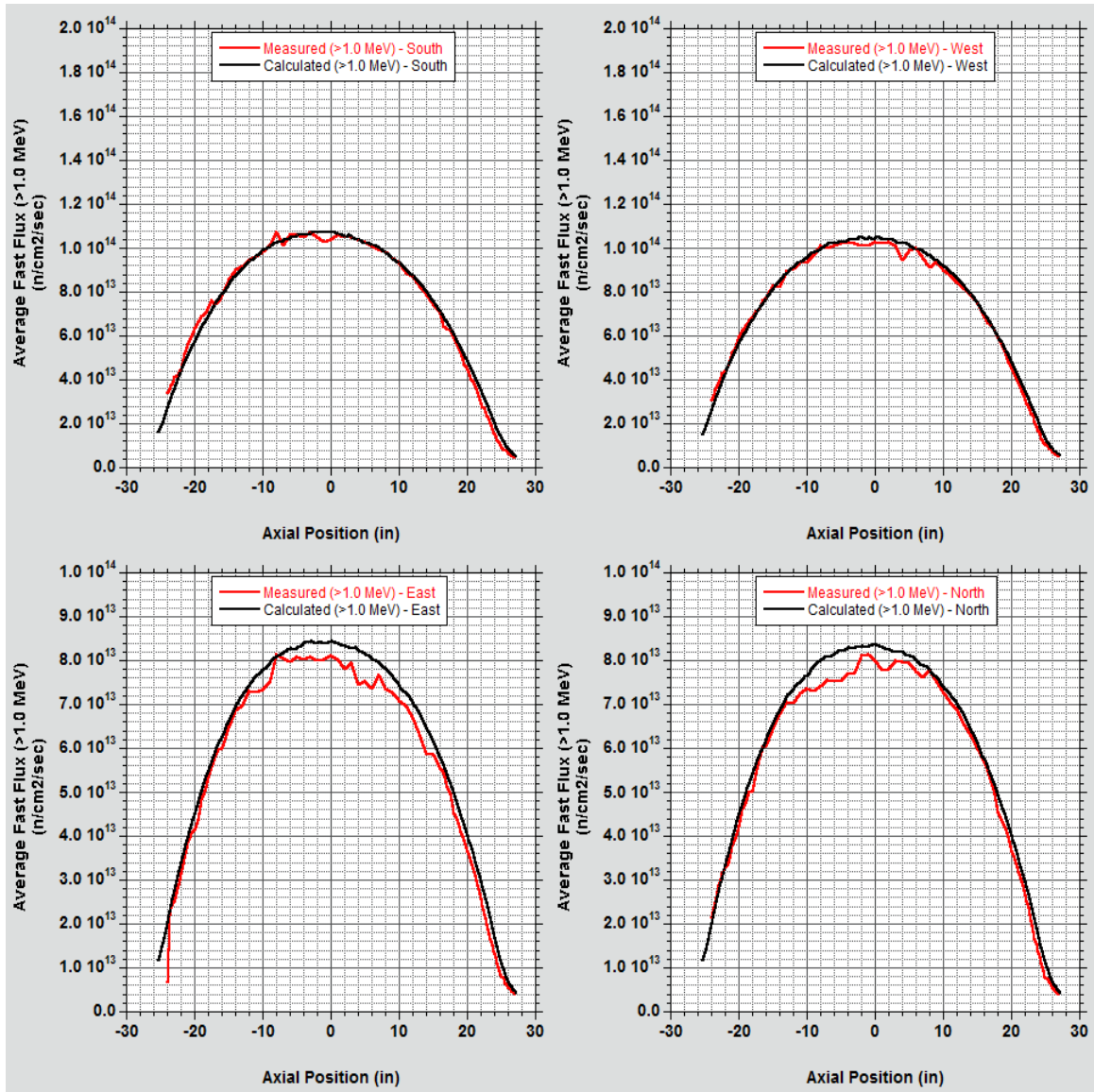


Figure 15. Average fast fluence rate or fast flux for the four flux wires (Cycle 154B).

### **3. THERMAL ANALYSIS**

The AGR-3/4 experiment was designed as a time-at-temperature experiment in which each capsule is thermally controlled in a range of temperatures suitable for the measurement of the diffusion of fission products. To meet the dual objectives of studying fission product release from the fuel and retention in the matrix and/or the graphite, temperature control was performed on fuel for six capsules and on graphite for the other six capsules. Specifically, Capsules 1, 3, 6, 7, 11, and 12 were controlled on peak fuel temperature, while Capsules 2, 4, 5, 8, 9, and 10 were controlled by maintaining their matrix ring or graphite ring mid-points at a constant temperature (Collin, 2015). The goal of the thermal predictions was to adjust the thermocouple set points as the fuel burned during irradiation to determine the proper sweep gas mixture required to maintain constant fuel or graphite temperature. This section describes the methodology and results of the finite element thermal analysis used to provide fuel temperatures and to generate predicted TC temperatures for use in the gas flow control system.

A quantification of the uncertainty on the calculated AGR-3/4 temperatures will be issued at a later date. The aim of this uncertainty analysis is to identify and analyze uncertainties in the thermal calculations from model parameters of potential importance, and to use the results of the numerical simulations in combination with statistical analysis methods to improve qualification of measured data. This is of particular importance for the AGR-3/4 experiment as the temperature simulation data are used for validation of fission product transport models.

#### **3.1 Thermal Calculation Methodology**

Three-dimensional finite element thermal calculations were performed on a daily basis using ABAQUS. The methods used in the thermal analysis summarized here are described in more detail in separate reports (Hawkes, 2015a and Hawkes, 2015b). These calculations were performed using heat generation rates for fuel compact and graphite components provided by the as-run neutronics analysis described in Sections 2.2 and 2.3 and with additional operational input for sweep gas composition versus time. Figure 16 shows a cutaway view of a capsule and the corresponding three-dimensional rendering of the finite element mesh formed from approximately 400,000 eight-noded hexahedral brick elements.

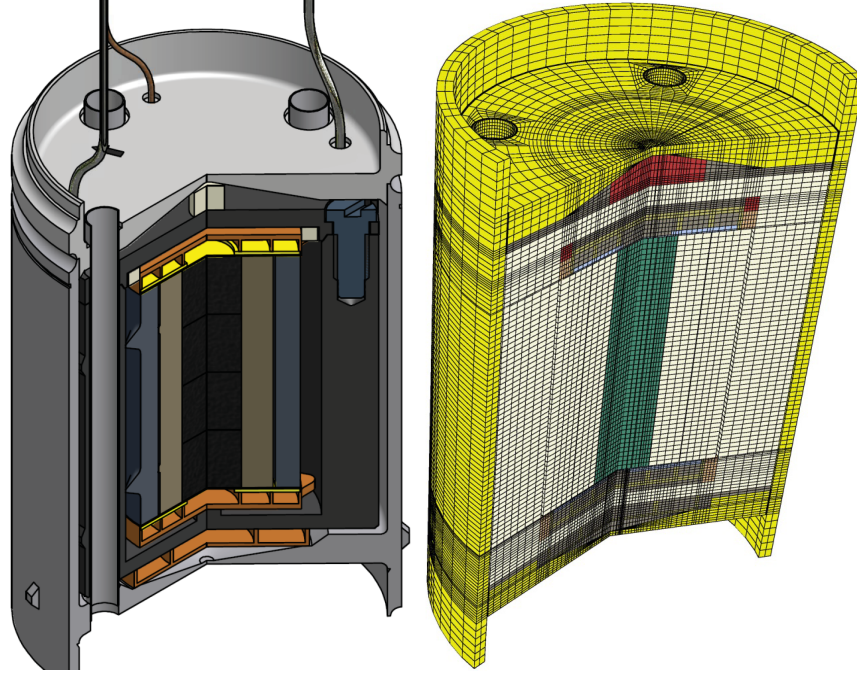


Figure 16. Cutaway view (left) and three-dimensional rendering of ABAQUS finite element mesh (right) of a single AGR 3/4 capsule.

Fuel compact thermal conductivity was obtained by combining compact matrix thermal conductivity and particle thermal conductivity, taking into account the particle volume packing fraction of the TRISO particles in the compacts. Matrix thermal conductivity was taken from correlations presented in (Gontard, 1990), which gives correlations for conductivity taking into account temperature, temperature of heat treatment, and neutron fluence. In this work, the convention used to quantify neutron damage to a material is fast fluence “E > 0.18 MeV”, yet (Gontard, 1990) used the dido nickel equivalent (DNE) unit. The following conversion was used to convert from the DNE convention to the “E > 0.18 MeV” fast neutron fluence:

$$\Gamma_{>0.18\text{MeV}} = 1.52 \times \Gamma_{\text{DNE}} \quad (1)$$

where  $\Gamma$  is neutron fluence in either the “E > 0.18 MeV” unit or DNE. Correlations reported in (Gontard, 1990) were further adjusted to account for differences in fuel compact density. The correlations were developed for a fuel compact matrix density of  $1.75 \text{ g/cm}^3$ , whereas the compact matrix used in AGR-3/4 had a density of approximately  $1.6 \text{ g/cm}^3$ . The thermal conductivities were scaled according to the ratio of densities (0.91) in order to correct for this difference.

The matrix thermal conductivity obtained from (Gontard, 1990) was combined with particle thermal conductivity obtained from (Folsom, 2015) following the approach described in (Gonzo, 2002). In this approach, the matrix thermal conductivity  $k_m$  and the particle thermal conductivity  $k_p$  are combined into an effective thermal conductivity  $k_{\text{eff}}$ :

$$\frac{k_{\text{eff}}}{k_m} = \frac{1 + 2\beta\varphi + (2\beta^3 - 0.1\beta)\varphi^2 + 0.05\varphi^3 e^{4.5\beta}}{1 - \beta\varphi} \quad (2)$$

where  $\beta = \frac{\kappa - 1}{\kappa + 2}$  and  $\kappa = \frac{k_p}{k_m}$ , and  $\varphi$  is the particle volume packing fraction.

Figure 17 shows the resulting three-dimensional plot of the fuel compact thermal conductivity varying with fast neutron fluence and temperature.

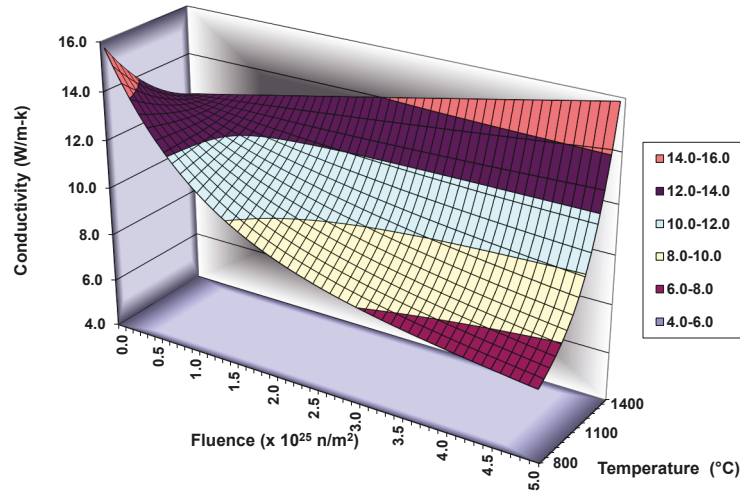


Figure 17. Three-dimensional plot of the AGR-3/4 fuel compact thermal conductivity as a function of fast neutron fluence ( $E > 0.18 \text{ MeV}$ ) and temperature.

The thermal conductivity of the matrix ring was taken from the fuel compact thermal conductivity correlation with a particle volume packing fraction of zero because no pure matrix material conductivity was available. Figure 18 shows the three-dimensional plot of the matrix thermal conductivity varying with fast neutron fluence and temperature.

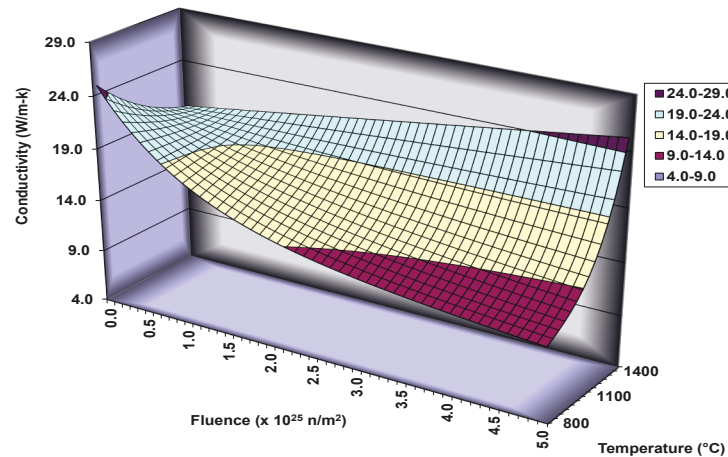


Figure 18. Three-dimensional plot of the AGR-3/4 matrix thermal conductivity as a function of fast neutron fluence ( $E > 0.18 \text{ MeV}$ ) and temperature.



The thermal conductivities of the unirradiated IG-110 and PCEA graphites were derived from measurements of their thermal diffusivities made at INL using their respective densities (Windes, 2013) and graphite specific heat capacity (ASTM, 2008). The effect of irradiation on the thermal conductivity of graphite was accounted for in this analysis using the following correlation by (Snead 1995):

$$\frac{k_{irr}}{k_0} = (0.25 - 0.00017 \times T_{irr}) \times A \times \log(dpa) + 0.000683 \times T_{irr} \quad (3)$$

$$A = -1.0$$

where  $k_0$  and  $k_{irr}$  are the thermal conductivities of unirradiated and irradiated graphite, respectively,  $T_{irr}$  is the irradiation temperature and dpa is displacements per atom. The multiplier used to convert fast fluence ( $E > 0.18$  MeV) to dpa is  $8.23 \times 10^{-26}$  dpa/(n/m<sup>2</sup>) (Sterbentz, 2009). Figure 19 shows a three-dimensional plot of the ratio of the irradiated over unirradiated thermal conductivity varying with temperature and dpa.

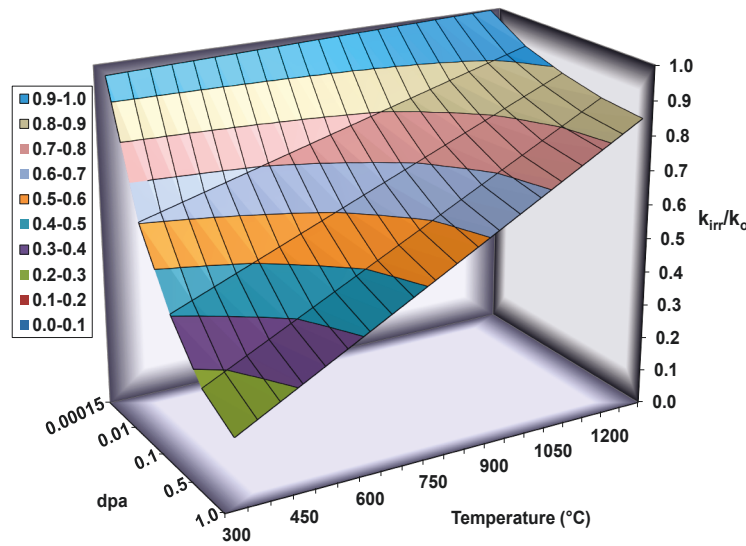


Figure 19. Three-dimensional plot of the ratio of irradiated over unirradiated AGR-3/4 graphite thermal conductivity as a function of temperature and displacements per atom (dpa).

Heat produced in the fuel compacts and graphite components is transferred through the gas gaps surrounding the compacts and components via a gap conductance model using the gap width and the conductivity of the sweep gas. Heat transfer across every gap was considered by both radiation and conduction but not by advection because of the low thermal capacitance of the sweep gas. Indeed, the convective heat transfer from the sweep gas would be less than 0.01% of the heat transfer across the gap because of its low density, low flow rate, and low thermal capacitance. Approximately 80 to 85% of that heat transfer is by conduction and 15 to 20% by radiation, depending on the temperature of the compacts. As a consequence of the low flow rate, the sweep gas is modeled as being stationary. Its thermal conductivity was determined using a set of correlations from Brown University for mixtures of noble gases (Kestin, 1984). Figure 20 shows a three-dimensional plot of the thermal conductivity of the helium/neon sweep gas thermal conductivity, varying with temperature and mole fraction of helium.

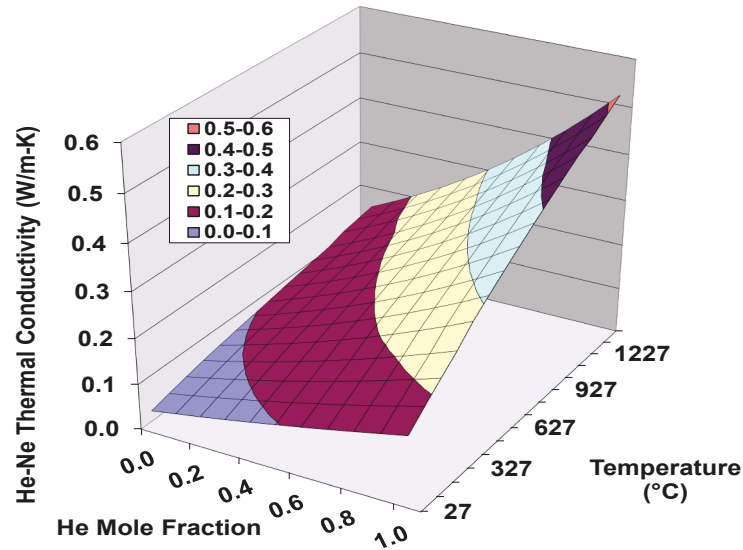


Figure 20. Three-dimensional plot of the AGR-3/4 sweep gas thermal conductivity as a function of temperature and helium mole fraction.

The radiation heat transfer across the gas gaps was implemented using emissivities of 0.9 for all graphite surfaces, 0.4 for stainless steel, and 0.5 for the zirconium-based components.

The daily gas mixtures were taken from NDMAS data. Data in NDMAS provide a separate flow rate for helium and neon for each capsule. Data were taken every 5 minutes and averaged by NDMAS to get a daily average.

Gamma heating rates for the non-fuel structural components were taken from (Sterbentz, 2015) and taken into account in the finite element thermal calculations.

Because of material irradiation-induced shrinkage, all gas gaps were modeled as changing with fast neutron fluence. This was accomplished by having the gas gap conductivity of each capsule change with neutron fluence. The original finite element mesh models in ABAQUS were created with the as-built dimensions for the gas gaps. Experimental data were used for irradiation-induced dimensional changes of the compacts, matrix rings, and graphite rings and sinks (Hawkes, 2015a and Hawkes, 2015b). The model assumed that both the inside and outside radii of the rings shrank inward.

Figure 21 shows a temperature contour plot cutaway view of Capsule 12 calculated by ABAQUS. In this example, the peak fuel compact temperature is 887°C at the center. Outside stainless steel capsule temperatures are near the temperature of the ATR primary coolant water temperature of 50°C. Gamma heating in the stainless steel end cap shows a radial temperature gradient. Several insulating materials were placed in the capsule to prevent heat from transferring in the axial direction and through the stainless steel end caps. The majority of the heat for these capsules is deposited in the fuel compacts about one-third) and the three graphitic ring layers (about two-thirds).



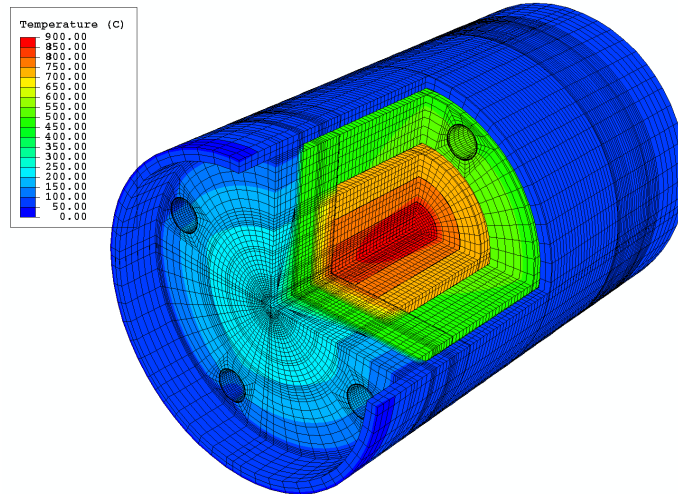


Figure 21. Temperature contour plot cutaway view Capsule 12.

Figure 22 and Figure 23 show the daily calculated fuel temperatures (capsule minimum, capsule maximum, and capsule-average) for each of the 12 capsules of the AGR-3/4 test train versus time in EFPD plotted using NDMAS. Figure 24 and Figure 25 show the corresponding time-average minimum, time-average maximum, and time-average volume-average (TAVA) fuel temperatures versus time for the 12 capsules.

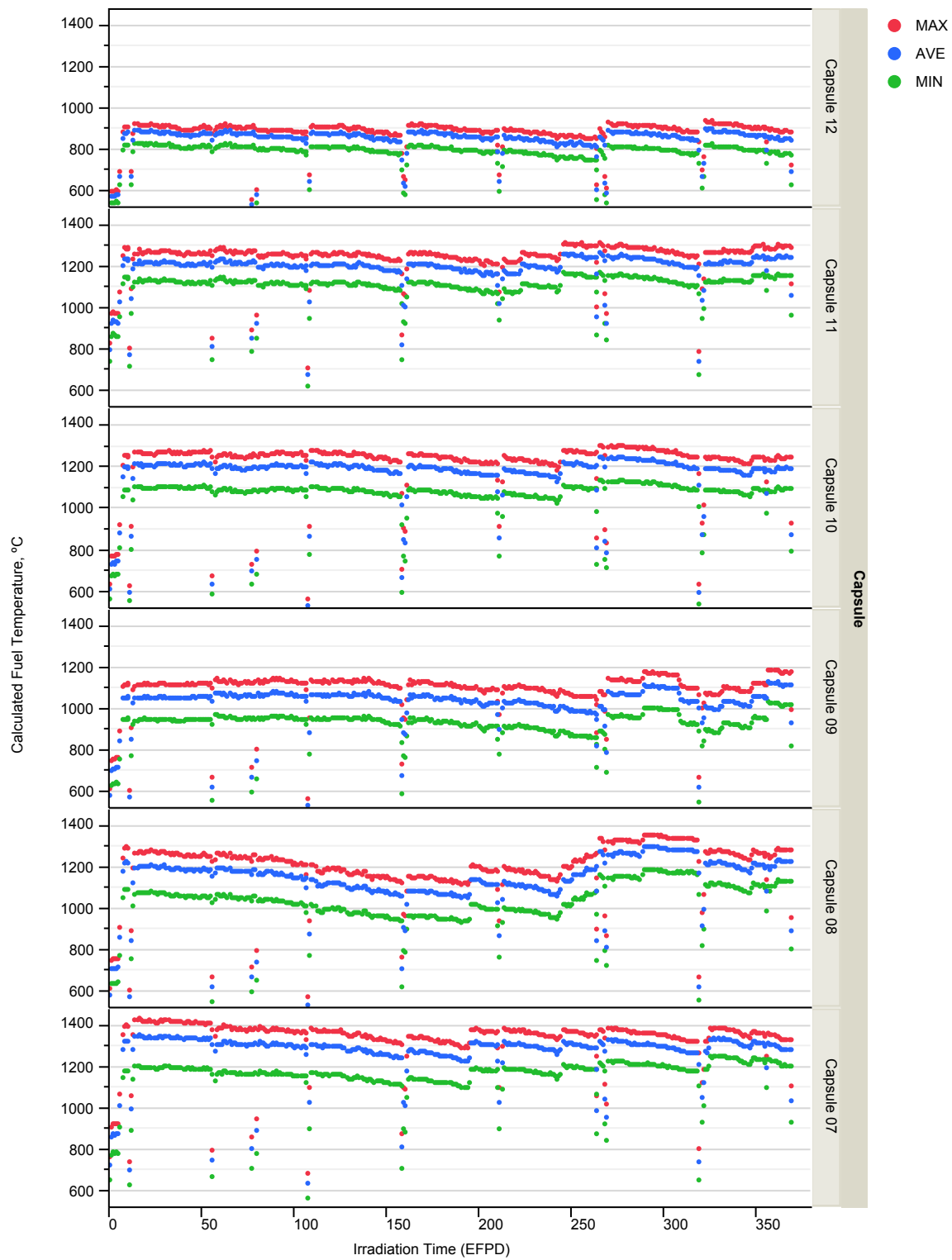


Figure 22. Calculated daily minimum, maximum, and volume-average fuel temperatures for Capsules 7-12.

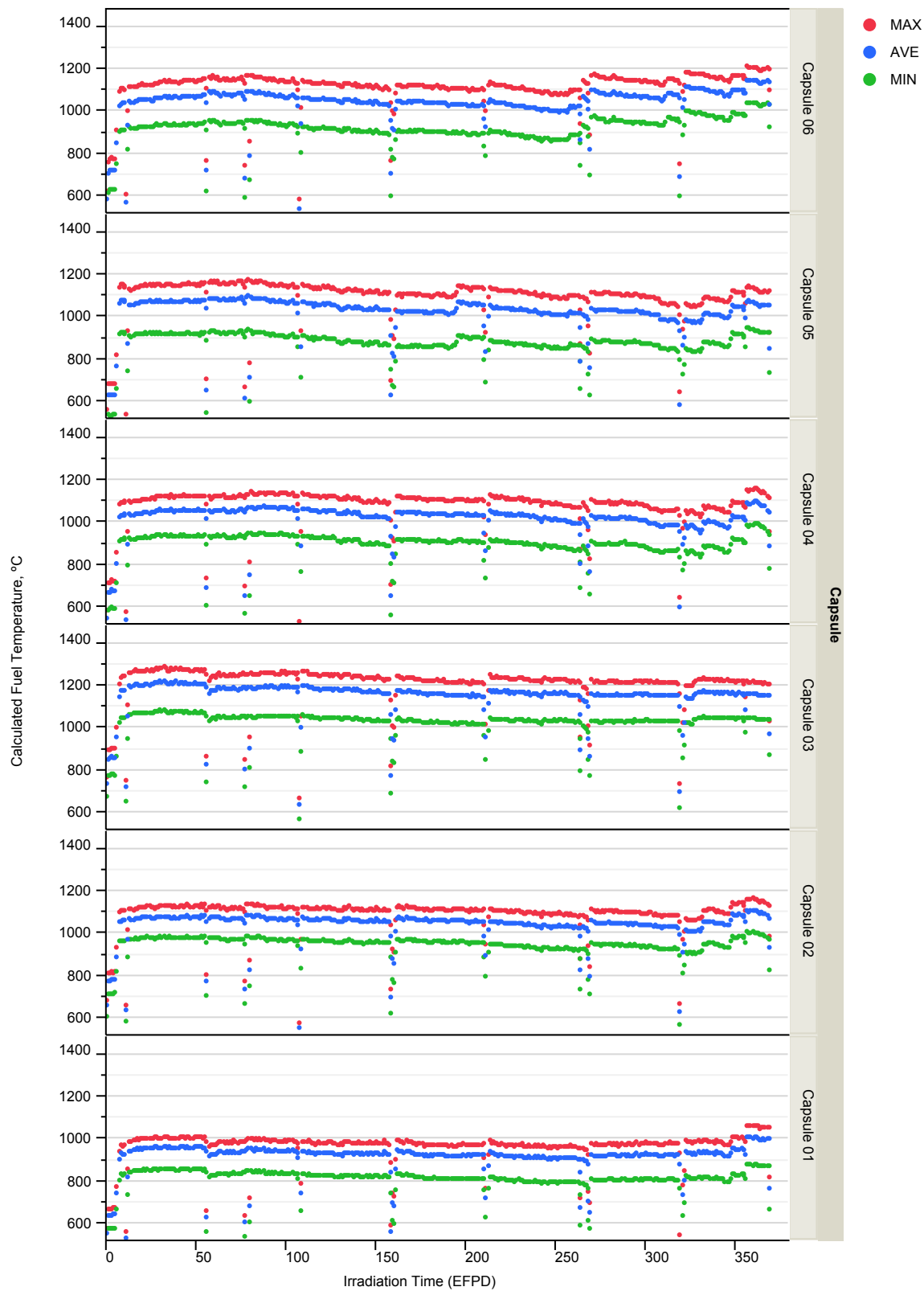


Figure 23. Calculated daily minimum, maximum, and volume-average fuel temperatures for Capsules 1-6.

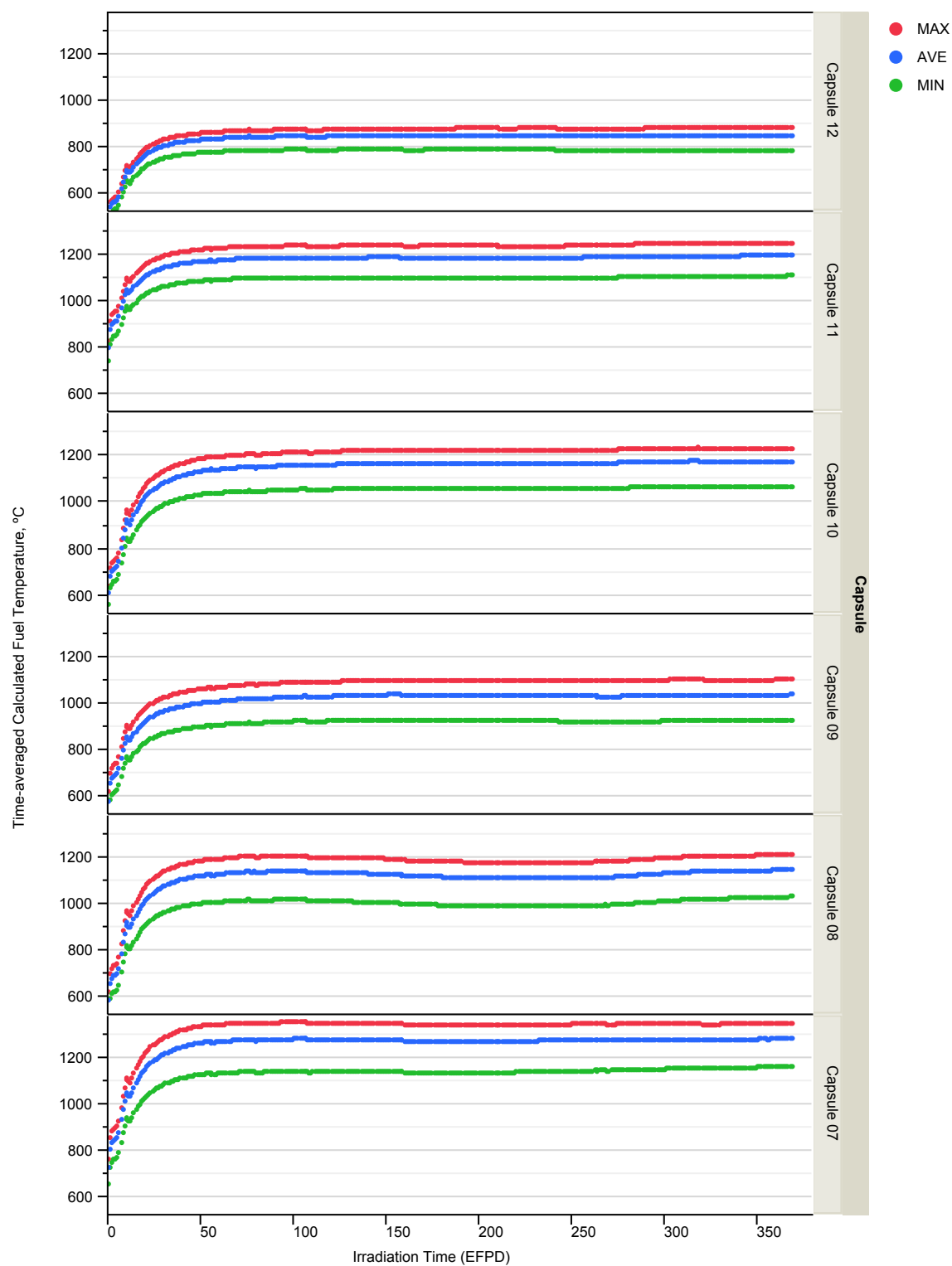


Figure 24. Calculated time-average minimum, time-average maximum, and time-average volume-average fuel temperatures for Capsules 7-12.

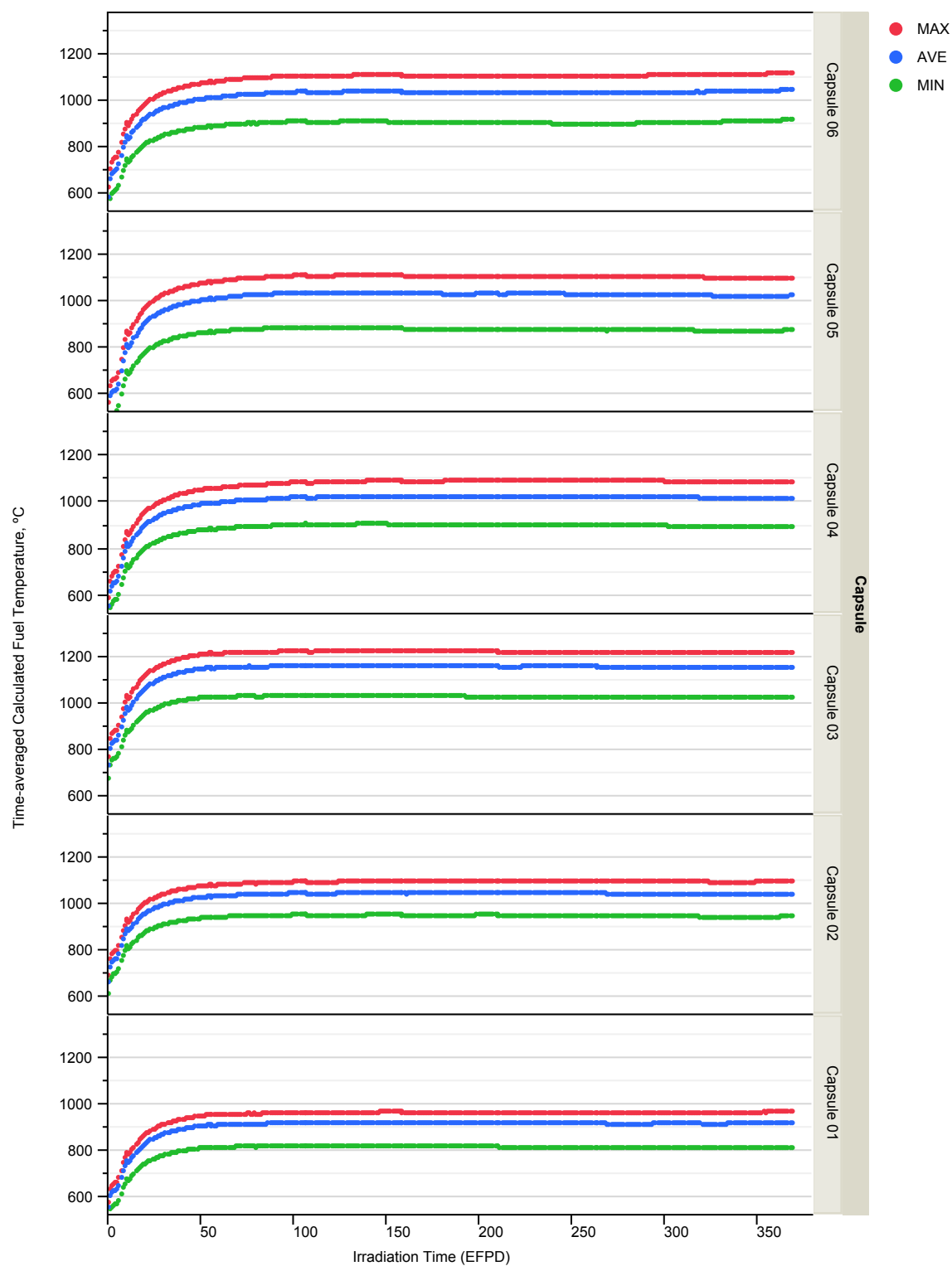


Figure 25. Calculated time-average minimum, time-average maximum, and time-average volume-average fuel temperatures for Capsules 1-6.

Figure 26 shows temperature contour plots for (a) fuel compacts, (b) matrix, (c) graphite ring, and (d) graphite sink. One goal of the AGR-3/4 experiment was to have as uniform temperature as possible in the fuel compacts and graphite rings and, in particular, to minimize axial gradients. In this example, the majority of the compact is between 820 and 870 °C (green to dark orange) as shown in Figure 26a. The very center is hottest, reaching 890°C, with outside edges coolest at 780°C. The calculated temperature distribution is typical of a heat-generating cylinder with heat transfer on all sides.

The matrix ring and graphite ring temperature contours are shown in Figure 26b and Figure 26c, respectively. They show temperature spreads of about 50 and 15°C, respectively. Figure 26d shows the graphite sink temperature contours without the top and bottom lids. The temperature ranges from 475 to 510°C. Hot spots are found on the inside in the four locations where the through tubes prevent heat from evenly transferring to the outside. Coolest temperatures are found on the top outside edges next to the through tube holes.

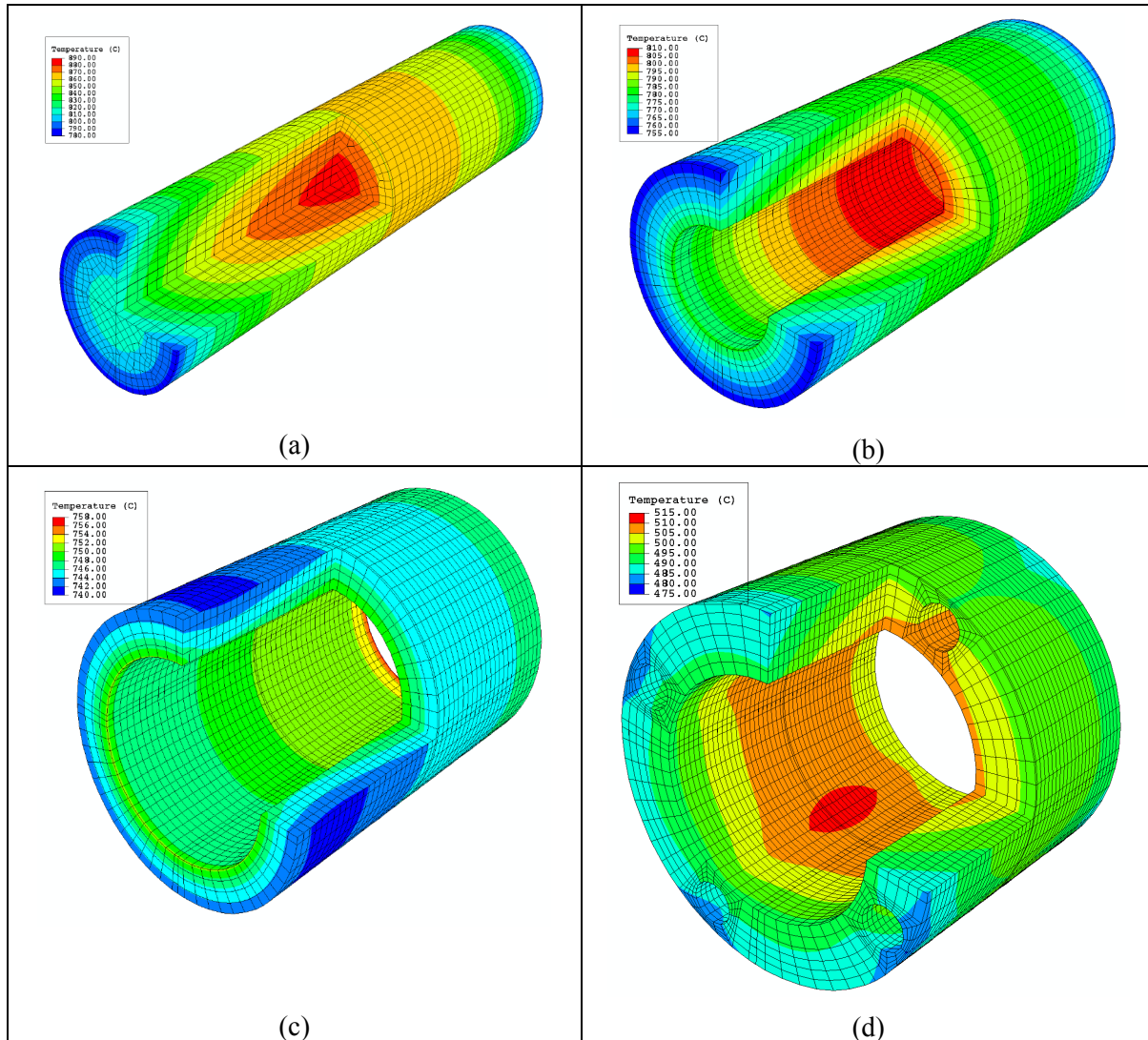


Figure 26. Temperature (°C) contour of compacts (a), matrix (b), graphite ring (c), and graphite sink (d).

Figures C-1 to C-12 in Appendix C show the calculated daily and time-average minimum, maximum, and volume-average temperatures for the matrix rings, graphite rings, and graphite sinks.

### 3.2 As-Run Thermal Analysis Results

Table 6, Table 7, and Figure 27 show the time-average minimum, time-average volume-average, and time-average peak temperatures on a compact basis for all 72 compacts in the AGR-3/4 test. Time-average volume-average fuel temperatures on a capsule basis at the end of irradiation ranged from 845°C in Capsule 12 to 1276°C in Capsule 7. In the AGR-3/4 Irradiation Test Specification (Maki, 2011), two goals of the experiment were specified related to the thermal conditions of the fuel during irradiation. These are listed below with comments on the performance of the experiment with respect to each:

- *The instantaneous peak temperature for each capsule shall be  $\leq 1800^{\circ}\text{C}$ .*

As can be seen in Figure 22 and Figure 23, this constraint was met in all capsules.

- *The time-average peak temperature shall be  $900 \pm 50^{\circ}\text{C}$  for one capsule,  $1100 \pm 50^{\circ}\text{C}$  for up to six capsules,  $1200 \pm 50^{\circ}\text{C}$  for up to four capsules, and  $1300 \pm 50^{\circ}\text{C}$  for one capsule.*

As can be seen in Table 6 and Table 7, this constraint was met. Capsule 12 had a time-average peak temperature of 874°C (within  $900 \pm 50^{\circ}\text{C}$ ), five capsules had time-average peak temperatures between 1088°C ( $>1050^{\circ}\text{C}$ ) and 1110°C ( $<1150^{\circ}\text{C}$ ), four capsules had time-average peak temperatures between 1201°C ( $>1150^{\circ}\text{C}$ ) and 1241°C ( $<1250^{\circ}\text{C}$ ), and Capsule 7 had a time-average peak temperature of 1335°C (within  $1300 \pm 50^{\circ}\text{C}$ ). Capsule 1 had a time-average peak temperature of 959°C, which does not fall into any specified range.

Additionally, the AGR-3/4 Irradiation Test Specification also requires that:

- *The instantaneous peak temperature for the sink material in each capsule shall be  $\leq 650^{\circ}\text{C}$ .*

Figures C-9 and C-10 in Appendix C show that this requirement is met only in Capsules 1, 3, and 12. The instantaneous peak temperature in the graphite sink of Capsules 2, 4, and 5 is below 650°C for the first six AGR-3/4 cycles and above 650°C during Cycle 155B, reaching about 700, 750, and 700°C, respectively. In Capsules 6 and 9, it is below 650°C for the first five AGR-3/4 cycles and above 650°C during Cycles 155A and 155B, reaching approximately 800 and 775°C, respectively. In Capsule 7, the instantaneous peak temperature in the graphite sink becomes greater than 650°C during Cycle 152B (third AGR-3/4 cycle) and remains greater than 650°C throughout the rest of irradiation with a maximum of 850°C. In Capsule 8, the instantaneous peak temperature increases above 650°C towards the end of Cycle 154A (fourth AGR-3/4 cycle) and stays greater thereafter, reaching a maximum of about 800°C. In Capsules 10 and 11, the instantaneous peak temperature is above 650°C during the entire irradiation, around 700 and 750°C during the first five cycles, and around 750 and 800°C during the last two cycles, respectively. Overall, the instantaneous peak temperature was kept below 800°C in all capsules that did not meet the requirement of 650°C, except Capsule 7 whose instantaneous peak temperature in the graphite sink reached around 850°C during the last AGR-3/4 cycle.

Figure 28 displays three-dimensional scatter plots of the irradiation characteristics of the AGR-3/4 compacts (black dots), along with their two-dimensional projections on the “Burnup – Fast Fluence” (blue dots), “Burnup – TAVA Temperature” (green dots), and “Fast Fluence – TAVA Temperature” (red dots) plans. Figure 29 and Figure 30 show the distribution of burnup and TAVA temperature and the distribution of fast fluence and TAVA temperature for the AGR-3/4 compacts. The plots show that AGR-3/4 covers a broad range of burnup, fast fluence, and irradiation temperatures in an effort to bound expected reactor irradiation characteristics.

Table 6. Compact temperature data for Capsules 7-12 at end of irradiation.

Capsule	Compact	Time-Average Minimum Temperature (°C)	Time-Average Volume-Average Temperature (°C)	Time-Average Peak Temperature (°C)
12	4	781	823	856
	3	836	855	875
	2	849	863	879
	1	792	840	874
All Capsule 12 compacts		781	845	879
11	4	1108	1168	1219
	3	1181	1212	1245
	2	1190	1218	1246
	1	1104	1173	1231
All Capsule 11 compacts		1104	1193	1246
10	4	1062	1147	1208
	3	1152	1187	1224
	2	1157	1190	1225
	1	1063	1151	1215
All Capsule 10 compacts		1062	1169	1225
9	4	930	1014	1083
	3	1010	1052	1098
	2	1012	1054	1099
	1	922	1012	1086
All Capsule 9 compacts		922	1033	1099
8	4	1030	1124	1195
	3	1121	1162	1207
	2	1121	1162	1207
	1	1026	1120	1194
All Capsule 8 compacts		1026	1142	1207
7	4	1165	1257	1327
	3	1259	1299	1341
	2	1257	1298	1341
	1	1157	1251	1325
All Capsule 7 compacts		1157	1276	1341



Table 7. Compact temperature data for Capsules 1-6 at end of irradiation.

Capsule	Compact	Time-Average Minimum Temperature (°C)	Time-Average Volume-Average Temperature (°C)	Time-Average Peak Temperature (°C)
6	4	935	1028	1103
	3	1019	1064	1114
	2	1014	1062	1114
	1	912	1012	1096
All Capsule 6 compacts		912	1041	1114
5	4	886	999	1083
	3	1000	1046	1095
	2	995	1043	1095
	1	868	984	1075
All Capsule 5 compacts		868	1018	1095
4	4	938	1026	1097
	3	1019	1061	1107
	2	1009	1055	1106
	1	908	1002	1083
All Capsule 4 compacts		908	1036	1107
3	4	1052	1142	1206
	3	1142	1176	1213
	2	1127	1167	1210
	1	1023	1115	1187
All Capsule 3 compacts		1023	1150	1213
2	4	981	1042	1090
	3	1035	1061	1092
	2	1015	1049	1087
	1	940	1004	1061
All Capsule 2 compacts		940	1039	1092
1	4	853	915	958
	3	929	946	964
	2	899	929	958
	1	807	869	919
All Capsule 1 compacts		807	915	964

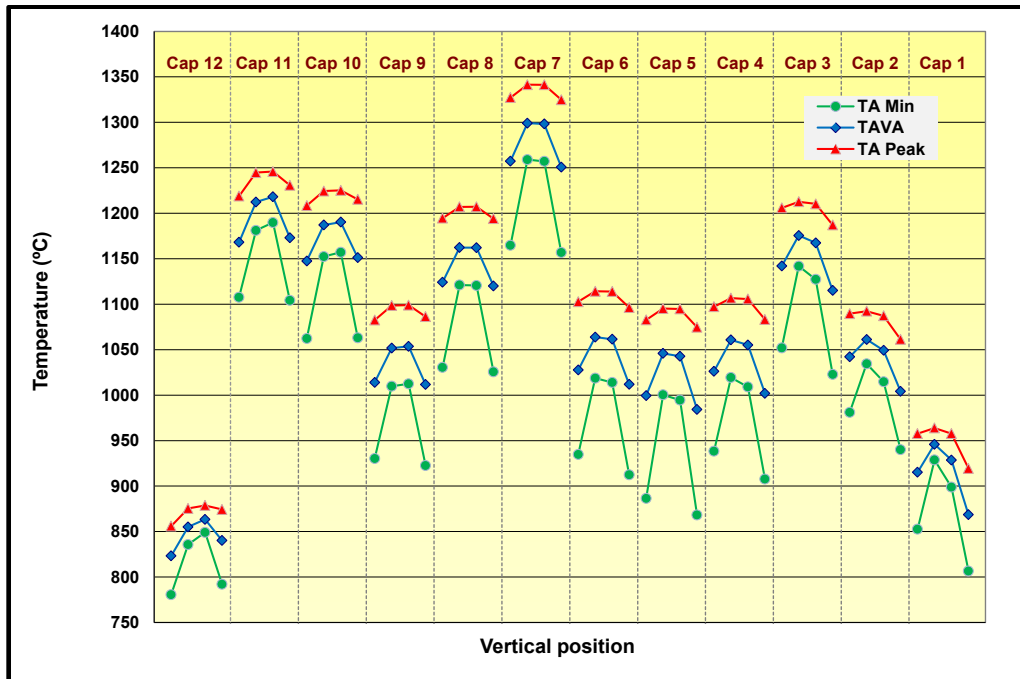


Figure 27. Time-average minimum (TA Min), time-average volume-average (TAVA), and time-average peak (TA Peak) temperatures of AGR-3/4 compacts.

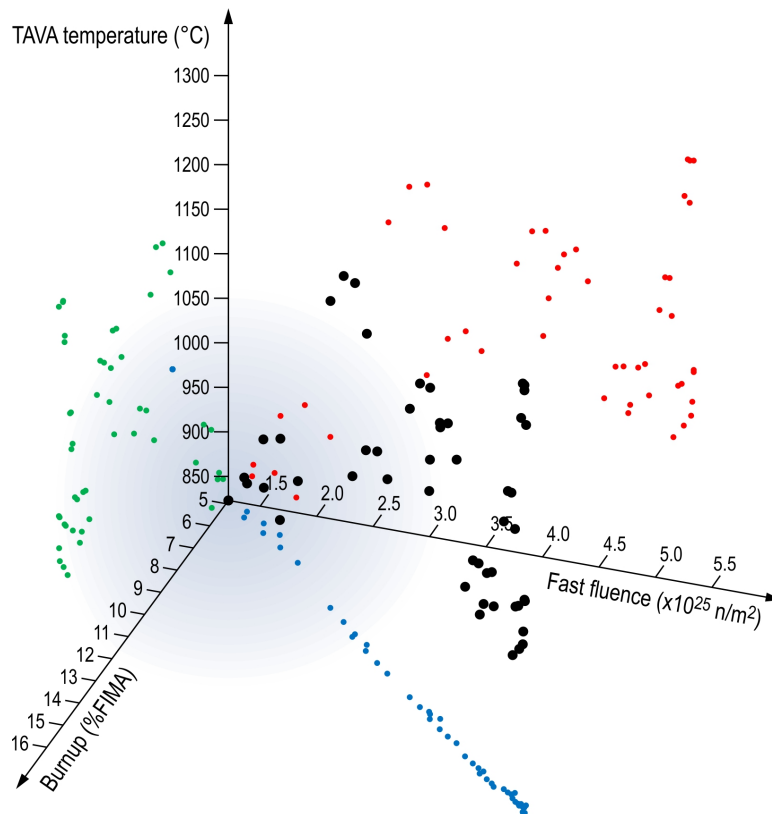


Figure 28. Three-dimensional scatter plots of the irradiation characteristics of the AGR 3/4 compacts, with projections on two-dimensional plans in blue (burnup vs. fast fluence), green (burnup vs. TAVA temperature), and red (fast fluence vs. TAVA temperature).

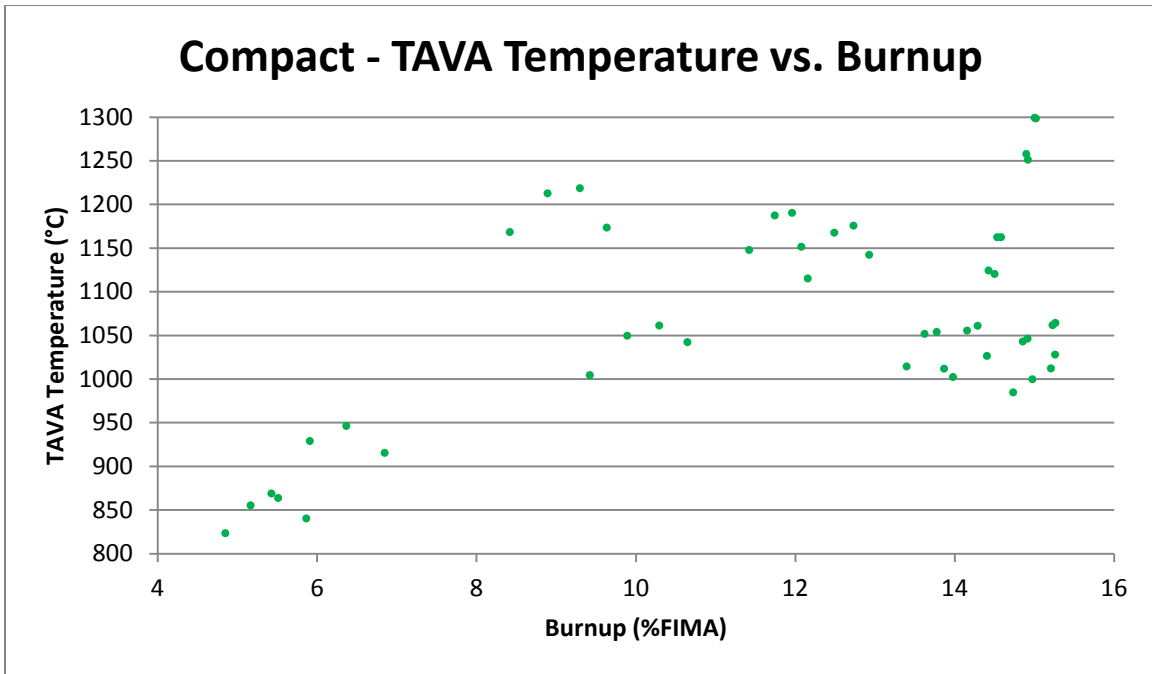


Figure 29. Time-average volume-average temperature (°C) versus burnup for AGR 3/4 compacts.

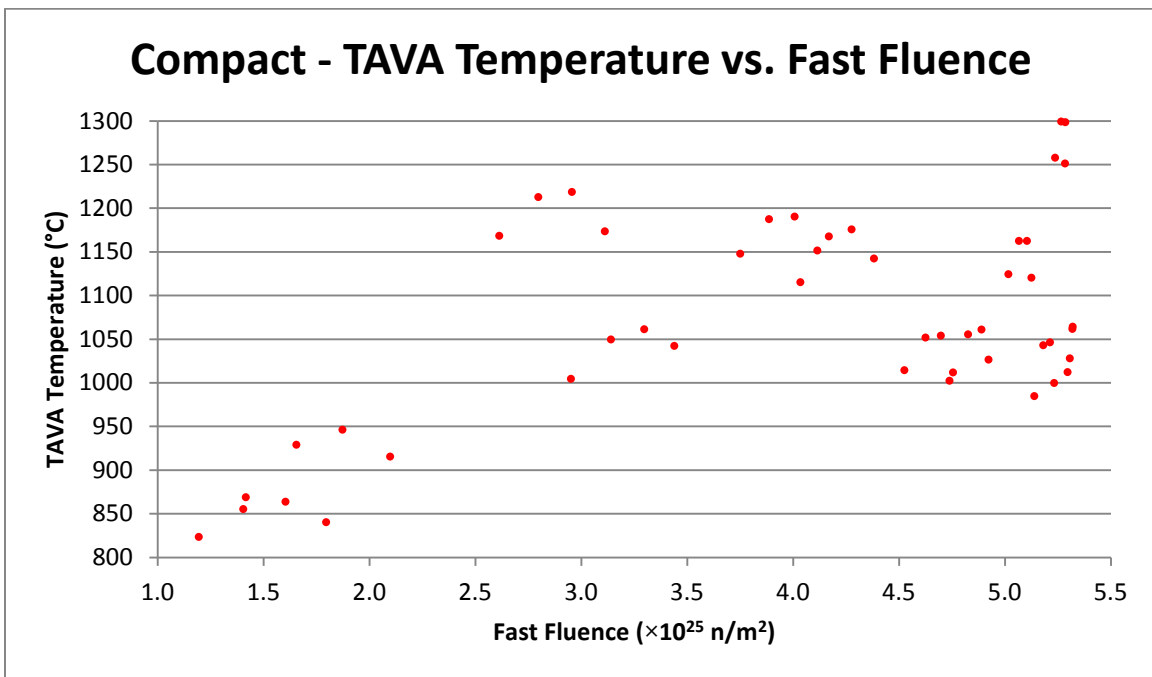


Figure 30. Time-average volume-average temperature (°C) versus fast neutron fluence ( $E > 0.18 \text{ MeV}$ ) for AGR 3/4 compacts.

## 4. FISSION PRODUCT GAS RELEASE ANALYSIS

The performance of a nuclear fuel test is typically evaluated using the release-to-birth ratio, which is the ratio of the released activity of an isotope from the fuel to the predicted creation rate of the isotope during irradiation. Fission product birth rates for the following isotopes were provided by as-run physics calculation: Kr-85m, Kr-87, Kr-88, Kr-89, Kr-90, Xe-131m, Xe-133, Xe-135, Xe-135m, Xe-137, Xe-138, and Xe-139. These nuclides were selected because they are chemically inert fission product gases with relatively short half-lives, allowing each isotope to reach equilibrium concentration in the fuel during each cycle. The FPMS described in Section 1.2 was used to quantify release rates during irradiation giving the R/B values for the radionuclides of interest. In the case of the AGR-3/4 experiment, the detection of fission gas release also served to monitor the failure count of the DTF particles.

As mentioned in Section 1, impurities were added to the sweep gas and injected in Capsule 11 during the last three cycles of AGR-3/4 to assess their effects on fuel performance and fission product transport. Injection of these impurities (50 ppmv CO, 10 ppmv H<sub>2</sub>O, and 50 ppmv H<sub>2</sub>) proceeded at 0.5 sccm into the main gas stream of 29.5 sccm blended helium/neon gas mixture. Injection was carried out briefly to establish design functionality starting near the beginning of Cycle 154B on August 26, 2013 and ending on September 5, 2013. The injection resumed in earnest, officially starting on September 9, 2013. During Cycle 154B, no effects of the impure gas injection were recognized in the routine monitoring of the release activities, signaling no appreciable impact of the impurities on intact and DTF fuel performance and subsequent fission product transport.

However, very small quantities of iodine isotope I-131 were identified during Cycle 155A outage in spectra from Capsule 11, several days after the end of Cycle 154B. It is suggested that the impurities helped to mobilize some of the I-131 capsule inventory (Scates, 2015). To verify this assumption, the injection of impurities during Cycle 155B was halted on February 21, 2014 and re-started on March 28, 2014. The FMPS observed a decrease in I-131 activity at the beginning of an unplanned reactor scram on March 21, 2014, but the activity rose after the re-start of the reactor on March 28, 2014. The measured inventory at the end of Cycle 155B on April 12, 2014 indicates that iodine had again been mobilized by the injected impurities.

I-131 was also detected in both FPM 7 and 8 after the first irradiation cycle. Because no impurities were injected into these capsules, it is suspected that some moisture was initially present in the graphite of these two capsules and off-gassed during the first few irradiation cycles providing mobility to the iodine inventory (Scates, 2015).

### 4.1 Birth Rate Calculations Methodology

The birth rates of noble gas fission products of interest were calculated using ORIGEN2 version 2.2 (Croff, 1983). These calculations used compact flux and reactions rates from MCNP (LANL, 2004). The ORIGEN2 libraries used in the calculation were modified to remove the isotope depletion methods (transmutation and decay) for the isotopes of interest for birth rates. The increase in the concentration of the isotope during the irradiation time interval divided by the irradiation time interval was determined to be the isotope birth rate of the isotope during the time interval. This was performed by two separate physics calculations with different time resolutions. One calculation used a four-point subdivision of each ATR cycle – once at the beginning of each cycle, once at the end, and two times during each cycle. The second high resolution calculation estimated birth rates on a daily basis. The data provided by the four-point interpolation method supplied the experiment team with information pertaining to fuel integrity during the multiyear irradiation. At conclusion of the AGR-3/4 experiment, the high-resolution daily depletion calculations were performed to provide daily compact and component heat rates for high resolution thermal analyses. The daily physics analysis also increased the number of tracked fission product isotopes in the TRISO particle compacts in order to assist in post-irradiation examination measurements and to better characterize the irradiated compacts.

## 4.2 Release Rate Calculations Methodology

As mentioned in Section 1, spectrometer detector systems measure the concentrations of various krypton and xenon isotopes in the sweep gas from each capsule. Eight-hour counting intervals were used to measure the concentrations of Kr-85m, Kr-87, Kr-88, Kr-89, Kr-90, Xe-131m, Xe-133, Xe-135, Xe-135m, Xe-137, Xe-138, and Xe-139.

The radionuclides of interest decay in transit from the capsule to the counters. Given a certain measured activity,  $A$  ( $\mu\text{Ci}$ ), the radionuclide release rate,  $R$  (at/s), of a particular nuclide can be calculated as (Scates 2015):

$$R = 3.7 \times 10^4 \frac{A e^{\lambda V_T/f}}{(1 - e^{-\lambda V_S/f})} \quad (5)$$

where  $V_S$  is the sample volume (mL),  $\lambda$  is the nuclide decay constant ( $\text{s}^{-1}$ ),  $f$  is the capsule volumetric flow rate (mL/s), and  $V_T$  is the transport volume from the capsule to the sample volume (mL). The transport volumes were determined during a lead-out flow experiment performed at the beginning of the AGR-3/4 irradiation (Scates, 2015). The method used to determine the transport volumes is similar to the one used for AGR-1, and it is described in (Hartwell, 2007). The ratio of the experimentally determined release rates to the calculated birth rates is then computed. The report (Scates, 2015) contains information about the software and hardware used to take and process these release rate measurements along with detailed R/B results, which are summarized in the following section.

## 4.3 Release Rate to Birth Rate Ratio Results

Figure 31 and Figure 32 shows R/B values versus time for Kr-85m, Kr-88 and Xe-138 plotted using NDMAS. The R/B values for this figure were computed using the high-resolution daily depletion method. These nuclides were selected for plotting because they have relatively short half-lives allowing them to come into equilibrium in each cycle. These are daily-average values filtered, such that data with uncertainty higher than 50% and sometimes data from short acquisition intervals (e.g., 20-minute intervals for neon testing at the beginning of each cycles) are removed.

Fission product R/B values reached values in the  $10^{-4}$ - $10^{-3}$  range early during irradiation as DTF particles started to fail during the first AGR-3/4 cycle. The hotter Capsule 7 reached the higher R/B value of around  $3 \times 10^{-3}$ .

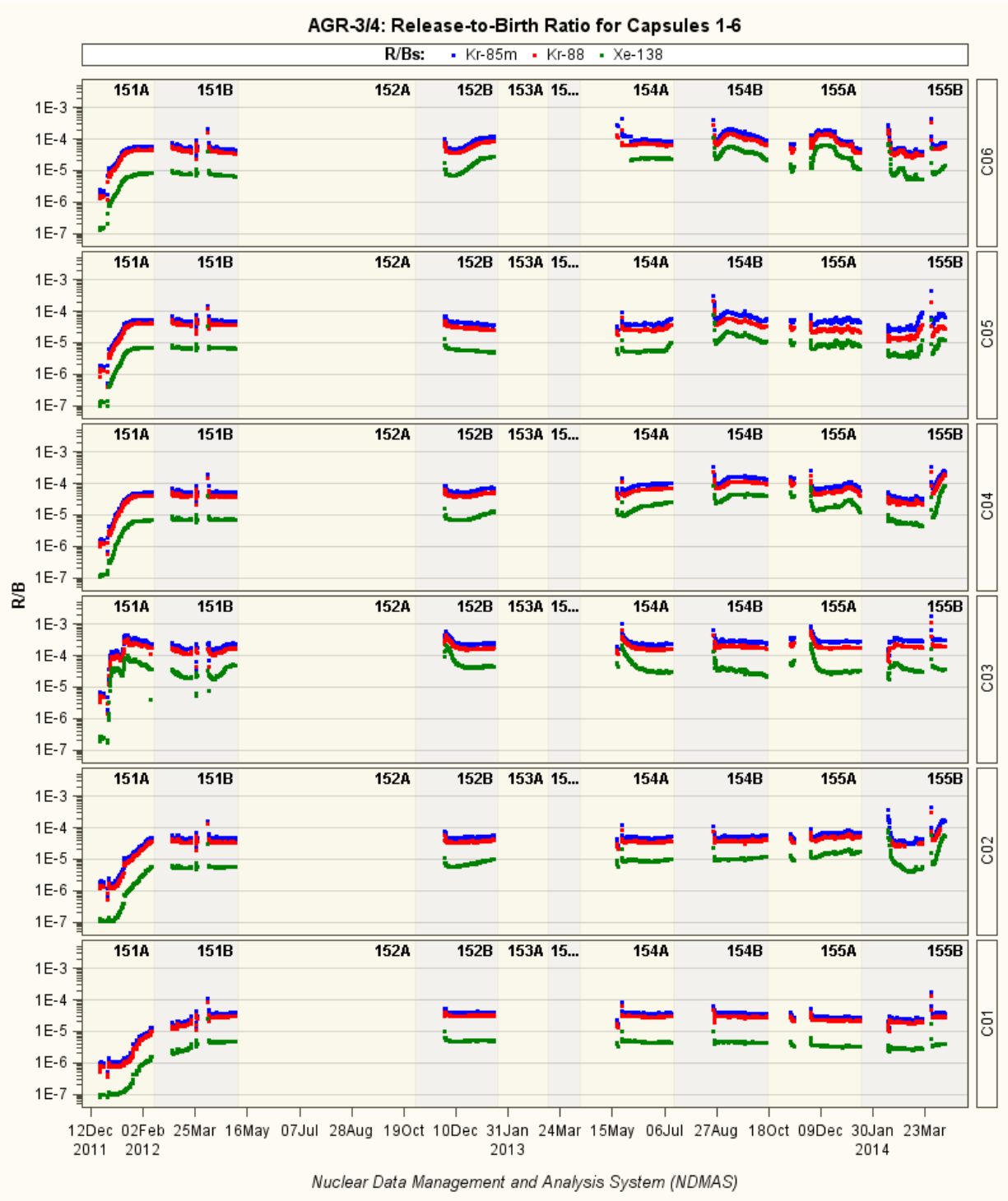


Figure 31. R/B values from daily birth rates for Kr 85m, Kr 88, and Xe 138 for Capsules 1-6.

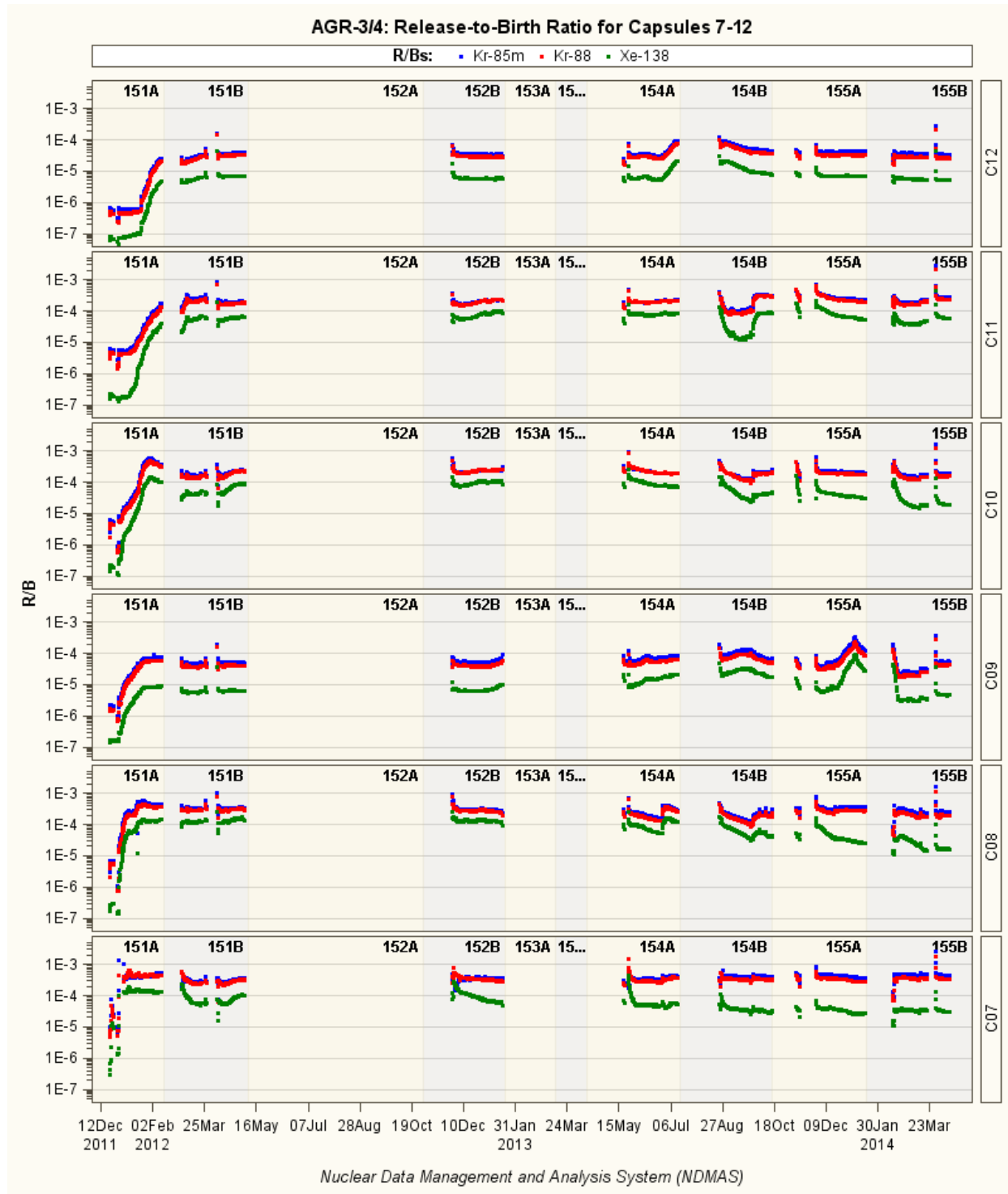


Figure 32. R/B values from daily birth rates for Kr 85m, Kr 88, and Xe 138 for Capsules 7-12.

## 4.4 Fuel Failure Particle Count

The in-pile failures of embedded DTF particles in each capsule are detected using the independent capsule-specific NaI(Tl) total radiation detector. Even though the gross gamma detector is sensitive to each fuel particle failure (up to 250 failures), visually counting the exact number of failed particles during the whole AGR-3/4 irradiation was a challenging task. This is because of multiple DTF fuel particles failing with little time separation, because of partial failures, and because of high background activity caused by release from already failed particles. Challenges in the failure detection process could lead to high uncertainty of particle failure counts in some capsules. Therefore, each inspection period provides three estimates of failure counts: (1) best-estimate (BE), (2) maximum, and (3) minimum (Scates, 2015). These values are summarized in Table 8 for each capsule. For Capsule 1, the three failure estimates are quite different from each other, indicating high counting uncertainty. By contrast, for Capsule 9, the three failure estimates are very similar, indicating low counting uncertainty or high confidence in the number of particle failures.

NDMAS received 732 records of weekly particle failure counts for 12 capsules throughout the AGR-3/4 irradiation (Pham, 2015). Each record contains the best-estimate, maximum, and minimum counts. Figure 33 plots the weekly cumulative best-estimated failure counts as a function of EFPDs for each of the 12 AGR-3/4 capsules. For most capsules, the fuel failures occurred during the first irradiation cycle (within the first 55 EFPDs). For a few of the capsules (e.g., Capsules 2 and 3), fuel failures occurred throughout irradiation. Based on best-estimate values, the final particle failure count ranges from 49 (Capsule 12) to 120% (Capsule 3) of the initial 80 DTF particles in each capsule. In particular, Capsules 2, 3, and 9 each have a final best-estimated failure count higher than 80 DTFs. Based on the AGR-1 irradiation fuel performance, it is reasonable to assume that there were no in-pile particle failures among the qualified driver fuel particles. Thus, the total number of fuel particle failures in each AGR-3/4 capsule should be capped at a maximum of 80 failures, as had been done in fission product data analysis.

Table 8. AGR-3/4 DTF fuel failure total count (best-estimate, maximum, and minimum).

Capsule	BE	Max	Min	Capsule	BE	Max	Min
1	41	81	21	7	52	75	38
2	91	168	51	8	78	129	54
3	96	146	53	9	90	99	88
4	76	100	57	10	47	75	36
5	54	92	36	11	69	92	48
6	47	53	42	12	39	49	38



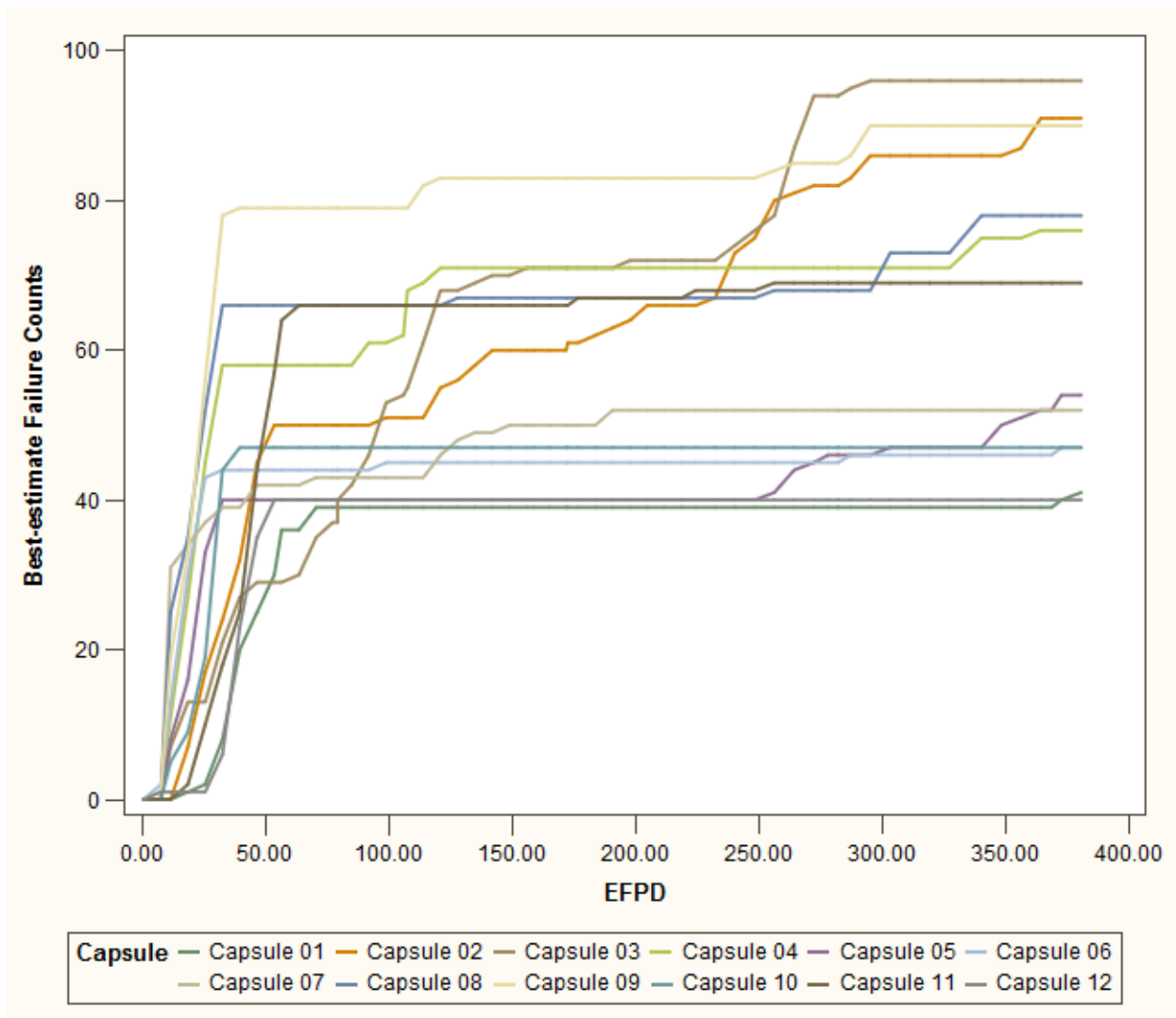


Figure 33. DTF best-estimate failure counts.

## 4.5 Release-to-Birth Ratio Per Failed Particle

The release-to-birth ratio is a measure of the ability of fuel kernels, particle coating layers and compact matrix material to retain fission gas species preventing their release into the sweep gas flow. In the absence of particle failure, this ratio is expected to be very low because standard particles within the specification limits are not expected to contribute to the release of fission products under normal operating conditions. On the other hand, in the presence of failed particles, the release of fission gas is significantly higher. The major factors that govern gaseous diffusion and release processes are found to be fuel material diffusion coefficient, temperature, and isotopic decay constant. Using the R/B values presented in Section 4.3 and the number of failed particles estimated in Section 4.4, it is possible to derive an R/B per failed particle and to correlate it with temperature and decay constant. Such an analysis was performed on AGR-3/4 data and presented in separate reports (Pham, 2014 and Einerson, 2014). The subsequent correlation can be used by reactor designers to estimate fission gas release from postulated, failed fuel particles in HTGR cores, which is a key safety factor for a fuel performance assessment.

## 5. AGR-3/4 OPERATIONAL ASSESSMENT

### 5.1 Power Increase

It was requested that the ATR power in the northeast lobe be increased during the course of the AGR-3/4 irradiation. A progressive power increase ensured that the temperature control could be maintained by the helium/neon sweep gas mixture as the fissile fuel content was consumed and the heat generation rate dropped. As mentioned in Section 2.1, the northeast lobe power was increased from about 14 MW (first two AGR-3/4 cycles) to about 16 MW (AGR-3/4 cycles 3 and 4), and then to about 18 MW (AGR-3/4 cycles 5 and 6), and finally to about 19 MW (last AGR-3/4 cycle).

### 5.2 Temperature Control

As mentioned in Section 3.1, Capsules 1, 3, 6, 7, 11, and 12 were controlled on peak fuel temperature, while Capsules 2, 4, 5, 8, 9, and 10 were controlled by maintaining their matrix ring or graphite ring mid-points at a constant temperature. Table 9 shows the temperature matrix that was planned prior to the start of irradiation (Collin, 2015).

Table 9. AGR-3/4 temperature matrix.

Capsule	Peak Fuel Temperature (°C) <sup>(a,b)</sup>	Matrix Ring Temperature (°C) <sup>(a,b,c)</sup>	Graphite Ring Temperature (°C) <sup>(a,b,c)</sup>	Initial Sink Temperature (°C) <sup>(c,d)</sup>
12	<b>900</b>	825-830	800-810	675-635
11	<b>1100</b>	985-1000	830-845	680-700
10	1130-1105	<b>980</b>	920-930	665-650
9	1080-1010	880-865	<b>800</b>	640-650
8	1180-1110	<b>980</b>	895-905	590-600
7	<b>1300</b>	1080-1175	1020-1115	585-690
6	<b>1100</b>	880-940	790-870	610-700
5	1040-960	830-810	<b>750</b>	580-570
4	1100-1050	890-870	<b>800</b>	610-630
3	<b>1250</b>	1080-1100	1025-1050	690-700
2	1050-1020	910-890	<b>850</b>	660-670
1	<b>950</b>	885	825	680

- Fuel temperature was controlled in Capsules 1, 3, 6, 7, 11 and 12 whereas graphite temperature was controlled in Capsules 2, 4, 5, 8, 9 and 10 (the matrix ring was replaced with graphite in Capsules 3, 8 and 10). Bold values are temperature specifications, other values result from calculations.
- When temperature ranges are shown, the first number is the estimated temperature at the beginning of the irradiation and second number is the estimated temperature at the end of the experiment.
- Temperatures at the center of the ring.
- The initial sink temperature is an acceptable range of temperatures for the center of the sink ring at the beginning of irradiation.

The objective of the AGR-3/4 experiment was to maintain the control temperatures as flat as possible throughout irradiation. The values reached at the beginning of Cycle 151A (first AGR-3/4 cycle) when full power was first achieved differed from the expected values shown in Table 9 because of erroneous physics models that resulted in incorrect thermal predictions. Subsequently, these observed values were used as target temperatures for the first three cycles, superseding the predicted values from Table 9. As shown in Figure 34 and Figure 35, the control temperatures remained relatively flat throughout these first three cycles. New thermal calculations were performed that included the modeling of varying gap width with irradiation. These new thermal predictions showed good agreement with the TC measurements for

these first three cycles (see Section 5.3) and they were deemed appropriate to determine the target control temperatures for the last four cycles of the AGR-3/4 experiment. This was done by setting these target values to the average values of the calculated control temperatures of the first three cycles. Temperature bands of  $\pm 75^{\circ}\text{C}$  and  $\pm 50^{\circ}\text{C}$  were defined for peak fuel temperature and graphite temperature, respectively, as acceptable boundaries for variation of the control temperatures around their target values. Figure 34 and Figure 35 show that the control temperatures were successfully kept in the temperature bands around their respective targets. In a few capsules (Capsules 4, 5, 8, and 9), temperatures in the compacts or rings started to drift upward during the last two cycles; however, no definite cause could be put forward to account for it. The rise of temperatures toward the end of irradiation did not call into question the validity of the experiment, which will still provide useful data on fission product transport over the range of temperatures of interest.

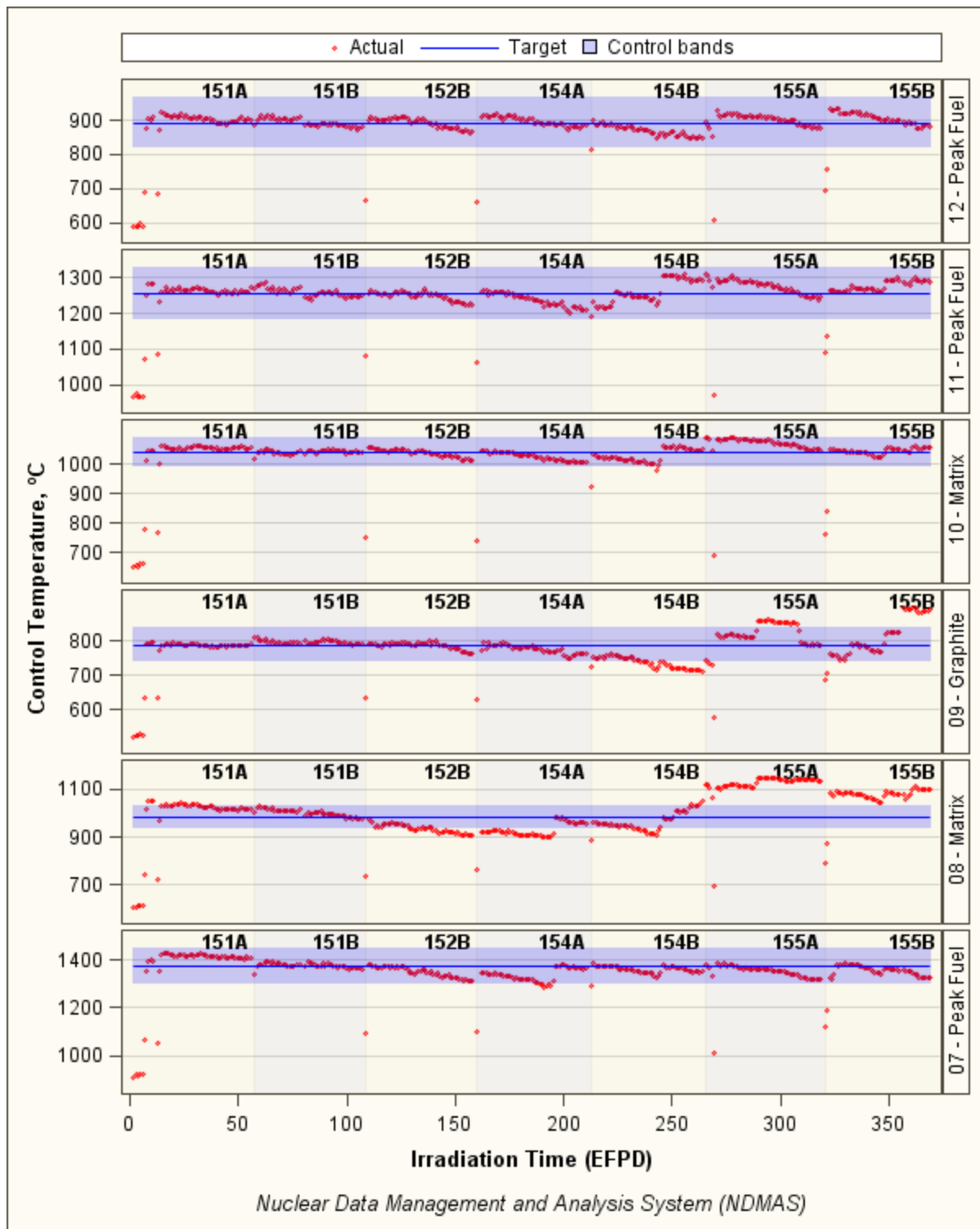


Figure 34. Calculated daily control temperatures for Capsules 7-12.

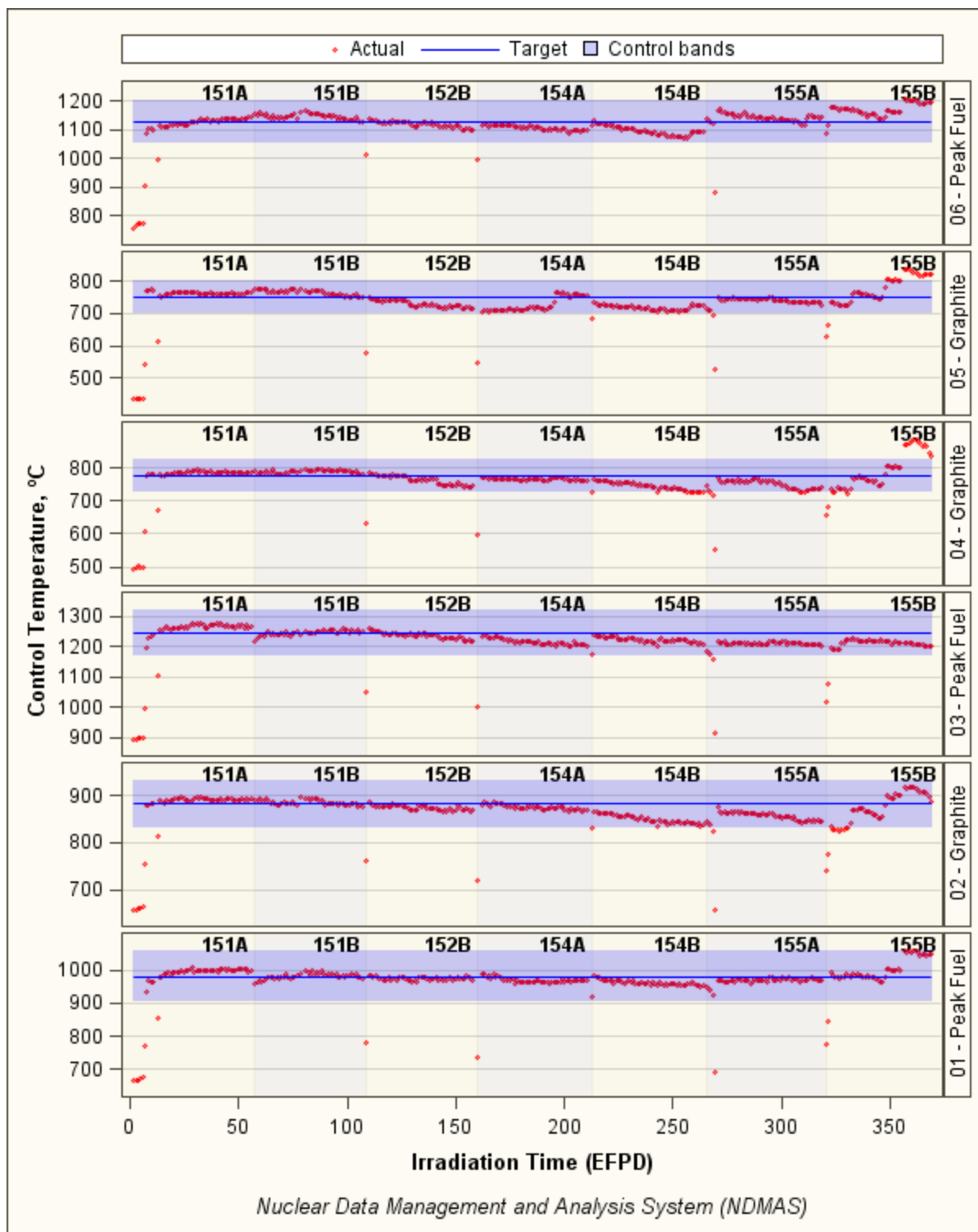


Figure 35. Calculated daily control temperatures for Capsules 1-6.

### 5.3 Thermocouple Performance

AGR-3/4 temperature measurements were performed by TCs terminating within the graphite sinks of each capsule and additional TCs located in the graphite rings of Capsules 5, 10, and 12. These measurements support temperature control of the experiment where designated control TCs provide feedback to the automated sweep gas control system, which adjusts gas blends to maintain reference temperatures. TC measurements are also used to support thermal analyses of the test train, which ultimately determine fuel temperatures.

Figure 36 gives a diagram of the locations of the TCs in a capsule with TC-1 in the southwest quadrant and TC-2 in the northeast quadrant. Both TCs were located in the graphite sink. When applicable, TC-3 was located in the northeast quadrant of the graphite ring. All TCs terminated at the midplane of the fuel stack. TC-1 was used as control TC in all Capsules except for Capsules 9 and 12. In Capsule 9, TC-2 was used as control TC because a connection error on TC-1 left a reading error of 15-20°C after correction. In Capsule 12, TC-3 was chosen as control TC because its location in the matrix ring was closer to the fuel stack, therefore providing more accuracy in temperature measurement in this capsule controlled on peak fuel temperature.

When a control TC failed during irradiation, the other sink TC within the same capsule was used as control TC and the reference control temperature was reset based on thermal analysis calculations. After both TCs in Capsule 3 failed near the end of Cycle 154B, the neon fraction in the gas mixture was set at 0.52 (15.6 sccm) for the rest of the cycle and increased for the last two cycles, as the temperature started to fall off. Thermal analysis showed that the projected peak fuel temperature could then be maintained within the desired control band of  $1250 \pm 75^\circ\text{C}$  with a neon fraction of 0.68 (20.4 sccm).

The AGR-3/4 TCs performed relatively well: of the 27 installed TCs, only five failed late during operation. AGR TCs deteriorate and sometimes fail because of the high irradiation and temperature conditions that occur during test reactor cycles. The two common failure mechanisms for TCs are the formation of virtual junctions and open circuit failures where the signal ceases altogether. Open circuit failures occur when the thermo-elements in the TC break, causing an open circuit. Failures from virtual junctions are caused by deterioration or damage to the TC sheath and/or dielectric insulating material that separates the TC thermal elements. This produces an electrical path (“virtual junction”) at some location along the TC wire other than at the terminal tip. Virtual junctions are detected by perturbing the temperature in a single capsule using gas flow, then observing the TC readings from capsules below this one to see if they respond. If a capsule TC responds to temperature changes in a capsule above it, it is likely that a virtual junction has formed and the TC can be considered failed. No evidence of virtual junctions was found during the operating lifetime of the AGR-3/4 TCs; therefore, all TC failures were attributed to open circuit failure (Pham, 2015).

Table 10 shows the TC locations and their failure status (failure date and cycle). TC-2 in Capsule 2 failed during the outage of Cycle 154A after the AGR-3/4 test train was reinserted in the NEFT from the ATR canal following PALM Cycle 153B. TC-1 in Capsule 3 also failed during the outage of Cycle 154A, two days before reactor start-up. TC-2 in Capsule 3 failed near the end of Cycle 154B while ATR was at full power, leaving Capsule 3 without any TC for the remainder of the irradiation. TC-1 in Capsule 5 also failed under full power, near the end of Cycle 155A. Finally, TC-1 in Capsule 6 failed during the powering up of Cycle 155B, the last cycle of the AGR-3/4 irradiation experiment (Pham, 2015).

Figure 37 and Figure 38 show the readings of all functioning TCs as function of EFPD, thus the plots are discontinued at the time of TC failures.

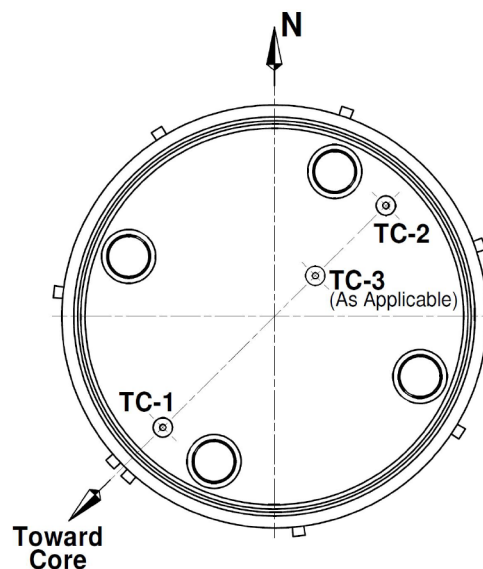


Figure 36. Cutaway view of a capsule showing the position of TCs.

Table 10. TC types, locations, and conditions in AGR 3/4 test train.

Capsule	Location	TC Type <sup>(a)</sup>	Sheath/ Insulation	Condition
12	2 sink 1 matrix	Type N (2.03 mm)	Inconel 600 / MgO	-
11	2 sink	Type N	Inconel 600 / MgO	-
10	2 sink 1 matrix	Type N	Inconel 600 / MgO	-
9	2 sink	Type N	Inconel 600 / MgO	-
8	2 sink	Type N	Inconel 600 / MgO	-
7	2 sink	Type N	Inconel 600 / MgO	-
6	2 sink	Type N	Inconel 600 / MgO	TC-1 failed on 02/13/2014 during the power-up phase of Cycle 155B
5	2 sink 1 matrix	Type N	Inconel 600 / MgO	TC-1 failed on 01/11/2014 near the end of Cycle 155A
4	2 sink	Type N	Inconel 600 / MgO	-
3	2 sink	Type N	Inconel 600 / MgO	TC-1 failed on 05/17/2013 during the outage of Cycle 154A
2	2 sink	Type N	Inconel 600 / MgO	TC-2 failed on 04/29/2013 during the outage of Cycle 154A
1	2 sink	Type N	Inconel 600 / MgO	-

a. All TCs are 1.02 mm in diameter unless noted as 2.03 mm in diameter.

The temperature difference between TCs in the same capsule should remain fairly constant over time. Any other trend or discontinuity in the data suggests that one of the TCs is drifting (Pham, 2015). However, continued correlation between TCs in the same capsule is no assurance that both TCs are not drifting. Indeed, out-of-pile TC testing showed that TCs of the same design and exposed to the same temperature conditions will tend to drift in similar ways, i.e., they could both drift and still maintain a fairly constant temperature difference over time. A control chart was used to monitor the temperature difference between two TCs in each capsule. The control chart uses an initial “baseline” period of data to calculate typical operating conditions. Then, it evaluates a subsequent “monitoring period” of data relative to the baseline conditions. A control chart centerline is calculated for a given TC pair in one capsule using the mean of the temperature difference between two TCs in that same capsule during the baseline period. Upper and lower control limits for the TC differences are then calculated as three standard deviations above and below the control chart mean difference. If, during the monitoring period, one TC indicates significantly higher or lower temperatures relative to another TC in that capsule, then one of the TCs may be drifting. However, a key control chart assumption is that there is a constant mean and standard deviation of the temperature differences between TC pairs within a capsule over both the baseline and monitoring periods. This assumption may not always be valid because of differential heating across TC pairs that may occur as the experiment progresses. Using this control chart, it was suggested that TC-3 in Capsule 10 started to drift from the middle of Cycle 154B. TCs in Capsules 2, 3, 5, 8, 11, and 12 were stable relative to each other for the duration of the irradiation, or until one TC failed in the case of Capsules 2, 3, and 5. In Capsules 6, 7, and 10 the TCs were not perfectly stable relative to each other but only TC-3 in Capsule 10 was considered drifting. Finally, TCs in Capsules 4 and 9 were not stable relative to each other but they were not considered drifting (Pham, 2015).

Figure 39 and Figure 40 show the differences between measured and calculated TC temperatures. There is a good agreement between measured and calculated TC temperatures, with differences within approximately  $\pm 60^{\circ}\text{C}$ , except for both TCs in Capsule 1, TC-3 in Capsule 5, and TC-1 in Capsule 8, which show differences extending to  $+90^{\circ}\text{C}$ .



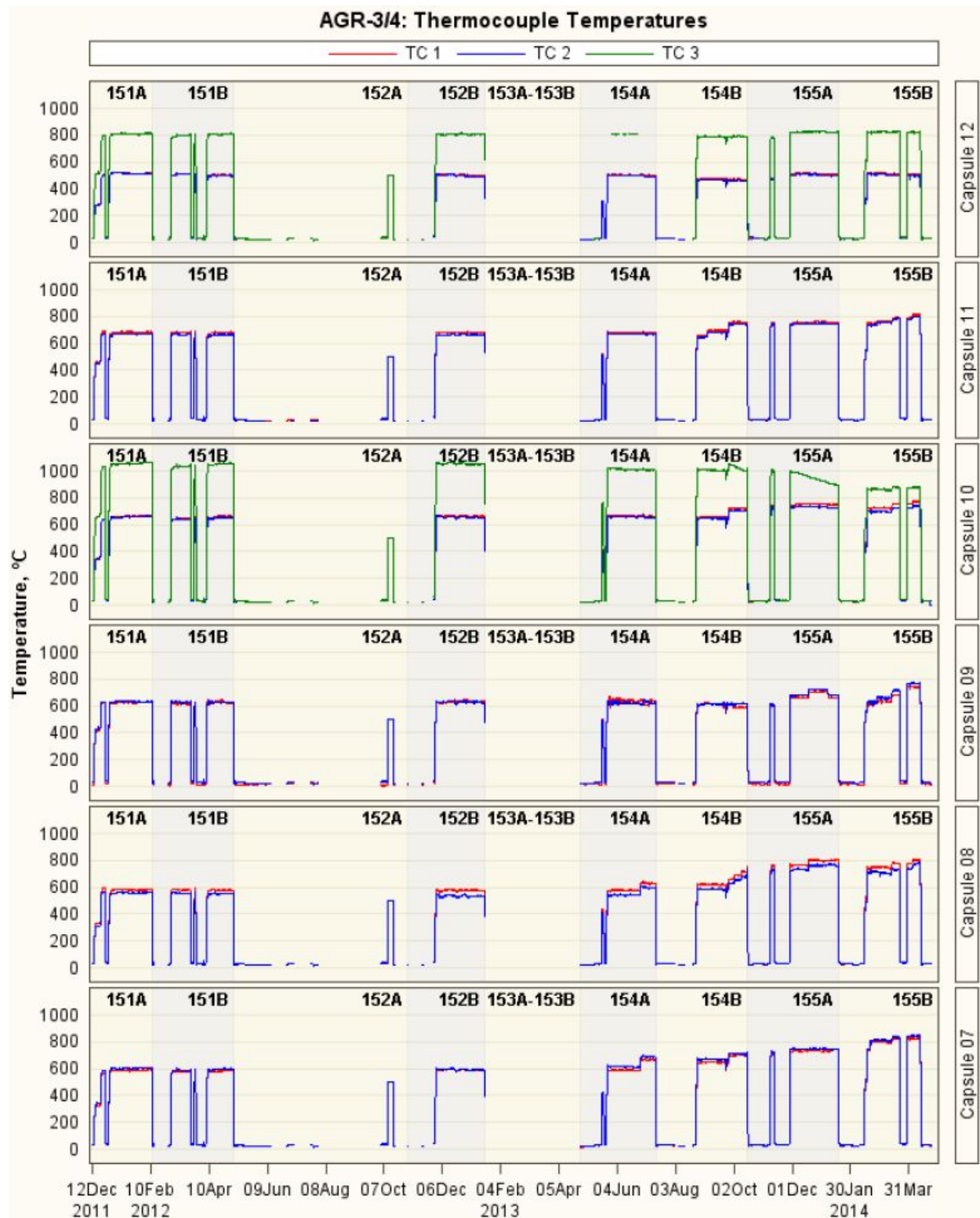


Figure 37. Measured TC temperatures for Capsules 7-12.

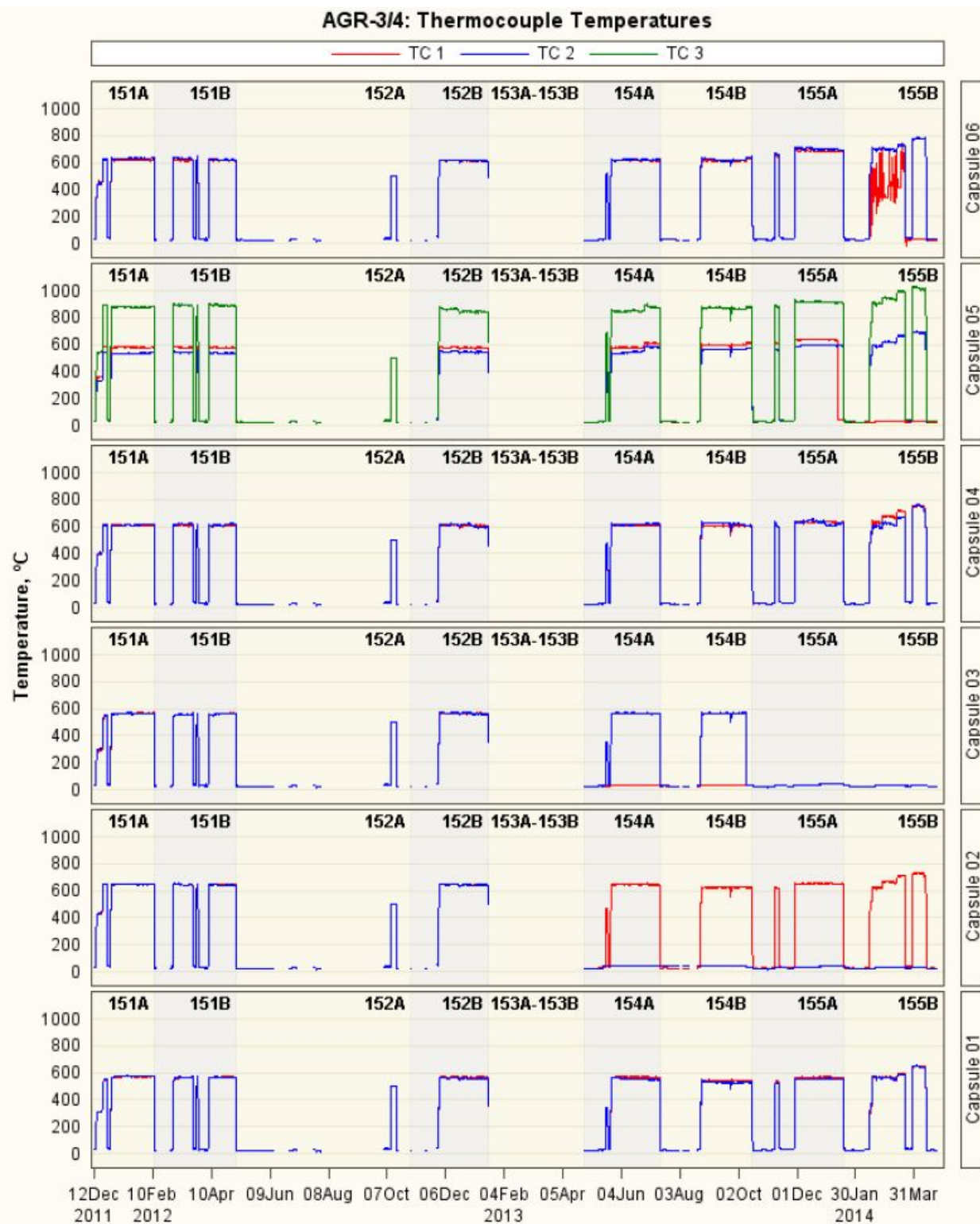


Figure 38. Measured TC temperatures for Capsules 1-6.

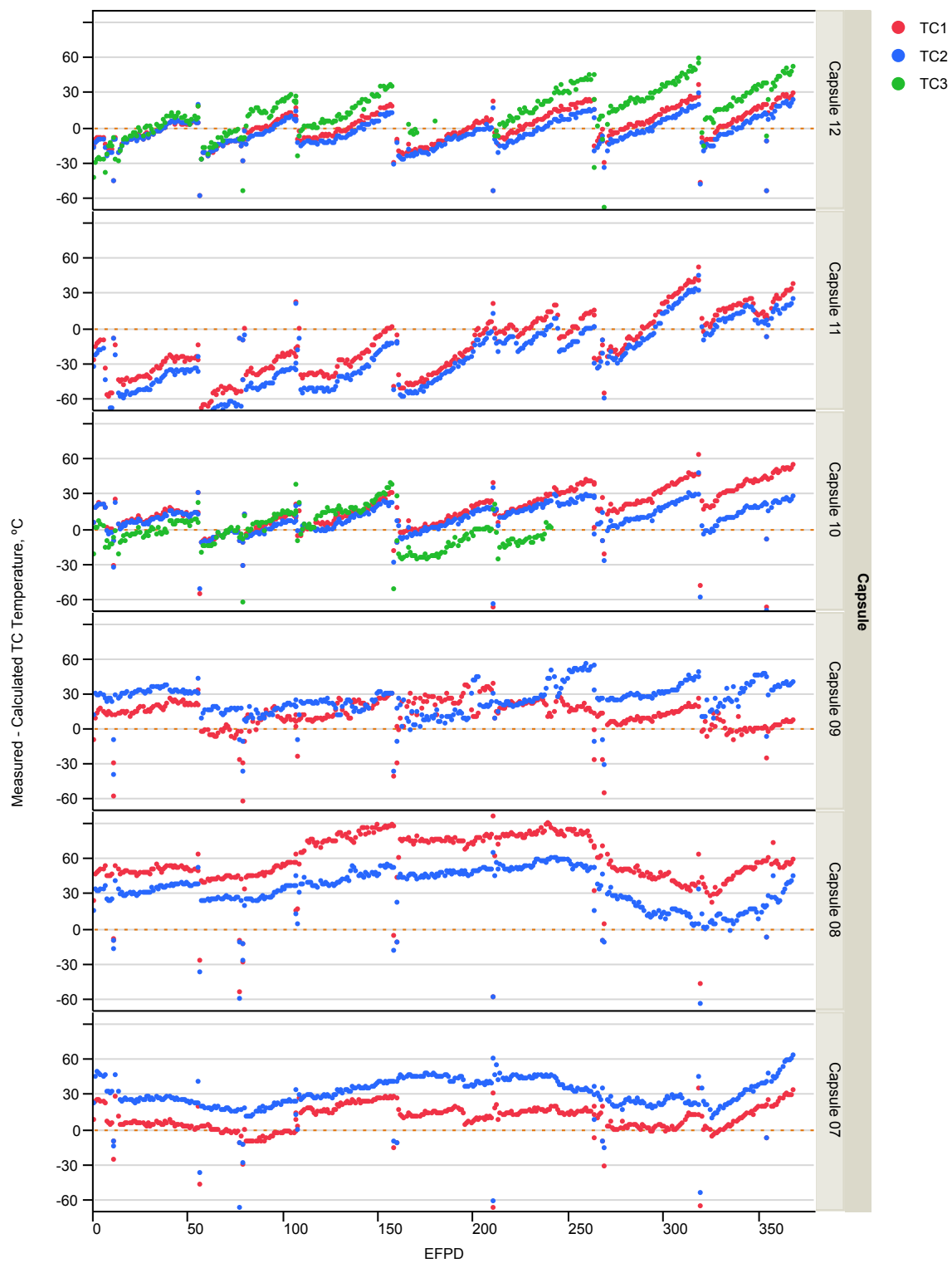


Figure 39. Difference between measured and calculated TC temperatures versus EFPD for Capsules 7-12.

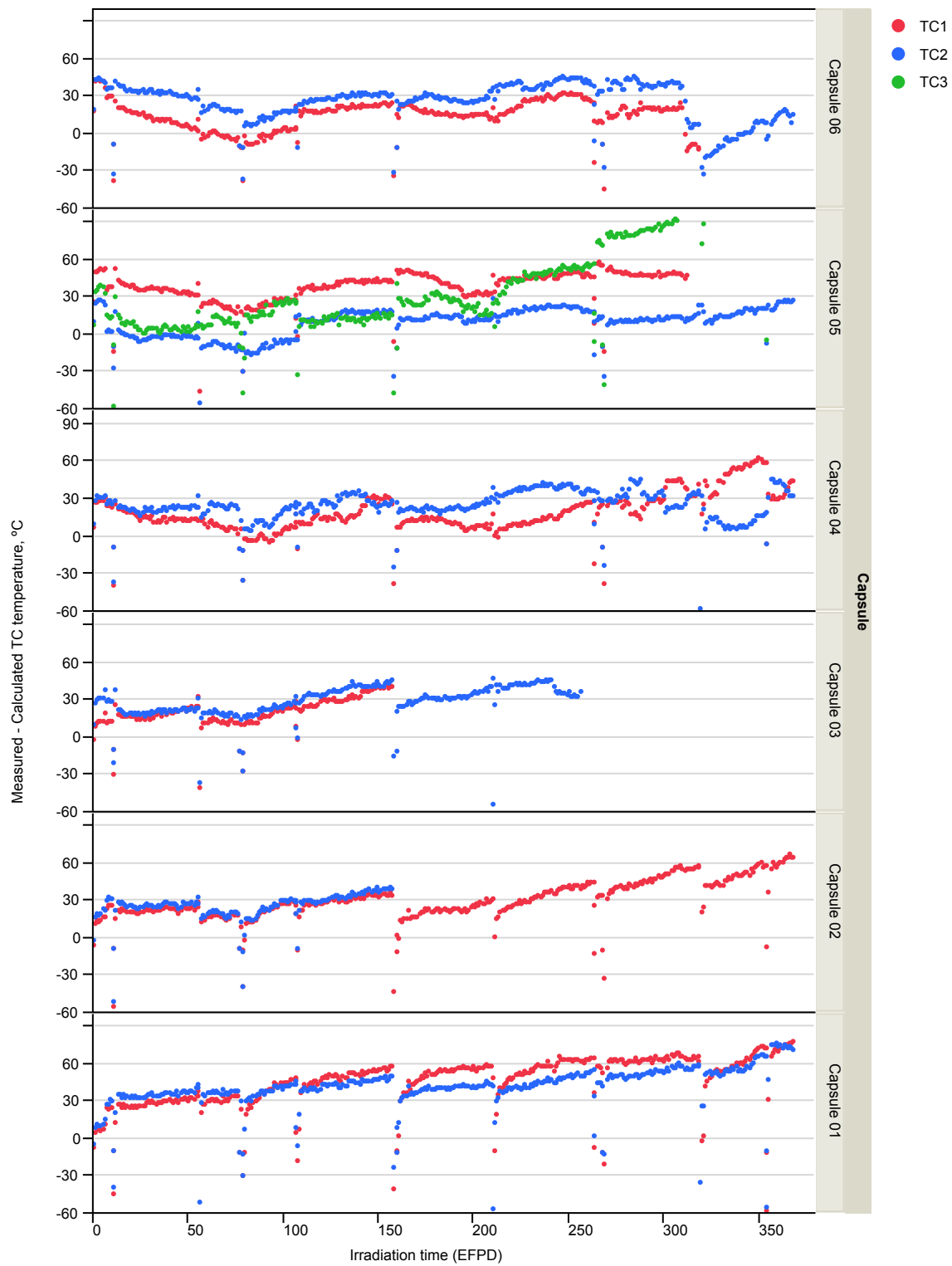


Figure 40. Difference between measured and calculated TC temperatures versus EFPD for Capsules 1-6.

## 5.4 Thermocouple Set Points Adjustments

As the irradiation progressed and the power was progressively increased, temperature adjustments were made to keep the capsules in their desired temperature bands (see Section 5.2). Thermocouple set points were redefined based on fission gas release measurements, TC readings and thermal calculations. The changes are listed below and summarized in Table 11. More details are given in (Scates, 2015).

On November 15, 2011, all control TCs were assigned set points.

### Cycle 151A

Following a reactor scram on December 25, 2011 and a restart on December 27, 2011, TC set points were changed on January 3, 2012 for Capsules 1, 3, 7, and 12.

### Cycle 154A

After TC-1 in Capsule 3 failed during the outage prior to the start of Cycle 154A, TC-2 became the control TC and assigned a new set point on May 20, 2014. As Cycle 154A progressed, some adjustments were made on June 27, 2013 to the TC set points of Capsules 5, 7, and 8.

### Cycle 154B

Two days prior to the start of Cycle 154B, all Capsules had their TC set points changed. Within six weeks, between September 4, 2013 and October 14, 2013, five adjustments were made, affecting Capsules 5, 6, 7, 8, 10, and 11.

### Cycle 155A

At the beginning of Cycle 155A, eight of the 12 TC set points were changed. Since the remaining TC (TC-2) in Capsule 3 had failed near the end of Cycle 154B, the neon gas flow was set to 20.4 sccm at the beginning of Cycle 155A, where it remained until the end of irradiation. Three other changes occurred during this cycle, affecting Capsules 5, 8, and 9.

### Cycle 155B

Prior to the start of Cycle 155B, seven of the 12 TC set points were changed. During Cycle 155B, there were five other TC set point adjustments affecting all capsules, except Capsule 3 that was running on a set neon gas flow since the loss of both of its TCs.

Table 11. AGR-3/4 capsule TC set points (°C). NF indicates capsule running on set neon flow.

Date	C1	C2	C3	C4	C5	C6	C7	C8	C9	C10	C11	C12
11/15/11	689	648	687	612	581	618	629	582	633	667	683	673
12/14/11	Start Cycle 151A / Start AGR-3/4											
1/3/12	570		568				591					808
5/19/13	Start Cycle 154A											
6/27/13					613		671	635				
7/7/13	End Cycle 154A											
8/21/13	545	625	568	606	598	614	648	623	617	656	658	790
8/23/13	Start Cycle 154B											
9/4/13											698	
9/26/13							700	663		721	758	
10/1/13								693				
10/8/13					613	634		718				
10/14/13			NF			649	720	768		751		
11/8/13	Start Cycle 155A											
11/13/13	568	654		636	636	687	749		680			823
12/17/13								803	720			
1/6/14									680			
1/13/14					591							
1/17/14	End Cycle 155A											
2/4/14		625		635			800	750	635	725	750	
2/13/14	Start Cycle 155B											
2/13/14						702						
2/25/14		665		675	621				665		765	
3/12/14	598	710		720	666	732	825	780	720	755	795	598
3/18/14	648	730		760	691	782		805	770	775	815	648
4/10/14		705		735								
4/12/14	End Cycle 155B / End AGR-3/4											

## 6. CONCLUSIONS

The AGR-3/4 fuel test was successful in irradiating its fuel compacts to their expected and specified burnup and fast fluence ranges with no definitive evidence of driver TRISO fuel particle failure.

- Capsule-average burnups ranged from 5.35% FIMA in Capsule 12 to 15.24% FIMA in Capsule 6.
- Capsule-average fast fluences ranged from  $1.50 \times 10^{25}$  n/m<sup>2</sup> in Capsule 12 to  $5.31 \times 10^{25}$  n/m<sup>2</sup> in Capsule 6.
- Time-average volume-average fuel temperatures on a capsule basis at the end of irradiation ranged from 845°C in Capsule 12 to 1276°C in Capsule 7.

The AGR-3/4 experiment was globally successful in keeping the control temperatures of the 12 capsules relatively flat in a range of temperatures suitable for measurement of fission product diffusion in compact matrix and structural graphite materials.

The TCs perform relatively well: of the 27 installed TCs, only five failed late during operation.

Fission product R/B values reached values in the  $10^{-4}$ - $10^{-3}$  range early during irradiation as DTF particles started to fail during the first AGR-3/4 cycle. The hotter Capsule 7 reached the higher R/B value of around  $3 \times 10^{-3}$ .

Impurities added to the sweep gas did not seem to have an appreciable impact on fuel performance or fission product transport, but very small quantities of iodine isotope I-131 were identified in the sweep gas following the injection of the impurities and its transport to the detection system is believed to have been facilitated by the injected moisture.

The results of this test will provide irradiation performance and fission product transport data (Demkowicz 2015). PIE for this experiment focuses on: (1) Determining the extent of fission product migration in the matrix and graphite rings during irradiation; (2) Determining the extent of fission product migration in the matrix and graphite rings at elevated temperatures during heating in pure helium; (3) Evaluating retention of fission products in fuel kernels and compact matrix during irradiation; and (4) Determining the extent of condensable and gaseous fission product release from fuel kernels and compact matrix at elevated temperatures during heating in pure helium. Once PIE is completed, this test will provide useful data on fission product diffusion, which are crucial for modeling of fission product transport and release from the reactor core during operation and during reactor accident scenarios, as well as additional AGR data that will form a link between fabrication processes, fuel product properties, and irradiation performance.

## 7. REFERENCES

- ASTM International, “Standard Practice for Testing Graphite and Boronated Graphite Materials for High-Temperature Gas-Cooled Nuclear Reactor Components”, C781-08, September 2008.
- Barnes, C.M., “AGR-1 Fuel Product Specification and Characterization Guidance”, EDF-4380, Rev. 8, April 25, 2006a.
- Barnes, C.M., “AGR-3 & 4 Fuel Product Specification”, EDF-6638, Rev. 1, September 14, 2006b.
- BWXT, “Industrial Fuel Fabrication and Development Lot G73V-20-69303”, Data Certification Package, June 6, 2006.
- Chang, G.S. and J.R. Parry, “Physics Evaluations for the AGR-3/4 Experiment Irradiated in the ATR NEFT in Support of Final Design Activities”, ECAR-1346, Rev. 1, September 13, 2011.
- Collin, B.P., “AGR-1 Irradiation Test Final As-Run Report”, INL/EXT-10-18097, Rev. 1, June 8, 2012.
- Collin, B.P., “AGR-3/4 Irradiation Experiment Test Plan”, PLN-3867, Rev.1, May 20, 2015.
- Croff, A.G., “ORIGEN2: A Versatile Computer Code for Calculating the Nuclide Compositions and Characteristics of Nuclear Materials”, Nuclear Technology Vol. 62 (1983) 335-352.
- Demkowicz, P.A., “AGR-3/4 Post-Irradiation Examination Plan”, PLN-4916, to be issued.
- Einerson, J.J., B.T. Pham, D.M. Scates, J.T. Maki, D.A. Petti, “Analysis of Fission Gas Release-to-Birth Ratio Data from AGR Irradiations,” HTR2014-31102, Proceedings of the HTR2014 Conference, Weihai, China, October 27-31, 2014.
- Folsom, C., C. Xing, C. Jensen, H. Ban, and D.W. Marshall, “Experimental measurement and numerical modeling of the effective thermal conductivity of TRISO fuel compacts”, Journal of Nuclear Materials 458 (2015) 198-205.
- GCM, “Graphite Contamination Measurements - Shiva ID U060802018 & U060802019 – P.O. #3400075184 – Job #UP4897”, August 8, 2006.
- Gontard, R. and H. Nabielek, “Performance Evaluation of Modern HTR TRISO Fuels”, Forschungszentrum Jülich GmbH, HTA-IB-05/90, July 31, 1990.
- Gonzo, E.E., “Estimating Correlations for the Effective Thermal Conductivity of Granular Materials,” Chemical Engineering Journal, Vol. 90, No. 3 (2002) 299-302.
- Hartwell, J.K., D.M. Scates, and M.W. Drigert, “Design and Expected Performance of the AGR-1 Fission Product Monitoring System”, INL/EXT-05-00073, September 2005.
- Hartwell, J.K., J.B. Walter, D.M. Scates, and M.W. Drigert, “Determination of the AGR-1 capsule to FPMS Spectrometer Transport Volumes from Leadout Flow Test Data”, INL/EXT-07-12494, April 2007.
- Hawkes, G.L., J.W. Sterbentz, and J.T. Maki, “Thermal Predictions of the AGR-3/4 Experiment with Time Varying Gas Gaps”, Nuclear Engineering and Radiation Science, NERS-15-1006, accepted March 12, 2015a.
- Hawkes, G.L., “AGR-3/4 Daily As-Run Thermal Analyses”, ECAR-2807, June 25, 2015b.
- Hull, L.C., “Nuclear Data Management and Analysis System Plan”, PLN-2709 Rev. 4, March 12, 2015.
- Hunn, J.D., “Data Compilation for AGR-3/4 Driver Fuel Coated Particle Composite LEU03-09T”, ORNL/TM-2007/019, March 2007.
- Hunn, J.D., “Data Compilation for AGR-3/4 Designed-To-Fail (DTF) Fuel Particle Batch LEU03-07DTF”, ORNL/TM-2011/109, April 2011a.



Hunn, J.D., “Data Compilation for AGR-3/4 Designed-to-Fail (DTF) Fuel Compact Lot (LEU03-10T-OP2/LEU03-07DTF-OP1)-Z”, ORNL/TM-2011/124, June 2011b.

Hunn, J.D., “Data Compilation for AGR-3/4 Matrix Matrix rings Lot ARB-B1”, ORNL/TM-2011/272, September 2011c.

INL, “Idaho National Laboratory Advanced Reactor Technologies Technology Development Office Quality Assurance Program Plan”, PLN-2690, Rev. 13, March 13, 2015a.

INL, “Technical Program Plan for the INL Advanced Reactor Technologies Technology Development Office/Advanced Gas Reactor Fuel Development and Qualification Program”, PLN-3636, Rev. 4, May 7, 2015b.

Kercher, A.K. and J. D. Hunn, “Results from ORNL Characterization of Nominal 350  $\mu\text{m}$  LEUCO Kernels (LEU03) from the BWXT G73V-20-69303 Composite”, ORNL/TM-2006/552, October 2006.

Kestin, J., K. Knierim, E.A. Mason, B. Najafi, S.T. Ro, and M. Waldman, “Equilibrium and Transport Properties of the Noble Gases and Their Mixtures at Low Density”, Journal of Physical and Chemical Reference Data, Vol. 13, No. 1 (1984) 229-303.

LANL, X-5 Monte Carlo Team, “MCNP—A General Monte Carlo N-Particle Transport Code, Version 5”, Volume I, LA-UR-03-1987, Los Alamos National Laboratory, April 24, 2003 (Revised 6/30/2004) and Volume II, LA-CP-0245, Los Alamos National Laboratory, April 24, 2003 (Revised 6/30/2004)

Maki, J.T., “AGR-3/4 Irradiation Test Specification”, SPC-1345, February 2, 2011.

Marshall, D.W., “AGR-3/4 DTF Fuel and Capsule Component Material Specifications”, SPC-1214, Rev. 1, June 21, 2011.

Petti, D.A., J.T. Maki, J. Buongiorno, R.R. Hobbins and G.K. Miller, “Key Differences in the Fabrication, Irradiation and Safety Testing of U.S. and German TRISO-coated Particle Fuel and Their Implications on Fuel Performance”, INEEL/EXT-02-00300, February 27, 2002.

Pham, B.T., J.J. Einerson, D.M. Scates, J.T. Maki, D.A. Petti, “AGR-2 and AGR-3/4 Release-to-Birth Ratio Data Analysis,” INL/EXT-14-32970, September 12, 2014.

Pham, B.T., “AGR-3/4 Final Data Qualification Report for ATR Cycles 151A through 155B-1”, INL/EXT-14-33780, March 17, 2015.

Scates, D.M., J.B. Walter, and J.W. Sterbentz, “Quantity of I-135 Released from the AGR-1, AGR-2, and AGR-3/4 Experiments and Discovery of I-131 at the FPMS Traps during the AGR-3/4 Experiment”, INL/EXT-14-32618, September 9, 2014.

Scates, D.M., “Release-to-Birth Ratios for AGR-3/4 Operating Cycles 151A through 155B”, ECAR-2457, Revision 1, June 5, 2015.

Snead, L.L. and T.D. Burchell, “Reduction in Thermal Conductivity Due to Neutron Irradiation”, 22<sup>nd</sup> Biennial Conference on Carbon, Extended Abstracts (1995) 774-775.

Sterbentz, J.W., “Fast Flux to DPA Multiplier”, E-mail communication to G.L. Hawkes, August 5, 2009.

Sterbentz, J.W., “JMOCUP As-Run Daily Depletion Calculation for the AGR-1 Experiment in ATR B-10 position”, ECAR-958, Rev. 2, September 3, 2013.

Sterbentz, J.W., “JMOCUP As-Run Daily Physics Depletion Calculation for the AGR-3/4 TRISO Particle Experiment in ATR Northeast Flux Trap”, ECAR-2753, June 6, 2015.

Tomberlin, T.A., “Advanced Test Reactor Critical Facility Measurements in Support of Advanced Test Experiments”, Engineering Design File No., TRA-ATRC-1546, Rev. 6, March 2000.

Windes, W.E., W.D. Swank, D.T. Rohrbaugh, and J.R. Lord, "AGC-2 Graphite Preirradiation Data Analysis Report", INL/EXT-13-28612, April 2, 2013.

# **Appendix A**

## **As-Manufactured Fuel Data**

Kernels for AGR-3/4 consist of LEU UCO fuel. The kernels were fabricated by BWX Technologies (BWXT, 2006) in accordance with the AGR-3/4 Fuel Product Specification (Marshall, 2011). Several production batches were combined into a single composite: Lot G73V-20-69303. Complete characterization data for this kernel lot are compiled in the Data Certification Package (BWXT, 2006). Selected kernel composite properties (from BWXT characterization except for kernel diameter and density which are from Oak Ridge National Laboratory (ORNL) characterization (Kercher, 2006)) and corresponding fuel product specifications are in Table A-1.

The UCO kernels were coated and characterized by ORNL (Hunn, 2007 and Hunn, 2011a). Coating was performed in accordance with the AGR-3/4 Fuel Product Specification (Barnes, 2006b and Marshall, 2011). Two particle composite lots comprised the fuel irradiated in AGR-3/4, one for each type of particles: Lot LEU03-09T for driver-coated particles and Lot LEU03-07DTF for designed-to-fail particles. A summary of selected properties, based on actual characterization data, for each of the two coated particle composites is listed in Table A-2.

After coating, AGR-3/4 fuel was formed into right cylindrical compacts. The compact matrix material is composed of a thermosetting carbonaceous material. Prior to compacting, the fuel particles were overcoated with thick layers of the compact matrix material. This overcoat is intended to prevent particle-to-particle contact and help achieve the desired packing fraction of fuel particles. A summary of selected properties, based on actual characterization data (Hunn, 2011b) and derived from these data, for each fuel type is listed in Table A-3.

The AGR-3/4 fuel compacts were surrounded by three concentric annular rings of test material consisting of fuel-compact matrix material (matrix ring) and fuel-element graphite (graphite ring and sink).

The matrix ring blanks, from which the matrix rings were machined, were made of the same graphite/resin blend that is expected to be used to fabricate the AGR-5/6 fuel compacts. A summary of selected properties, based on actual characterization data (Hunn, 2011c and GCM, 2006) and derived from these data, is listed in Table A-4. Table A-4 specifies the uranium contamination, which is given to ensure that the contribution of fission products from uranium contamination in the graphite and matrix rings combined with exposed kernels in the compacts will be less than 2.1% of that contributed by the DTF particles (Marshall, 2011).

Table A-1. Selected properties for kernel Lot G73V-20-69303.

Kernel Property	Specified Range for Mean Value	Actual Mean Value $\pm$ Population Standard Deviation
Diameter ( $\mu\text{m}$ )	$350 \pm 10$	$357.3 \pm 10.5^{(a)}$
Density ( $\text{Mg/m}^3$ )	$\geq 10.4$	$11.098 \pm 0.025$
U-235 enrichment (wt%)	$19.80 \pm 0.10$	$19.717 \pm 0.014$
Carbon/uranium (atomic ratio)	$0.50 \pm 0.20$	$0.361 \pm 0.004$
Oxygen/uranium (atomic ratio)	$1.50 \pm 0.20$	$1.43 \pm 0.00$
[Carbon + oxygen]/uranium (atomic ratio)	$\leq 2.0$	$1.8 \pm 0.0$
Total uranium (wt %)	$\geq 87.0$	$89.101 \pm 0.041$
Sulfur impurity (ppm – wt)	$\leq 1500$	$456 \pm 29$
Phosphorus impurity(ppm – wt)	$\leq 1500$	$\leq 30$
All other impurities	$\leq 100$	Below minimum detection limits and within specification

- a. 95% upper confidence diameter exceeds specifications. Justification of acceptance: the minor deviation has limited impact on the fission product release characteristics (BWXT, 2006).

Table A-2. Selected properties for AGR-3/4 coated particle composites.

Driver Fuel Property	Specified Range for Mean Value	Actual Mean Value $\pm$ Population Standard Deviation
Buffer thickness ( $\mu\text{m}$ )	$100 \pm 15$	$109.7 \pm 7.7$
IPyC thickness ( $\mu\text{m}$ )	$40 \pm 4$	$40.4 \pm 2.3$
SiC thickness ( $\mu\text{m}$ )	$35 \pm 3$	$33.5 \pm 1.1$
OPyC thickness ( $\mu\text{m}$ )	$40 \pm 4$	$41.3 \pm 2.1$
Buffer density ( $\text{Mg}/\text{m}^3$ )	$1.03 \pm 0.15$	$1.10 \pm 0.04$
IPyC density ( $\text{Mg}/\text{m}^3$ )	$1.90 \pm 0.05$	$1.904 \pm 0.014$
SiC density ( $\text{Mg}/\text{m}^3$ )	$\geq 3.19$	$3.203 \pm 0.002$
OPyC density ( $\text{Mg}/\text{m}^3$ )	$1.90 \pm 0.05$	$1.901 \pm 0.012$
IPyC anisotropy (BAF)	$\leq 1.035$	$1.027 \pm 0.002$
OPyC anisotropy (BAF)	$\leq 1.035$	$1.021 \pm 0.002$
IPyC anisotropy post compact anneal (BAF)	Not specified	Not measured
OPyC anisotropy post compact anneal (BAF)	Not specified	Not measured
OPyC sphericity (aspect ratio)	Mean not specified <sup>(a)</sup>	1.056
Particle diameter <sup>(b)</sup> ( $\mu\text{m}$ )	Mean not specified	$818.9 \pm 14.2$
Particle mass (mg)	Mean not specified	$0.774 \pm 0.002$
DTF Property	Specified Range for Mean Value	Actual Mean Value $\pm$ Population Standard Deviation
Pyrocarbon thickness ( $\mu\text{m}$ )	$20 \pm 5$	$20.0 \pm 0.9$
Pyrocarbon density ( $\text{Mg}/\text{m}^3$ )	$1.95 \pm .05$	$1.988 \pm 0.009$
Anisotropy (BAF)	$\geq 1.151$	$1.243 \pm 0.019$
Anisotropy post compact anneal (BAF)	Not specified	Not measured
Pyrocarbon surface-connected porosity ( $\text{ml}/\text{m}^2$ )	Information only	0.079
Sphericity at seal coat (aspect ratio)	Not specified	1.024
Particle diameter <sup>(c)</sup> ( $\mu\text{m}$ )	Mean not specified	$400.0 \pm 9.2$
Particle mass (mg)	Mean not specified	$0.280 \pm 0.001$

a. Critical region is specified such that  $\leq 1\%$  of the particles shall have an aspect ratio  $\geq 1.14$ . One particle in 1584 analyzed particles has an aspect ratio  $\geq 1.14$ .

b. Based on mean average particle measurements, not sums of mean layer thicknesses.

c. Based upon mean average particle measurements, not sums of mean layer thicknesses.

Table A-3. Selected properties for AGR-3/4 compacts.

Property	Specified Range for Mean Value	Actual Mean Value $\pm$ Population Standard Deviation
Compact mass (g)	Not specified	$2.998 \pm 0.002$
Mean uranium loading (g U/compact)	$0.45 \pm 0.03$	$0.450 \pm 0.003$
Diameter <sup>(b)</sup> (mm)	12.2 – 12.4	$12.310 \pm 0.017$
Length <sup>(b)</sup> (mm)	12.4 – 12.6	$12.510 \pm 0.025$
Number of driver particles per compact <sup>(a)</sup>	Not specified	1872
Number of DTF particles per compact	20	20
Particle volume packing fraction (%)	Not specified	37
Effective overall compact density <sup>(a)</sup> (Mg/m <sup>3</sup> )	Not specified	2.01
Compact matrix density (Mg/m <sup>3</sup> )	$\geq 1.45$	$1.603 \pm 0.010$
Compact weight % U <sup>(a)</sup>	Not specified	15.010
Compact weight % O <sup>(a)</sup>	Not specified	1.446
Compact weight % Si <sup>(a)</sup>	Not specified	7.046
Compact weight % C <sup>(a)</sup>	Not specified	76.498
Iron content ( $\mu\text{g}$ Fe outside of SiC/compact)	$\leq 12$	$1.39 \pm 0.06$
Chromium content ( $\mu\text{g}$ Cr outside of SiC/compact)	$\leq 25$	$0.157 \pm 0.012$
Manganese content ( $\mu\text{g}$ Mn outside of SiC/compact)	$\leq 25$	$0.064 \pm 0.003$
Cobalt content ( $\mu\text{g}$ Co outside of SiC/compact)	$\leq 25$	$0.055 \pm 0.002$
Nickel content ( $\mu\text{g}$ Ni outside of SiC/compact)	$\leq 25$	$0.218 \pm 0.011$
Calcium content ( $\mu\text{g}$ Ca outside of SiC/compact)	$\leq 50$	$17 \pm 7$
Aluminum content ( $\mu\text{g}$ Al outside of SiC/compact)	$\leq 25$	$4.8 \pm 1.9$
Titanium content ( $\mu\text{g}$ Ti outside of SiC/compact)	Note (c)	$4.48 \pm 0.17$
Vanadium content ( $\mu\text{g}$ V outside of SiC/compact)	Note (c)	$13.6 \pm 0.4$
U contamination fraction <sup>(d)</sup> (g exposed U/g U in compact)	$\leq 1.0 \times 10^{-4}$	$< 3.5 \times 10^{-5}$
Defective SiC coating fraction <sup>(d)</sup>	$\leq 1.0 \times 10^{-4}$	$< 3.5 \times 10^{-5}$
Defective IPyC coating fraction <sup>(e)</sup>	$\leq 1.0 \times 10^{-4}$	$< 8.7 \times 10^{-5}$
Defective OPyC coating fraction <sup>(e)</sup>	$\leq 1.0 \times 10^{-2}$	$< 2.5 \times 10^{-5}$

a. Calculated value derived from other characterized properties.

b. Allowable range corresponding to upper and lower critical limits specified with no compacts exceeding the limits, which require 100 % inspection of all compacts.

c. Mean value specification of  $\leq 120 \mu\text{g}$  Ti+V outside of SiC per compact.

d. 80% confidence defect fraction.

e. 95% confidence defect fraction.

Table A-4. Selected properties for AGR-3/4 matrix ring blanks and graphite ring and sink.

Property	Specified Range for Mean Value	Actual Mean Value $\pm$ Population Standard Deviation
<b><i>Matrix ring blank</i></b>		
Mass (g)	Not specified	57.14 $\pm$ 0.16
Outer diameter (mm)	26.0 $\pm$ 1.0	25.70 $\pm$ 0.06
Length (mm)	63.0 $\pm$ 2.0	62.26 $\pm$ 0.48
Density (g/cm <sup>3</sup> ) <sup>(a)</sup>	1.65 $\pm$ 0.15	1.770 $\pm$ 0.020 <sup>(b)</sup>
Iron content (ppmw)	$\leq$ 20	2.90
Chromium content (ppmw)	$\leq$ 10	0.05
Manganese content (ppmw)	$\leq$ 10	< 0.0011
Cobalt content (ppmw)	$\leq$ 10	< 0.0038
Nickel content (ppmw)	$\leq$ 10	< 0.0328
Calcium content (ppmw)	$\leq$ 45	7.29
Aluminum content (ppmw)	$\leq$ 20	24.6 <sup>(c)</sup>
Titanium + Vanadium content (ppmw)	$\leq$ 85	3.98
Uranium contamination (ppmw)	$\leq$ 0.5	0.6 <sup>(d)</sup>
<b><i>Graphite ring &amp; sink</i></b>		
Uranium contamination (ppmw) <sup>(e)</sup>	$\leq$ 0.5	< 0.05 <sup>(f)</sup>

- Critical lower limit: < 1.50. No ring blank was found below the critical lower limit.
- Nineteen ring blanks were outside the specified range for density, with average measured densities ranging from 1.80 to 1.83 g/cm<sup>3</sup>. The non-conformance was reported in the Non-Conformance Report X-AGR-11-01 (Hunn, 2011c) with the recommendation of shipping only conforming ring blanks to INL.
- The measured aluminum content of the ring blanks exceeds the specification. The non-conformance was reported in the Non-Conformance Report X-AGR-11-02 (Hunn, 2011c) with the agreement to accept the ring blanks for use, as the Al content was not expected to affect the AGR-3/4 irradiation.
- One of four ring blank samples analyzed for uranium contamination showed an abnormally high content of 1.95 ppmw compared to an average of 0.10 ppmw for the other three samples. This resulted in an average value of 0.6 ppmw that exceeds the specification. The non-conformance was reported in the Non-Conformance Report X-AGR-11-03 (Hunn, 2011c) with the agreement to accept the ring blanks for use because the anomaly is a statistical anomaly.
- 80% confidence level. Values based on uranium contamination + “exposed” uranium being lower than 2.1% of the fuel content in 20 DTF particles/compact.
- Identical limit for both PCEA and IG-110 graphites.



## **Appendix B**

### **Compact Burnup and Fast Fluence by Cycle**

Table B-1. Compact burnup and fast fluence for capsules 7-12 after cycle 151A (AGR-3/4 cycle 1).

Capsule	Compact	Burnup (% FIMA)	Fast Neutron Fluence ( $10^{25}$ n/m <sup>2</sup> , E > 0.18 MeV)
12	4	0.72	0.17
	3	0.77	0.20
	2	0.82	0.22
	1	0.87	0.25
Capsule 12 Average		0.79	0.21
11	4	1.29	0.36
	3	1.37	0.39
	2	1.44	0.41
	1	1.50	0.43
Capsule 11 Average		1.40	0.40
10	4	1.81	0.51
	3	1.88	0.53
	2	1.91	0.55
	1	1.92	0.56
Capsule 10 Average		1.88	0.54
9	4	2.18	0.61
	3	2.24	0.62
	2	2.27	0.63
	1	2.28	0.63
Capsule 9 Average		2.24	0.62
8	4	2.38	0.66
	3	2.40	0.67
	2	2.40	0.67
	1	2.38	0.67
Capsule 8 Average		2.39	0.67
7	4	2.45	0.68
	3	2.48	0.69
	2	2.48	0.69
	1	2.46	0.69
Capsule 7 Average		2.47	0.69

Table B-2. Compact burnup and fast fluence for capsules 1-6 after cycle 151A (AGR-3/4 cycle 1).

Capsule	Compact	Burnup (% FIMA)	Fast Neutron Fluence ( $10^{25}$ n/m <sup>2</sup> , E > 0.18 MeV)
6	4	2.52	0.69
	3	2.54	0.70
	2	2.54	0.70
	1	2.51	0.69
Capsule 6 Average		2.53	0.70
5	4	2.48	0.69
	3	2.48	0.69
	2	2.47	0.68
	1	2.43	0.68
Capsule 5 Average		2.46	0.69
4	4	2.38	0.66
	3	2.36	0.65
	2	2.34	0.65
	1	2.30	0.64
Capsule 4 Average		2.35	0.65
3	4	2.10	0.59
	3	2.07	0.58
	2	2.03	0.57
	1	1.95	0.55
Capsule 3 Average		2.04	0.57
2	4	1.68	0.48
	3	1.63	0.46
	2	1.55	0.44
	1	1.47	0.41
Capsule 2 Average		1.58	0.44
1	4	1.04	0.29
	3	0.96	0.26
	2	0.88	0.23
	1	0.81	0.20
Capsule 1 Average		0.92	0.25

Table B-3. Compact burnup and fast fluence for capsules 7-12 after cycle 151B (AGR-3/4 cycle 2).

Capsule	Compact	Burnup (% FIMA)	Fast Neutron Fluence ( $10^{25}$ n/m <sup>2</sup> , E > 0.18 MeV)
12	4	1.38	0.32
	3	1.48	0.38
	2	1.58	0.44
	1	1.68	0.49
Capsule 12 Average		1.53	0.41
11	4	2.47	0.70
	3	2.63	0.75
	2	2.76	0.79
	1	2.87	0.83
Capsule 11 Average		2.68	0.77
10	4	3.46	0.99
	3	3.57	1.02
	2	3.64	1.05
	1	3.68	1.08
Capsule 10 Average		3.59	1.04
9	4	4.13	1.17
	3	4.23	1.19
	2	4.28	1.21
	1	4.30	1.22
Capsule 9 Average		4.23	1.20
8	4	4.48	1.27
	3	4.52	1.28
	2	4.52	1.29
	1	4.47	1.29
Capsule 8 Average		4.50	1.28
7	4	4.61	1.31
	3	4.66	1.32
	2	4.66	1.32
	1	4.62	1.32
Capsule 7 Average		4.64	1.32

Table B-4. Compact burnup and fast fluence for capsules 1-6 after cycle 151B (AGR-3/4 cycle 2).

Capsule	Compact	Burnup (% FIMA)	Fast Neutron Fluence ( $10^{25}$ n/m <sup>2</sup> , E > 0.18 MeV)
6	4	4.75	1.33
	3	4.77	1.33
	2	4.76	1.33
	1	4.73	1.33
Capsule 6 Average		4.75	1.33
5	4	4.66	1.32
	3	4.65	1.32
	2	4.63	1.31
	1	4.56	1.30
Capsule 5 Average		4.62	1.31
4	4	4.49	1.26
	3	4.47	1.25
	2	4.41	1.24
	1	4.33	1.22
Capsule 4 Average		4.43	1.24
3	4	3.97	1.14
	3	3.91	1.12
	2	3.83	1.09
	1	3.70	1.06
Capsule 3 Average		3.85	1.10
2	4	3.21	0.92
	3	3.10	0.88
	2	2.96	0.84
	1	2.80	0.79
Capsule 2 Average		3.02	0.86
1	4	1.99	0.57
	3	1.85	0.51
	2	1.70	0.45
	1	1.57	0.39
Capsule 1 Average		1.78	0.48

Table B-5. Compact burnup and fast fluence for capsules 7-12 after cycle 152B (AGR-3/4 cycle 3).

Capsule	Compact	Burnup (% FIMA)	Fast Neutron Fluence ( $10^{25}$ n/m <sup>2</sup> , E > 0.18 MeV)
12	4	2.07	0.49
	3	2.21	0.57
	2	2.35	0.65
	1	2.52	0.73
Capsule 12 Average		2.29	0.61
11	4	3.68	1.06
	3	3.91	1.13
	2	4.10	1.19
	1	4.26	1.25
Capsule 11 Average		3.99	1.16
10	4	5.13	1.50
	3	5.29	1.55
	2	5.38	1.59
	1	5.44	1.63
Capsule 10 Average		5.31	1.57
9	4	6.11	1.78
	3	6.25	1.81
	2	6.32	1.84
	1	6.36	1.86
Capsule 9 Average		6.26	1.82
8	4	6.63	1.94
	3	6.69	1.96
	2	6.69	1.97
	1	6.63	1.97
Capsule 8 Average		6.66	1.96
7	4	6.84	2.01
	3	6.90	2.02
	2	6.91	2.02
	1	6.85	2.02
Capsule 7 Average		6.87	2.02

Table B-6. Compact burnup and fast fluence for capsules 1-6 after cycle 152B (AGR-3/4 cycle 3).

Capsule	Compact	Burnup (% FIMA)	Fast Neutron Fluence ( $10^{25}$ n/m <sup>2</sup> , E > 0.18 MeV)
6	4	7.03	2.03
	3	7.06	2.04
	2	7.04	2.04
	1	7.00	2.03
Capsule 6 Average		7.03	2.03
5	4	6.89	2.01
	3	6.88	2.01
	2	6.85	2.00
	1	6.76	1.98
Capsule 5 Average		6.84	2.00
4	4	6.63	1.92
	3	6.59	1.91
	2	6.51	1.88
	1	6.40	1.85
Capsule 4 Average		6.53	1.89
3	4	5.88	1.73
	3	5.79	1.69
	2	5.65	1.66
	1	5.48	1.60
Capsule 3 Average		5.70	1.67
2	4	4.75	1.38
	3	4.59	1.33
	2	4.39	1.27
	1	4.15	1.19
Capsule 2 Average		4.47	1.29
1	4	2.96	0.85
	3	2.75	0.76
	2	2.54	0.67
	1	2.33	0.58
Capsule 1 Average		2.64	0.72

Table B-7. Compact burnup and fast fluence for capsules 7-12 after cycle 154A (AGR-3/4 cycle 4).

Capsule	Compact	Burnup (% FIMA)	Fast Neutron Fluence ( $10^{25}$ n/m <sup>2</sup> , E > 0.18 MeV)
12	4	2.73	0.65
	3	2.92	0.77
	2	3.11	0.87
	1	3.33	0.98
Capsule 12 Average		3.02	0.82
11	4	4.84	1.42
	3	5.14	1.52
	2	5.39	1.60
	1	5.59	1.68
Capsule 11 Average		5.24	1.55
10	4	6.72	2.01
	3	6.93	2.09
	2	7.06	2.14
	1	7.13	2.20
Capsule 10 Average		6.96	2.11
9	4	8.00	2.41
	3	8.17	2.46
	2	8.26	2.49
	1	8.32	2.52
Capsule 9 Average		8.19	2.47
8	4	8.67	2.64
	3	8.74	2.66
	2	8.76	2.68
	1	8.69	2.69
Capsule 8 Average		8.72	2.67
7	4	8.96	2.74
	3	9.04	2.75
	2	9.06	2.76
	1	8.97	2.76
Capsule 7 Average		9.01	2.75



Table B-8. Compact burnup and fast fluence for capsules 1-6 after cycle 154A (AGR-3/4 cycle 4).

Capsule	Compact	Burnup (% FIMA)	Fast Neutron Fluence ( $10^{25}$ n/m <sup>2</sup> , E > 0.18 MeV)
6	4	9.20	2.77
	3	9.23	2.78
	2	9.20	2.78
	1	9.16	2.77
Capsule 6 Average		9.20	2.78
5	4	9.01	2.74
	3	8.99	2.74
	2	8.95	2.72
	1	8.84	2.70
Capsule 5 Average		8.95	2.72
4	4	8.66	2.60
	3	8.60	2.59
	2	8.51	2.56
	1	8.37	2.51
Capsule 4 Average		8.54	2.56
3	4	7.69	2.33
	3	7.57	2.28
	2	7.40	2.23
	1	7.18	2.16
Capsule 3 Average		7.46	2.25
2	4	6.23	1.86
	3	6.01	1.78
	2	5.76	1.70
	1	5.46	1.60
Capsule 2 Average		5.87	1.73
1	4	3.91	1.14
	3	3.63	1.02
	2	3.35	0.90
	1	3.08	0.77
Capsule 1 Average		3.49	0.96

Table B-9. Compact burnup and fast fluence for capsules 7-12 after cycle 154B (AGR-3/4 cycle 5).

Capsule	Compact	Burnup (% FIMA)	Fast Neutron Fluence ( $10^{25}$ n/m <sup>2</sup> , E > 0.18 MeV)
12	4	3.48	0.84
	3	3.71	0.98
	2	3.96	1.12
	1	4.23	1.26
Capsule 12 Average		3.85	1.05
11	4	6.12	1.82
	3	6.49	1.95
	2	6.80	2.06
	1	7.05	2.16
Capsule 11 Average		6.62	2.00
10	4	8.43	2.60
	3	8.68	2.69
	2	8.85	2.77
	1	8.93	2.84
Capsule 10 Average		8.72	2.72
9	4	9.97	3.11
	3	10.17	3.17
	2	10.28	3.22
	1	10.35	3.25
Capsule 9 Average		10.20	3.19
8	4	10.79	3.42
	3	10.87	3.45
	2	10.90	3.47
	1	10.82	3.48
Capsule 8 Average		10.84	3.46
7	4	11.14	3.55
	3	11.23	3.57
	2	11.25	3.58
	1	11.15	3.58
Capsule 7 Average		11.19	3.57

Table B-10. Compact burnup and fast fluence for capsules 1-6 after cycle 154B (AGR-3/4 cycle 5).

Capsule	Compact	Burnup (% FIMA)	Fast Neutron Fluence ( $10^{25}$ n/m <sup>2</sup> , E > 0.18 MeV)
6	4	11.43	3.60
	3	11.45	3.61
	2	11.43	3.61
	1	11.39	3.59
Capsule 6 Average		11.42	3.60
5	4	11.20	3.55
	3	11.17	3.54
	2	11.12	3.52
	1	11.01	3.50
Capsule 5 Average		11.13	3.53
4	4	10.77	3.36
	3	10.70	3.34
	2	10.59	3.31
	1	10.43	3.24
Capsule 4 Average		10.62	3.31
3	4	9.61	3.01
	3	9.46	2.95
	2	9.26	2.88
	1	8.99	2.79
Capsule 3 Average		9.33	2.91
2	4	7.83	2.39
	3	7.56	2.29
	2	7.25	2.18
	1	6.88	2.06
Capsule 2 Average		7.38	2.23
1	4	4.95	1.46
	3	4.60	1.31
	2	4.25	1.16
	1	3.91	0.99
Capsule 1 Average		4.43	1.23

Table B-11. Compact burnup and fast fluence for capsules 7-12 after cycle 155A (AGR-3/4 cycle 6).

Capsule	Compact	Burnup (% FIMA)	Fast Neutron Fluence ( $10^{25}$ n/m <sup>2</sup> , E > 0.18 MeV)
12	4	4.19	1.02
	3	4.47	1.20
	2	4.77	1.37
	1	5.08	1.53
Capsule 12 Average		4.63	1.28
11	4	7.33	2.23
	3	7.75	2.39
	2	8.11	2.52
	1	8.42	2.65
Capsule 11 Average		7.90	2.45
10	4	10.02	3.19
	3	10.31	3.31
	2	10.50	3.41
	1	10.61	3.50
Capsule 10 Average		10.36	3.35
9	4	11.81	3.84
	3	12.03	3.92
	2	12.16	3.99
	1	12.24	4.03
Capsule 9 Average		12.06	3.95
8	4	12.75	4.25
	3	12.85	4.29
	2	12.89	4.32
	1	12.81	4.34
Capsule 8 Average		12.82	4.30
7	4	13.18	4.43
	3	13.27	4.45
	2	13.29	4.47
	1	13.19	4.46
Capsule 7 Average		13.23	4.45

Table B-12. Compact burnup and fast fluence for capsules 1-6 after cycle 155A (AGR-3/4 cycle 6).

Capsule	Compact	Burnup (% FIMA)	Fast Neutron Fluence ( $10^{25}$ n/m <sup>2</sup> , E > 0.18 MeV)
6	4	13.51	4.48
	3	13.52	4.50
	2	13.48	4.49
	1	13.46	4.48
Capsule 6 Average		13.49	4.49
5	4	13.24	4.42
	3	13.19	4.41
	2	13.14	4.38
	1	13.02	4.35
Capsule 5 Average		13.15	4.39
4	4	12.73	4.17
	3	12.63	4.14
	2	12.51	4.09
	1	12.34	4.02
Capsule 4 Average		12.55	4.11
3	4	11.38	3.72
	3	11.20	3.64
	2	10.98	3.55
	1	10.67	3.43
Capsule 3 Average		11.06	3.58
2	4	9.32	2.93
	3	9.00	2.81
	2	8.64	2.68
	1	8.22	2.52
Capsule 2 Average		8.80	2.74
1	4	5.94	1.79
	3	5.52	1.60
	2	5.11	1.41
	1	4.70	1.21
Capsule 1 Average		5.32	1.50

Table B-13. Compact burnup and fast fluence for capsules 7-12 after cycle 155B (AGR-3/4 cycle 7).

Capsule	Compact	Burnup (% FIMA)	Fast Neutron Fluence ( $10^{25}$ n/m <sup>2</sup> , E > 0.18 MeV)
12	4	4.85	1.19
	3	5.17	1.41
	2	5.52	1.60
	1	5.87	1.80
Capsule 12 Average		5.35	1.50
11	4	8.42	2.61
	3	8.89	2.80
	2	9.30	2.96
	1	9.64	3.11
Capsule 11 Average		9.06	2.87
10	4	11.43	3.75
	3	11.75	3.89
	2	11.96	4.01
	1	12.08	4.12
Capsule 10 Average		11.80	3.94
9	4	13.40	4.53
	3	13.63	4.63
	2	13.78	4.70
	1	13.87	4.76
Capsule 9 Average		13.67	4.65
8	4	14.43	5.02
	3	14.54	5.07
	2	14.58	5.11
	1	14.51	5.13
Capsule 8 Average		14.51	5.08
7	4	14.90	5.24
	3	15.00	5.27
	2	15.02	5.29
	1	14.92	5.28
Capsule 7 Average		14.96	5.27

Table B-14. Compact burnup and fast fluence for capsules 1-6 after cycle 155B (AGR-3/4 cycle 7).

Capsule	Compact	Burnup (% FIMA)	Fast Neutron Fluence ( $10^{25}$ n/m <sup>2</sup> , E > 0.18 MeV)
6	4	15.26	5.31
	3	15.27	5.32
	2	15.23	5.32
	1	15.21	5.30
Capsule 6 Average		15.24	5.31
5	4	14.98	5.23
	3	14.92	5.22
	2	14.86	5.18
	1	14.74	5.14
Capsule 5 Average		14.87	5.19
4	4	14.41	4.92
	3	14.29	4.89
	2	14.16	4.83
	1	13.98	4.74
Capsule 4 Average		14.21	4.85
3	4	12.93	4.38
	3	12.73	4.28
	2	12.49	4.17
	1	12.16	4.04
Capsule 3 Average		12.58	4.22
2	4	10.65	3.44
	3	10.29	3.30
	2	9.90	3.14
	1	9.43	2.95
Capsule 2 Average		10.07	3.21
1	4	6.85	2.10
	3	6.37	1.87
	2	5.91	1.66
	1	5.43	1.42
Capsule 1 Average		6.14	1.76

## **Appendix C**

### **Matrix ring, graphite ring, and graphite sink temperatures**



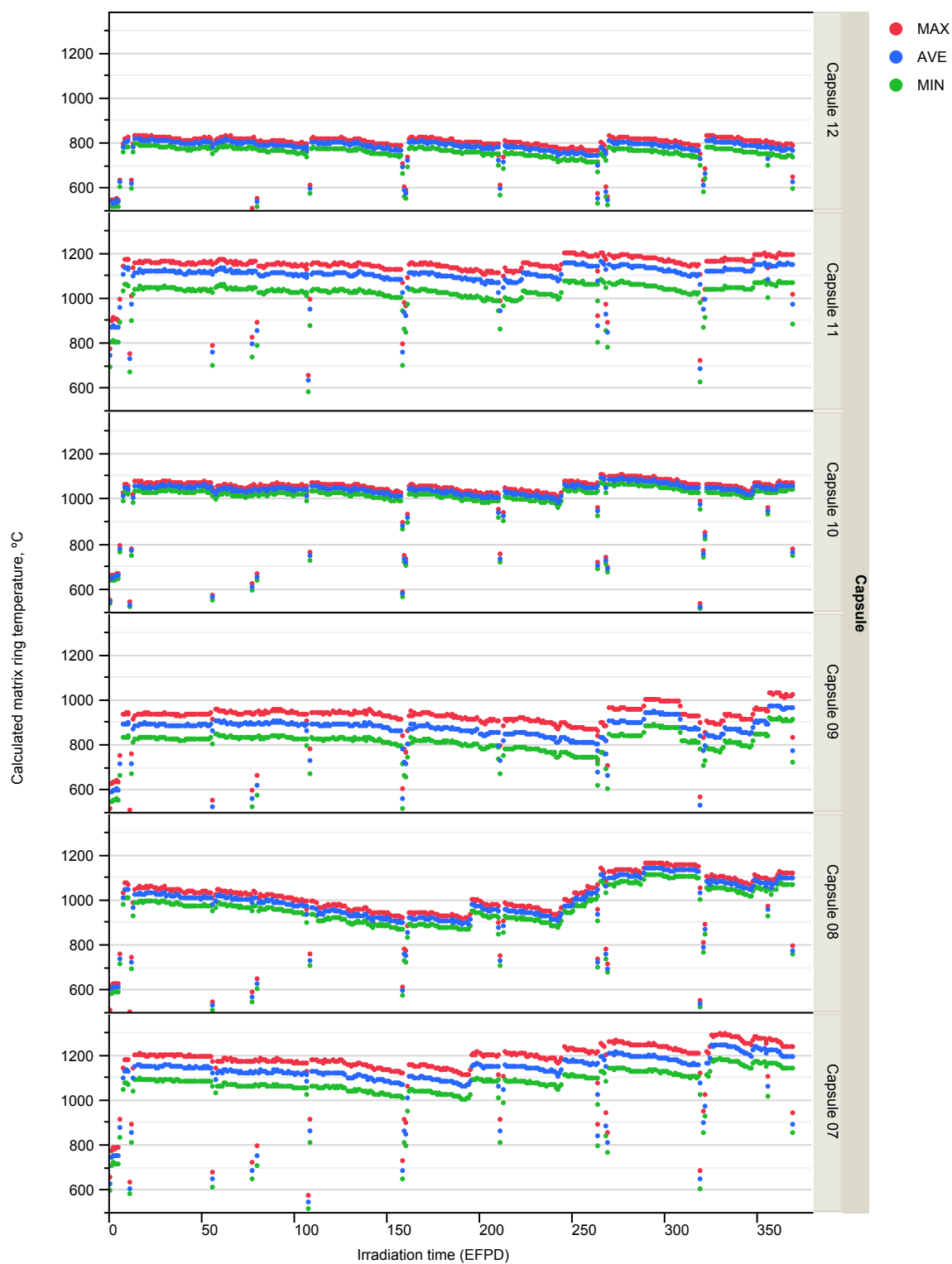


Figure C-1. Calculated daily minimum, maximum, and volume-average matrix ring temperatures for Capsules 7-12.

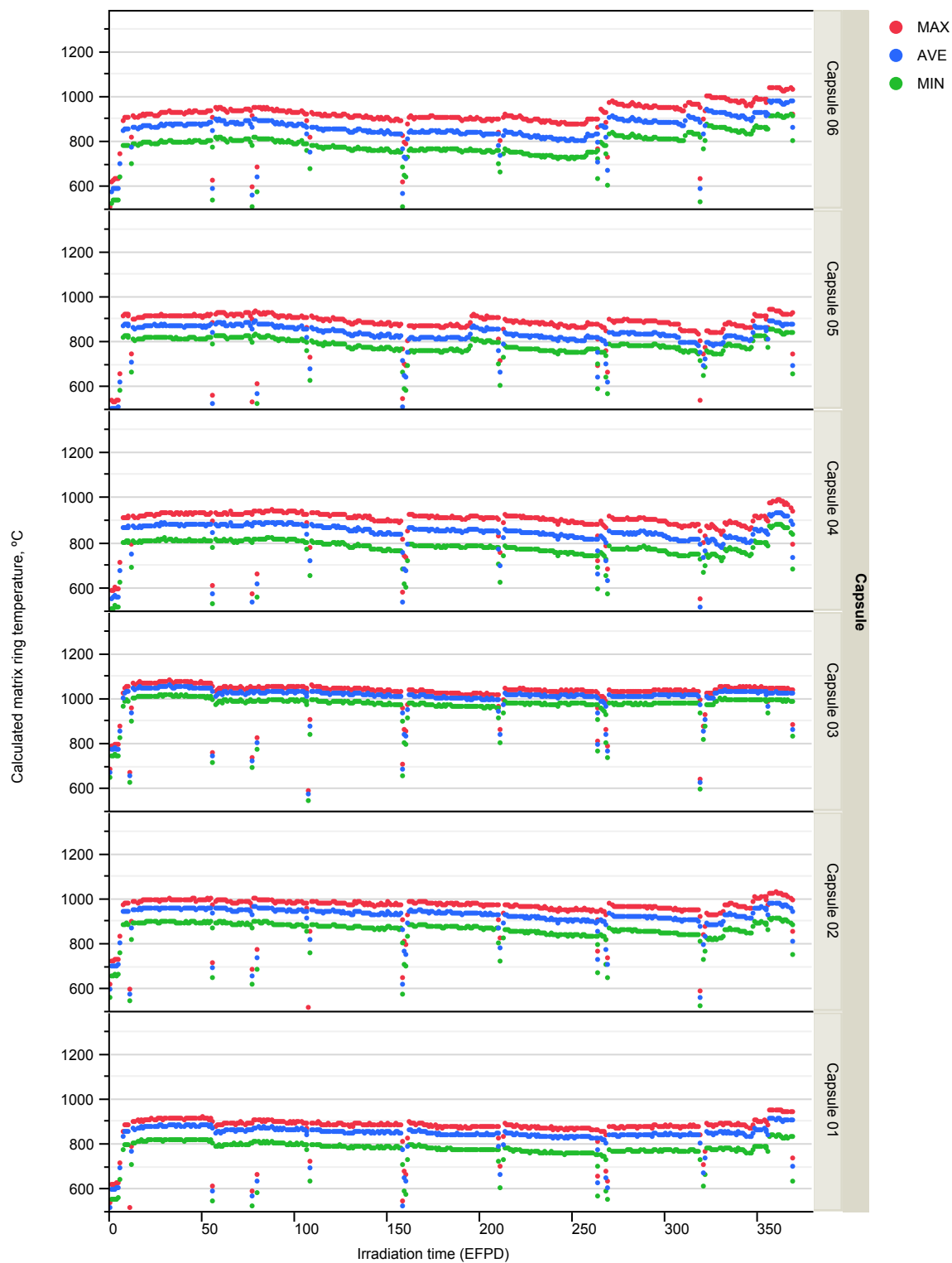


Figure C-2. Calculated daily minimum, maximum, and volume-average matrix ring temperatures for Capsules 1-6.

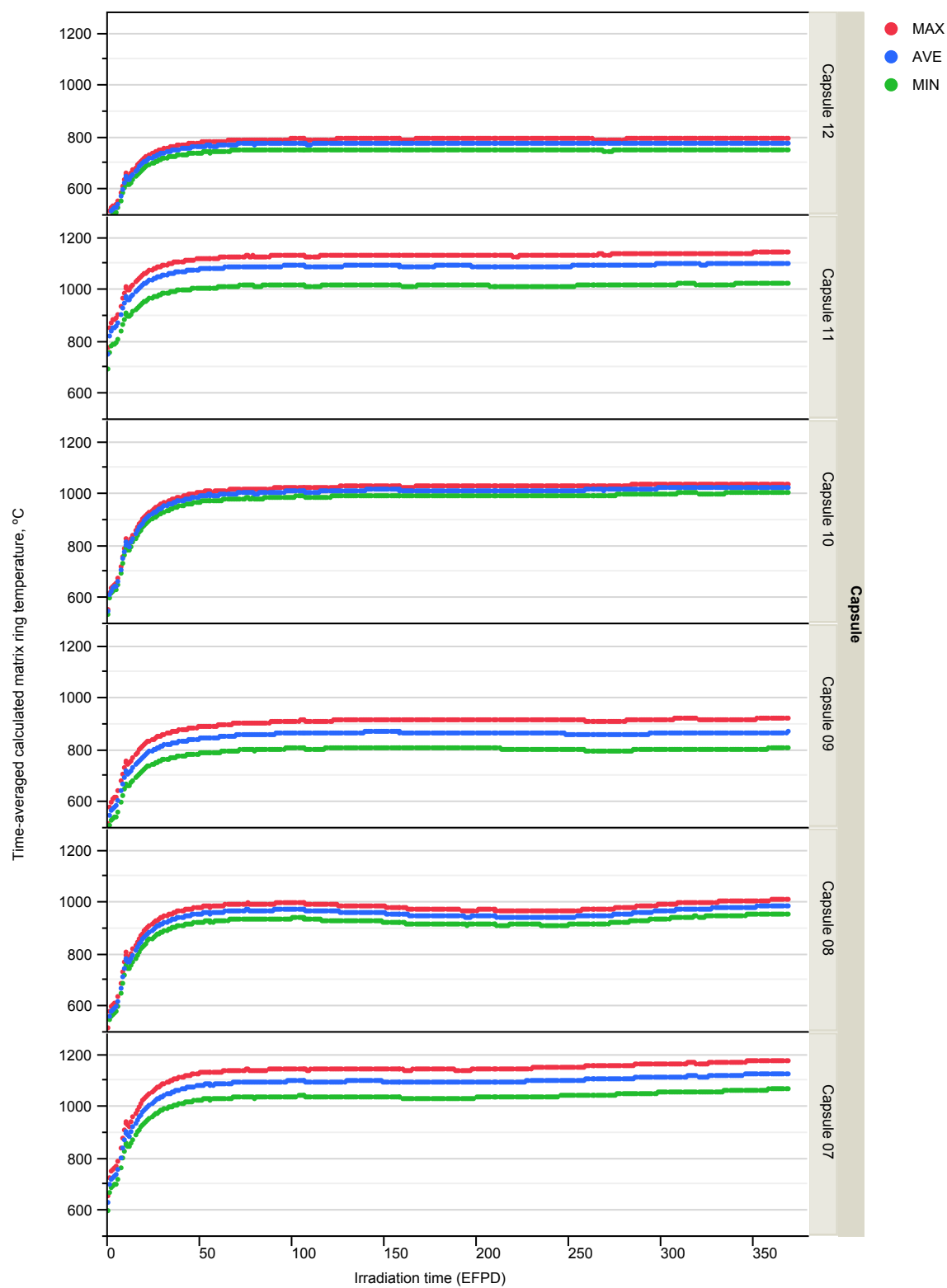


Figure C-3. Calculated time-average minimum, time-average maximum, and time-average volume-average matrix ring temperatures for Capsules 7-12.

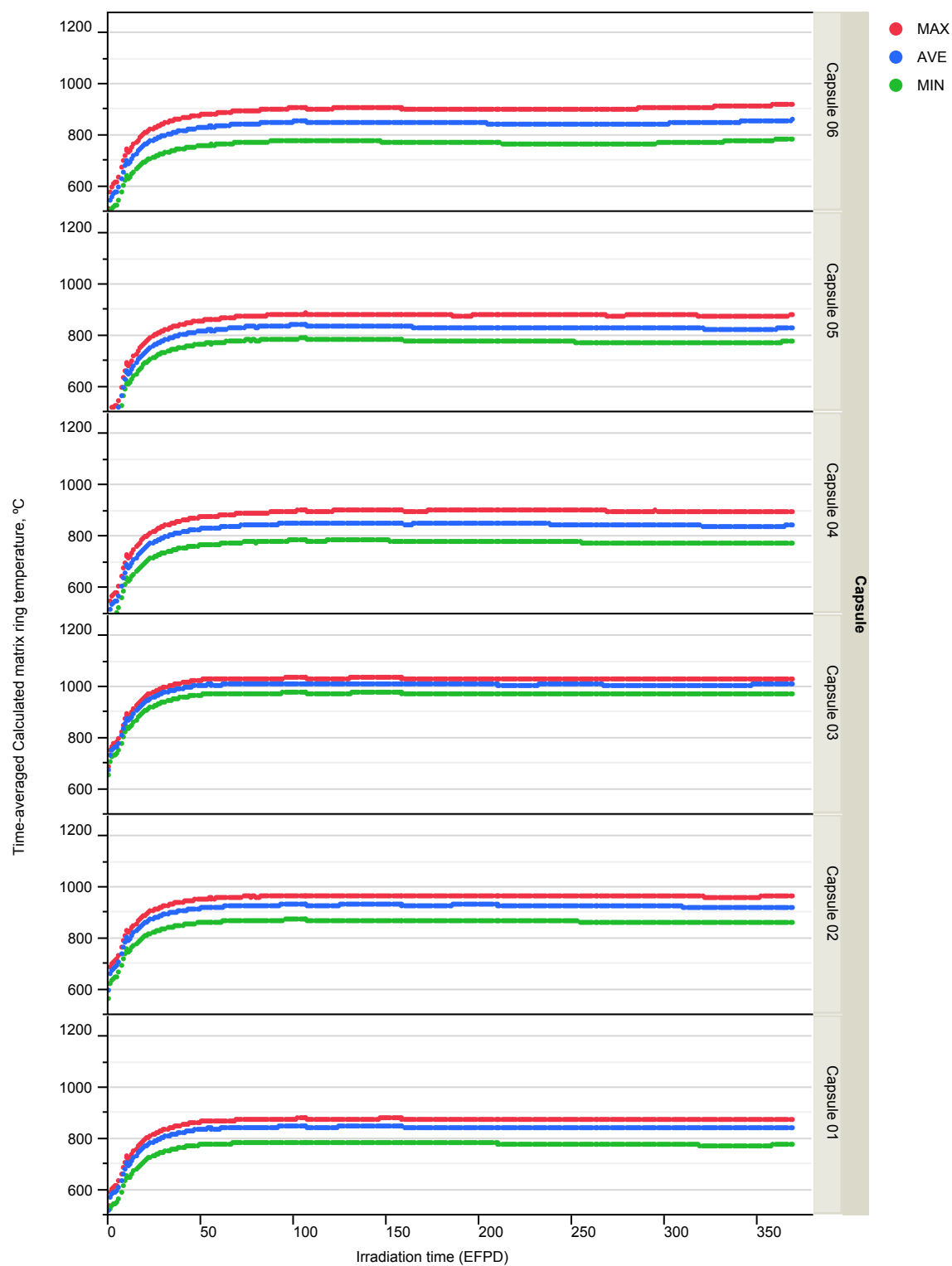


Figure C-4. Calculated time-average minimum, time-average maximum, and time-average volume-average matrix ring temperatures for Capsules 1-6.

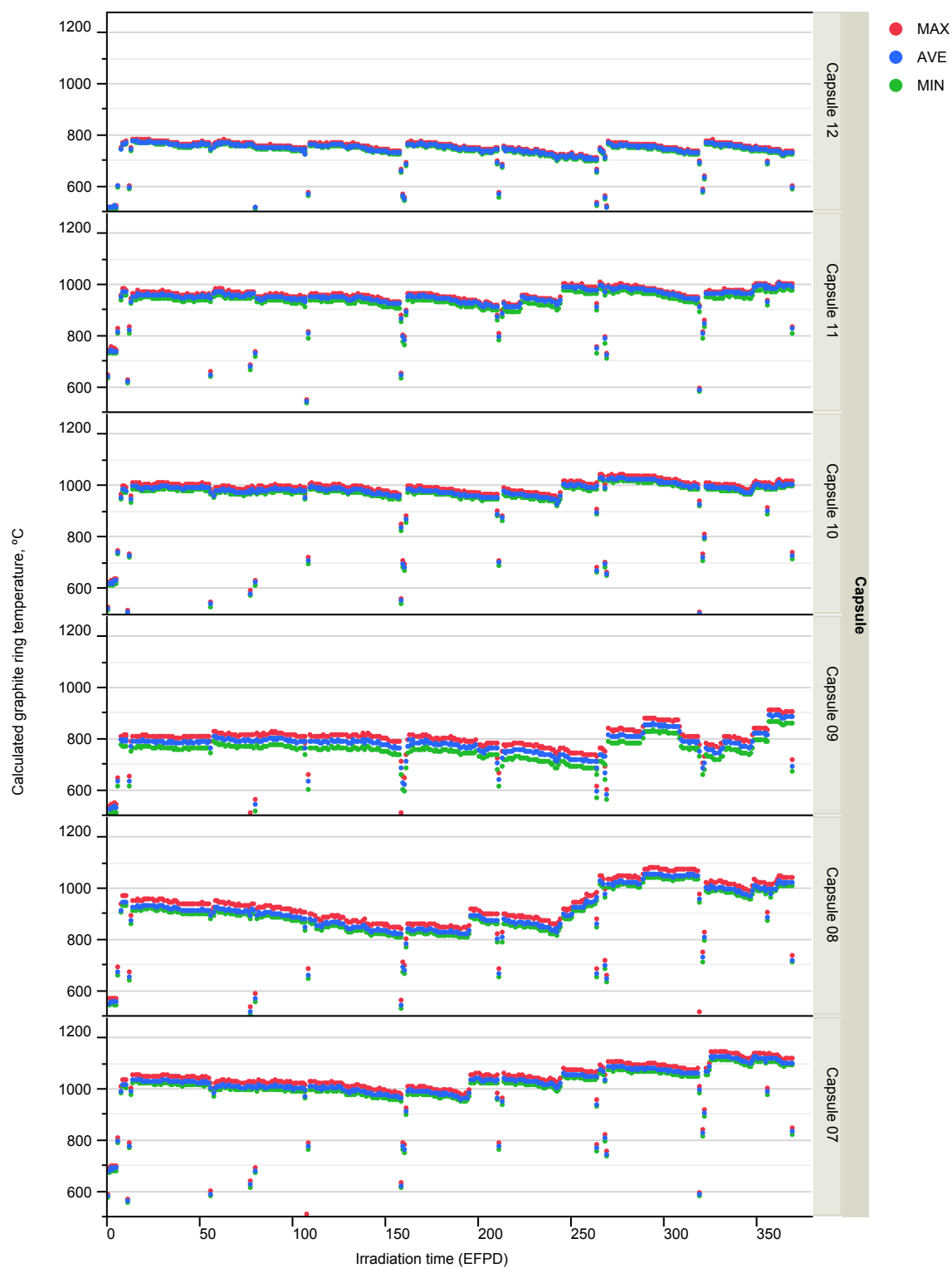


Figure C-5. Calculated daily minimum, maximum, and volume-average graphite ring temperatures for Capsules 7-12.

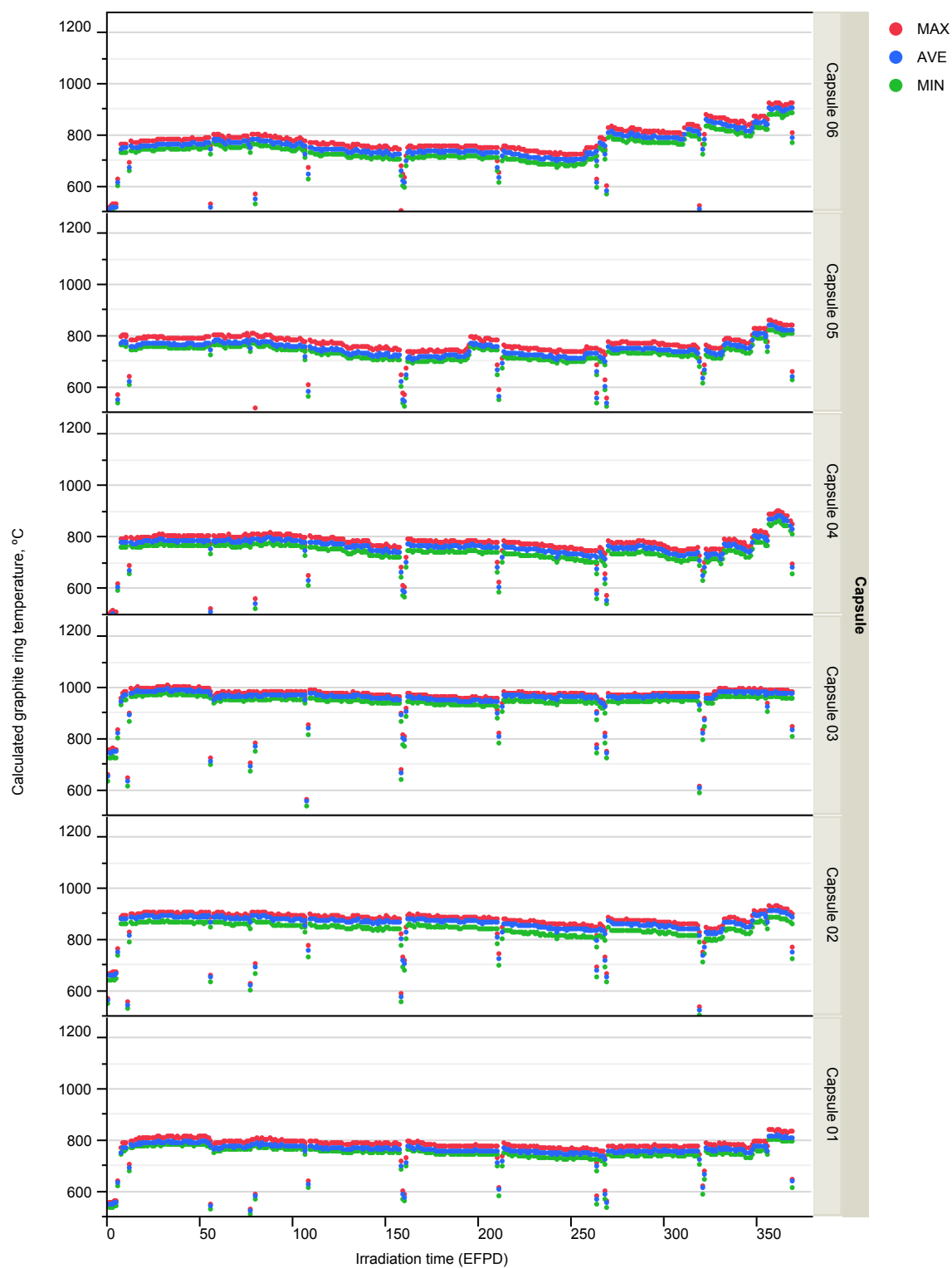


Figure C-6. Calculated daily minimum, maximum, and volume-average graphite ring temperatures for Capsules 1-6.

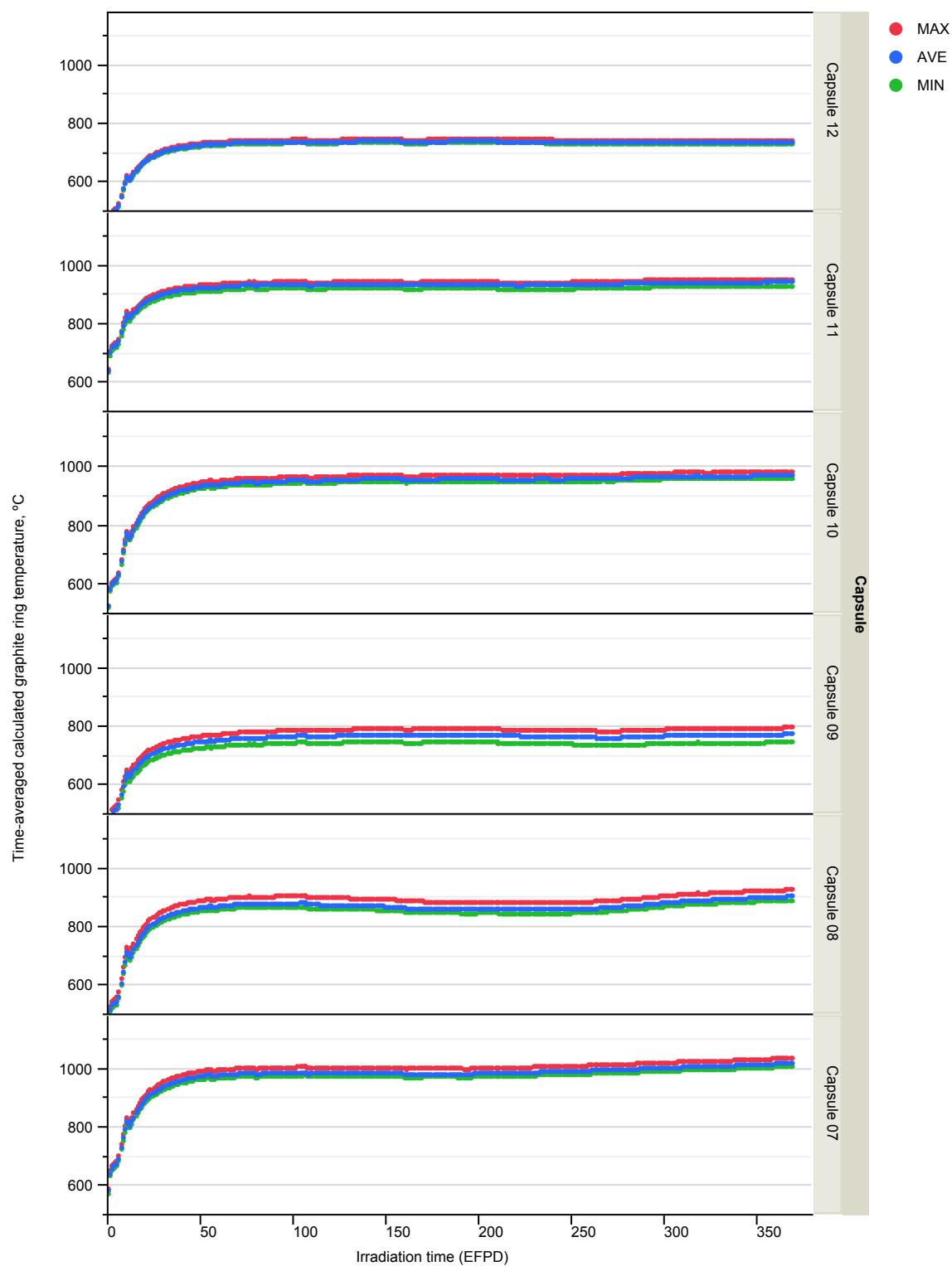


Figure C-7. Calculated time-average minimum, time-average maximum, and time-average volume-average graphite ring temperatures for Capsules 7-12.

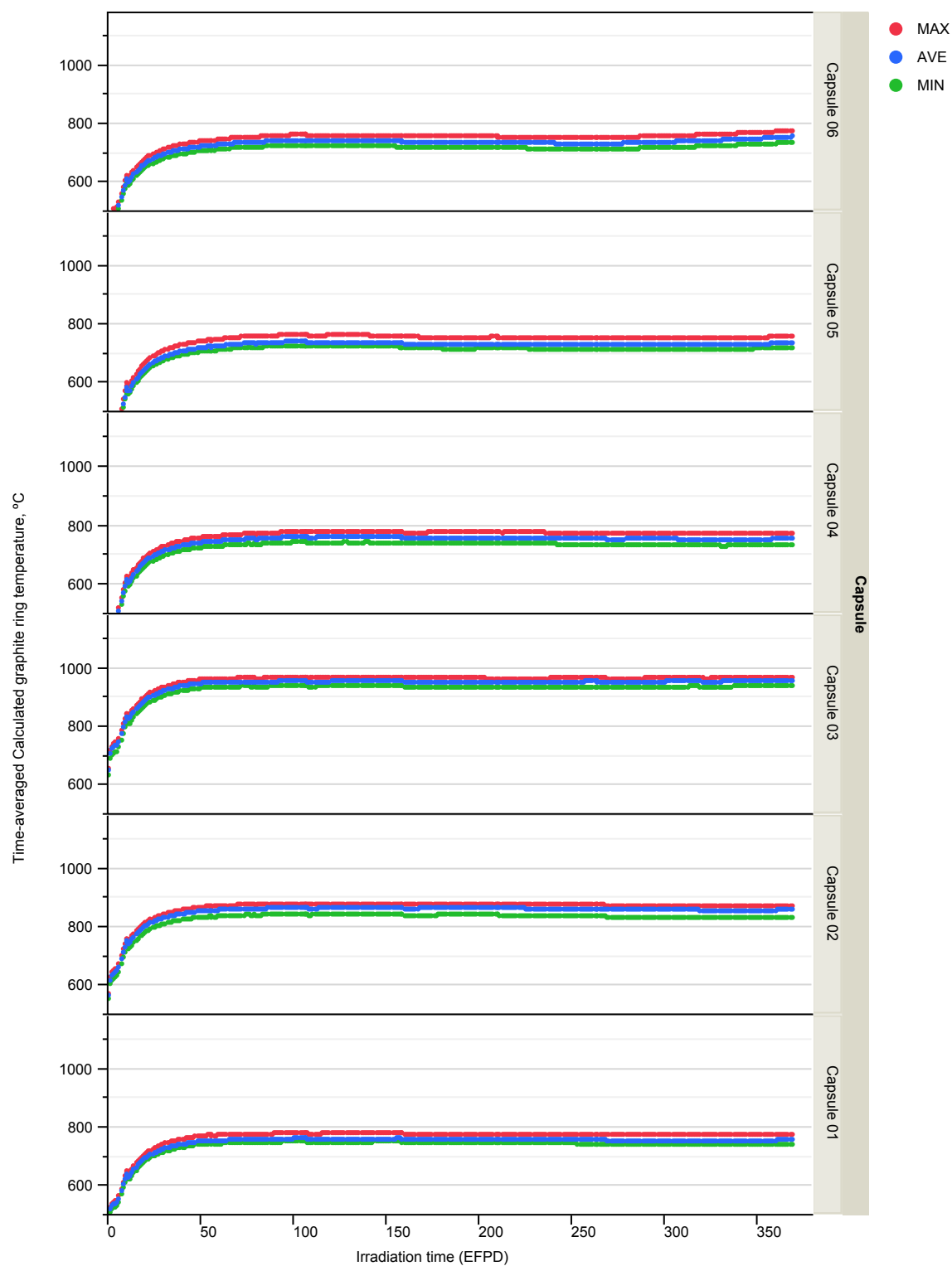


Figure C-8. Calculated time-average minimum, time-average maximum, and time-average volume-average graphite ring temperatures for Capsules 1-6.



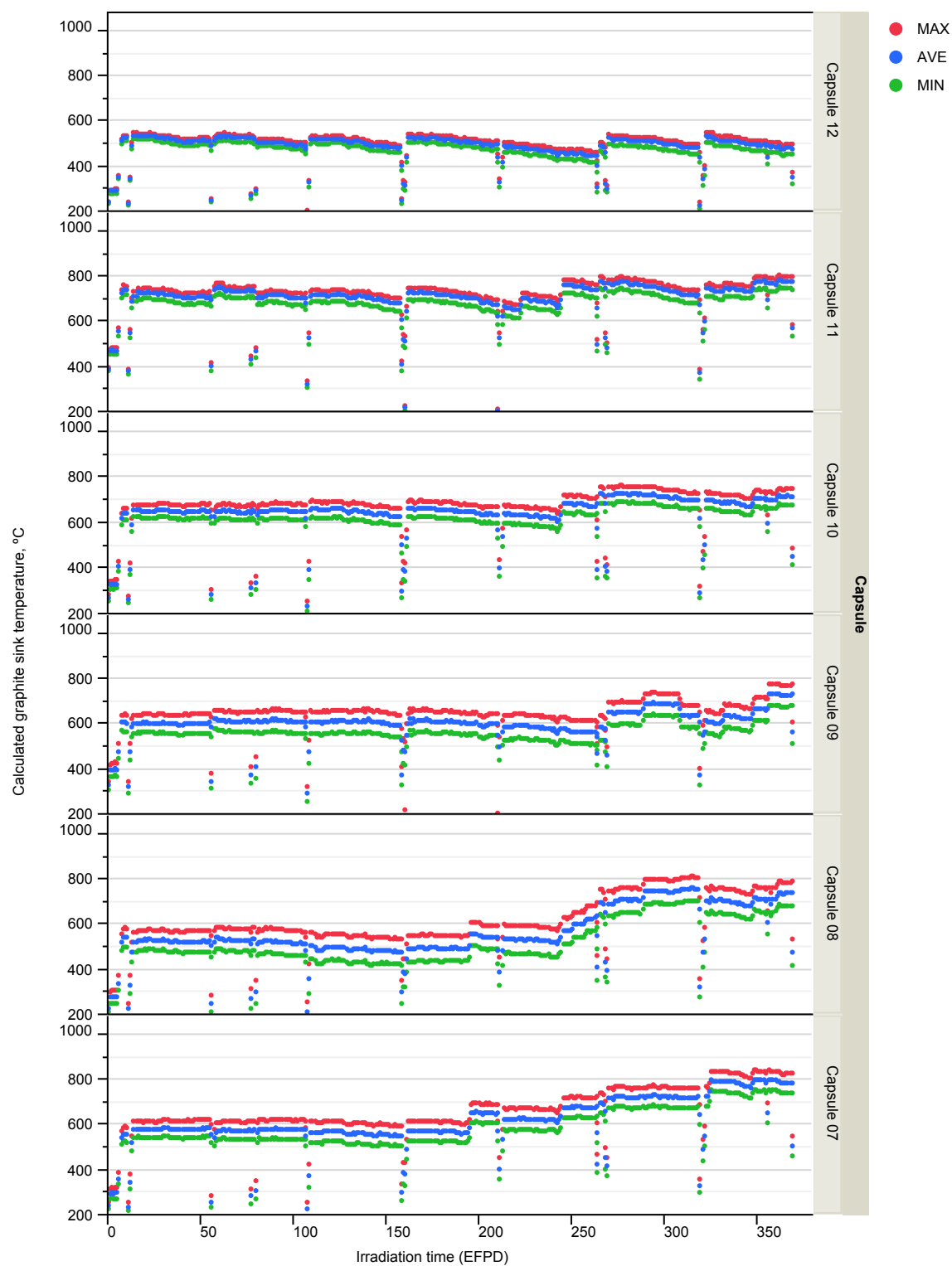


Figure C-9. Calculated daily minimum, maximum, and volume-average graphite sink temperatures for Capsules 7-12.

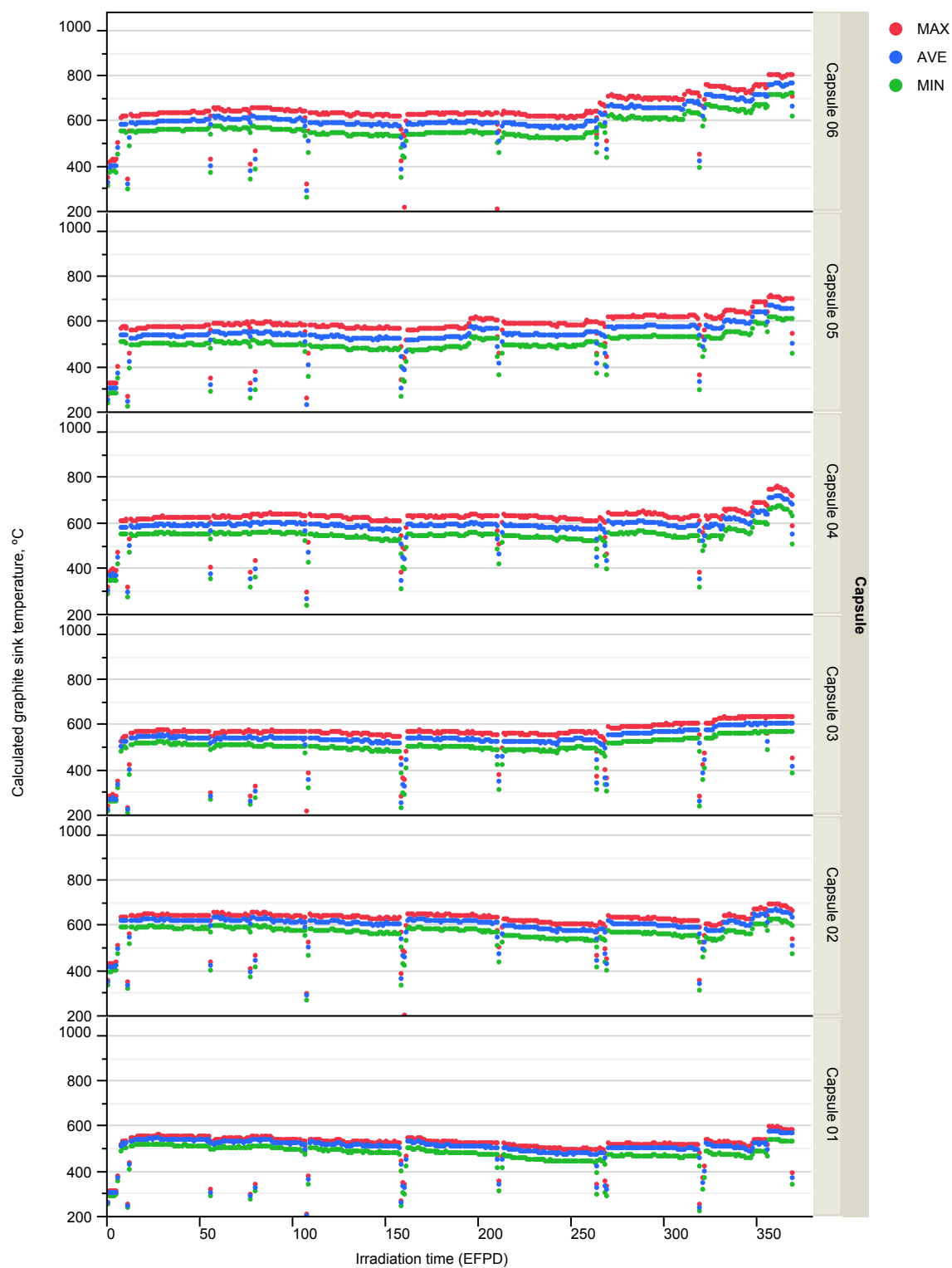


Figure C-10. Calculated daily minimum, maximum, and volume-average graphite sink temperatures for Capsules 1-6.

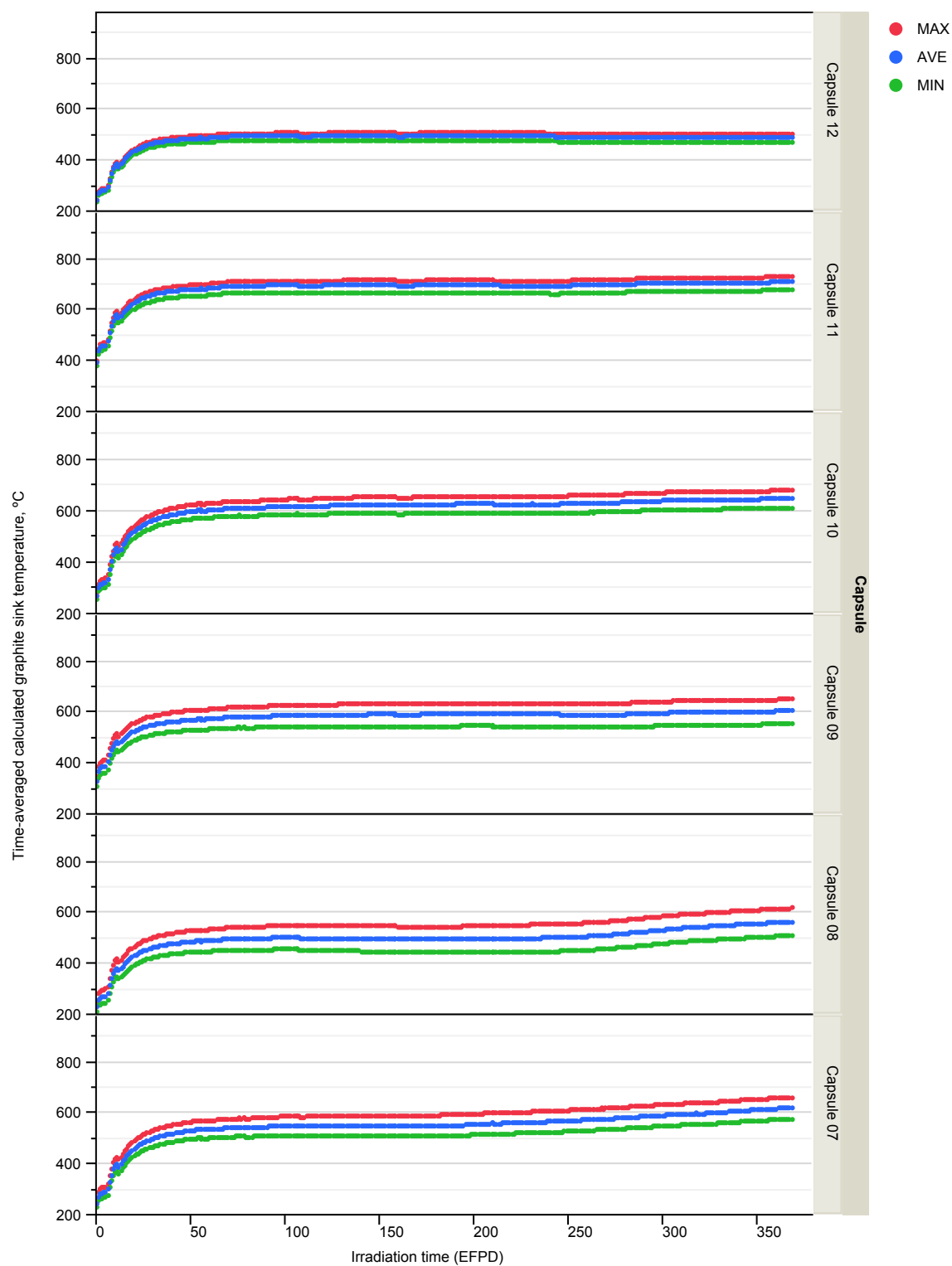


Figure C-11. Calculated time-average minimum, time-average maximum, and time-average volume-average graphite sink temperatures for Capsules 7-12.

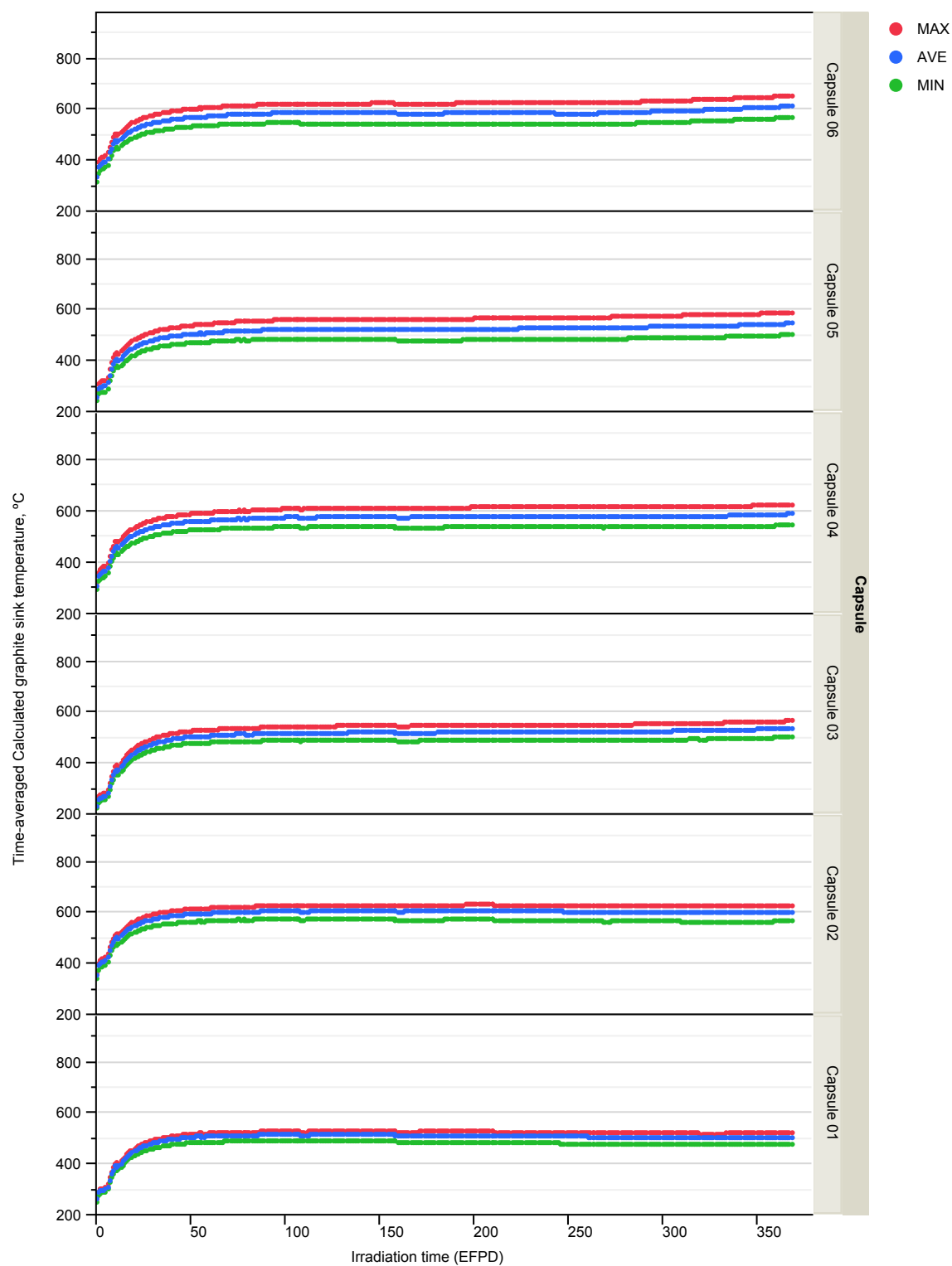


Figure C-12. Calculated time-average minimum, time-average maximum, and time-average volume-average graphite sink temperatures for Capsules 1-6.